Design, Optimization, and Sensorless Control of a Linear Actuator

THÈSE N^{O} 5187 (2011)

PRÉSENTÉE LE 4 NOVEMBRE 2011

À LA FACULTÉ SCIENCES ET TECHNIQUES DE L'INGÉNIEUR

LABORATOIRE D'ACTIONNEURS INTÉGRÉS

PROGRAMME DOCTORAL EN SYSTÈMES DE PRODUCTION ET ROBOTIQUE

ÉCOLE POLYTECHNIQUE FÉDÉRALE DE LAUSANNE

POUR L'OBTENTION DU GRADE DE DOCTEUR ÈS SCIENCES

PAR

Joël MARIDOR

acceptée sur proposition du jury:

Prof. M.-O. Hongler, président du jury
Prof. Y. Perriard, Dr M. Markovic, directeurs de thèse
Prof. H. Bleuler, rapporteur
Prof. C. Espanet, rapporteur
Dr D. Ladas, rapporteur

ÉCOLE POLYTECHNIQUE
FÉDÉRALE DE LAUSANNE

Suisse
2011

Maman quand j’s’rais grand
J’voudrais pas être étudiant
Alors tu seras un moins que rien
Ah oui ça j’veux bien

— Renaud

Remerciements

J'aimerais remercier toutes les personnes qui ont permis l'écriture de cette thèse par leurs conseils, avis, soutien et pardonnez-moi si j'en oublie certains ou si les mots n'expriment pas toute la gratitude que vous méritez.

Je remercie tout d'abord Yves qui m'a accueilli pendant 4 ans et a su créer un environnement de travail propice à un enrichissement professionnel et personnel.

J'aimerais ensuite remercier Mika, mon co-directeur de thèse, qui m'a suivi, soutenu, conseillé, éclairé et qui est en grande partie responsable de la réussite de cette thèse, Dimitrios et ses collègues de Schneider Electric, qui ont apporté un regard industriel à mon travail ainsi que Paolo, Christian et André qui ont été indispensables au bon déroulement pratique de la thèse.

Je veux bien sûr remercier tous les collègues du LAI. Vous avez tous contribué à l'excellente ambiance qui règne au Labo. Les pauses, les sorties, les Noëls, les vacances seront autant de moments qui vont me manquer.

Merci aussi aux étudiants de semestre et de master qui m'ont aidé à résoudre bien des problèmes techniques grâce à leur travail.

Le travail n'étant pas tout, merci à la famille, à ma filleule Julie, aux amis, au FAYLYS, au foot, et à tous ceux qui ont aussi permis que je passe 4 ans formidables.

Je tiens finalement à remercier tout spécialement mes frères Steve et Yann, mes potes de toujours ainsi que mes parents, Rose-Marie et Raymond, qui m'ont toujours encouragé, soutenu et sans qui rien n'aurait été possible.

Abstract

Electrical contactors are relays for interputing high currents (up to 2000 A). They consist of three main distinct parts: the low voltage circuit, the high voltage circuit and the linear actuator that moves the contact. The purpose of this thesis is to design, optimize and control the moving part of a linear actuator without external sensor.

Indeed, it is very important to control the closing speed of the actuator in order to minimize the contacts wear. The speed should not be too fast so as not to damage the silver contacts at the impact and not too slow to avoid multiple arcs, which erode the contacts.

The thesis is divided into different themes: the sensorless position detection, the optimization of the actuator, the signal processing of the position and the speed by adapting the Kalman filter, and finally the sensorless speed control of the actuator's moving part.

Industrial constraints impose, for reasons of cost, a position detection without sensor. To do this, a high frequency signal (1250 Hz), named scan current, is superimposed to the one that drives the actuator's moving part. Then, the total current is filtered to obtain only the scan current. Its amplitude depends on the position because the inductance of the actuator windind varies greatly with the value of the airgap. It is therefore possible to detect the position using only the provided low voltage circuit.

The optimization of the actuator is made by combining genetic algorithms and finite element modeling (FEM). The first objective to be achieved by the optimizer is to minimize the material cost of the actuator. Then, knowing the minimum price of the actuator, the cost becomes a constraint when optimizing for the best position detection. The optimal configuration presented in the thesis promotes the variation of inductance versus the position and thus allows the best position detection following the constraints defined by the specifications.

The speed of the moving part is the derivative of the position but as this signal is noisy, the resulting speed is not exploitable as it is. Because the memory of the microcontroller is limited, an adapted Kalman filter method, simple and appropriate, is developed to allow filtering of the position and speed.

Finally, the study of the speed control is first simulated using Matlab-Simulink in order to test different control strategies in both open and closed loops. They are then verified on the test bench with the industrial contactor and the optimized one.

The results allow the validation of the different levels of the method of design, optimization and sensorless control of a linear actuator.

Keywords: Linear actuator, design for self-sensing, genetic algorithms, optimization, sensorless position detection, Kalman filter, speed control.

Résumé

Les contacteurs électriques sont des relais permettant d'interrompre de forts courants (jusqu'à 2000 A). Ils sont constitués de trois parties principales distinctes : le circuit basse tension, le circuit haute tension et l'actionneur linéaire qui permet de déplacer les contacts. L'objet de cette thèse est de concevoir, d'optimiser et de contrôler sans capteur externe la partie mobile d'un actionneur linéaire.

En effet, il est très important de contrôler la vitesse de fermeture de l'actionneur pour pouvoir minimiser l'usure des contacts. La vitesse ne doit pas être trop rapide afin de ne pas détériorer les contacts en argent à l'impact, ni trop lente pour éviter de multiples arcs électriques qui éroderaient les contacts.

La thèse est divisée en différents thèmes : la détection de position sans capteur, l'optimisation de l'actionneur, le traitement des signaux de position et de vitesse par une adaptation du filtre de Kalman et, finalement, le contrôle sans capteur de la vitesse de la partie mobile de l'actionneur.

Les contraintes industrielles imposent, pour des raisons de coût, une détection de position sans capteur. Pour ce faire, un courant haute fréquence (1250 Hz), dit de mesure, est superposé au courant permettant la conduite de la partie mobile de l'actionneur. Ensuite, le courant total est filtré pour n'obtenir que le courant de mesure. L'amplitude de celui-ci est dépendante de la position car l'inductance de la bobine de l'actionneur varie fortement avec l'entrefer. Il est dès lors possible de détecter la position en utilisant uniquement le circuit basse tension à disposition.

L'optimisation de l'actionneur est faite en combinant les algorithmes génétiques à la modélisation par éléments finis (FEM). Le premier objectif que doit atteindre l'optimiseur est de minimiser le coût matière de l'actionneur. Ensuite, connaissant le prix minimal de l'actionneur, le coût devient une contrainte lors de l'optimisation pour une meilleure détection de la position. La configuration optimale présentée dans la thèse favorise la variation de l'inductance en fonction de la position et permet donc la meilleure détection de position selon les contraintes définies par le cahier des charges.

La vitesse de la partie mobile est la dérivée de la position, mais ce signal étant bruité, la vitesse résultante n'est pas du tout exploitable telle quelle. La mémoire du microcontrôleur étant limitée, une méthode adaptée du filtre de Kalman a été développée pour permettre le filtrage de la position et de la vitesse de manière simple et adéquate.

Pour finir, l'étude du contrôle de la vitesse a tout d'abord été simulée à l'aide de Matlab-Simulink afin de pouvoir tester différentes stratégies de contrôle tant en boucle ouverte qu'en boucle fermée.

Elles ont ensuite pu être vérifiées sur le banc de mesure avec le contacteur industriel, puis le contacteur optimisé.

Les résultats permettent de valider les différents paliers de la méthode de conception, d'optimisation et de contrôle sans capteur d'un actionneur linéaire.

Keywords : Actionneur linéaire, conception pour l'auto-détection, algorithmes génétiques, optimisation, détection de position sans capteur, filtre de Kalman, contrôle de la vitesse.

Contents

List of Figures

List of Tables

1 Introduction

1.1 Introduction

The electrical contactors have existed since the early 20^{th} century. Their duty was, as now, to interrupt and establish current in an electrical circuit.

The power grid becoming denser and the industrial production accelerating, the electrical contactor was increasingly important to the economy of industrialized countries. Gradually, the contactors evolved from manual to automatic and then became increasingly more compact and efficient. Until today, the electrical contactors operate in "all or nothing", which means they are open when not powered and closed when supplied. This power supply is constant and there is no control over the speed of the moving part of the linear actuator, the mover, which is the motor of the contactor, and over the impact when both parts, fixed and mobile, come into contact.

Schneider Electric has contacted the LAI at the end of the year 2007 with the objective to develop a new generation of contactors with a sensorless speed control of the mover.

The overall goal is to have an actuator which is controllable in speed and position along the length of the stoke between two extreme positions (open and contact closed). The objective is to control the actuator speed profile and to get an optimal speed during closing. The impact between the contacts has to be done with a speed sufficiently small to avoid rebounds, and large enough not to generate unnecessary arcs. As it appeared not as crucial as for the closing, the opening is not studied in this thesis. Finally, the actuator speed must be controlled without any position sensors.

1.2 Contactor and linear actuator

In this thesis, we will speak about contactor and linear actuator.

A contactor (Figs. 1.1 and 1.2) is an electrically controlled relay used for switching a power circuit. A contactor is controlled by a circuit which has a much lower power level than the

switched circuit. In the case of the contactor that we study in this thesis, the range of current that the contactor has to switch can reach 2 kA and the circuit that drives the switch operates at a voltage between 24 and 220 V for a current under 5 A.

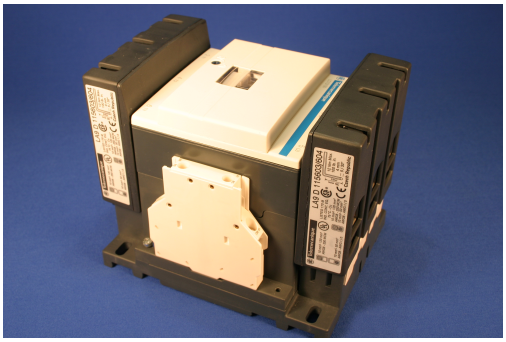

Figure 1.1: Industrial contactor - Telemecanique LC1D150

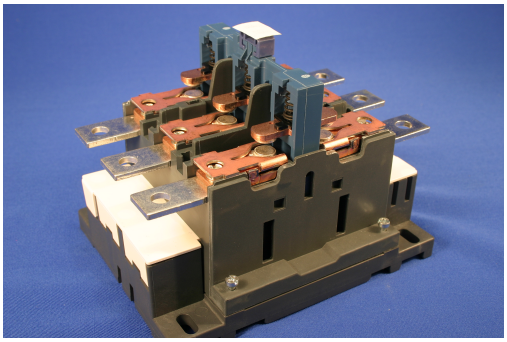

Figure 1.2: Contactor - view of the power contacts

The linear actuator (Fig. 1.1) is the “motor” of the contactor that drives the mover to pass from the open position to the closed one and vice versa. It is the low power part of the contactor and is the one that is studied in the thesis since it is the part that drives the speed of the mover.

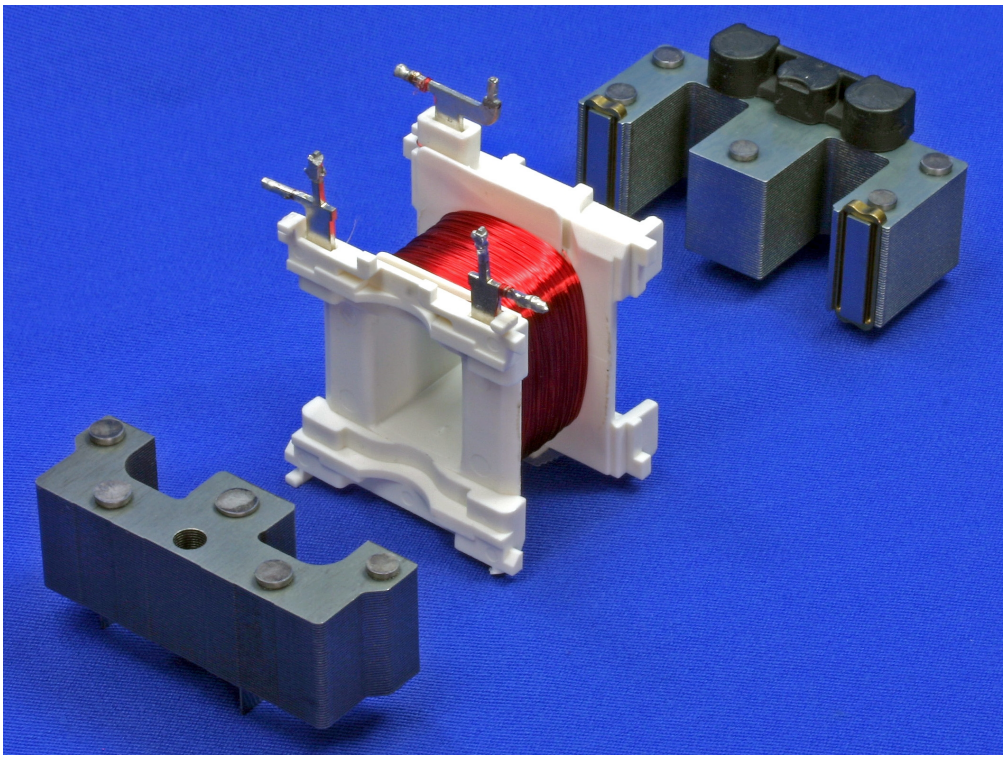

Figure 1.3: Linear actuator inside the contactor LC1D150

1.3 Sensorless versus self-sensing

As the specifications (which will be given in section 2.4.2) require a speed control without any sensor, it is natural to speak about sensorless control. But, as the control is done with the only information given by current and voltage in the winding, the winding itself can be regarded as an internal sensor, we also can speak about self-sensing. In the thesis, even if the term "self-sensing" is sometimes used for the optimization as it is known in literature as "design for self-sensing", the term "sensorless" is preferred and more often used.

1.4 Thesis structure

The thesis shows a complete method to design, optimize and control a linear actuator without any external sensor and it is divided in 4 main chapters:

- Design of the electromechanical actuator for its sensorless speed control.
- Sensorless position estimation for the electromechanical actuator.
- Adapted Kalman filter for filtering noisy position and speed signals.
- Sensorless speed control of the electromechanical actuator.

1.4.1 Design of the electromechanical actuator for its sensorless speed control (Chapter 2)

In this chapter, the main contribution is the static optimization for dynamical transients with the objective to reduce the optimization calculation time. The idea is to take into account the displacement by adding the force due to the acceleration $F_{ma} = m_{mob}w$ to the load F_L and consequently to perform only static optimizations that resolve the following equation at different chosen values of airgap:

$$F_{em,x} = m_{mob}w_x - F_{Lx} \tag{1.1}$$

Where F_{em} is the electromechanical force, m_{mob} the mass of the mover and w its acceleration. The indication x corresponds to the values of airgap.

The final objective is to design a new configuration of actuator, the cheapest possible and designed for self-sensing. In the first part of the chapter 2, in order to explain how to perform optimization for dynamical transient, the mass is minimized and the optimization is performed at different values of airgap. The system has to respect different constraints like speed reference, force, dimension or current density.

Although the method is described using mass optimization, the chapter will end with design

for self-sensing which is the second main contribution and uses inductance as a parameter for the optimization. Design for self-sensing is performed in order not to minimize mass or cost but to optimize position detection by maximizing the difference of inductance for two extreme positions of the mover. We will see in chapter 3 that we use a secondary signal, named scan signal, superimposed to the one that drives the mover in order to detect the position. The amplitude difference of the scan signal is maximized, and consequently, the moverposition is better detected. The basic configuration of the linear actuator is improved and the mass and the cost are not objectives but constraints.

1.4.2 Sensorless position estimation for the electromechanical actuator (Chapter 3)

The first part of this chapter is a state-of-the-art of the different possibilities for sensorless position detection. The chosen method is to superimpose to the main signal a scan signal which gives the position information when filtered.

The demonstration is done on an industrial contactor (Schneider Electric - Telemecanique LC1D150) and position detection is shown by moving manually the mover and comparing it with the position measured with an external sensor.

This chapter describes how to practically perform the position detection using electronic filters and a DSP that calculates the position of the actuator in the real time.

We will end the chapter by validating the method on the prototype designed and described in chapter 2.

1.4.3 Adapted Kalman filter for filtering noisy position and speed signals (Chapter 4)

When the position is detected, the goal is not reached yet. Actually, the measured position is noisy and the resulting speed obtained when the measured position is derived, is unusable. This chapter presents an adaptation of the Kalman filter that allows to filter a signal in real time by comparing it to its reference without needing much memory and computing time.

The adaptation of the Kalman filter is applied to the position and the speed of the prototype's mover in order to have the best filtered signal. The filtered position is derived to obtain the speed which is also filtered using the same method. The filter parameters are determined through Matlab simulations by minimizing the difference between the real speed and the measured one.

1.4.4 Sensorless speed control of the electromechanical actuator (Chapter 5)

In order to study the speed control, a Simulink model of a simple actuator is described. This model allows testing of different control strategies in closed and open loops. The methods of control are skimmed through and allow analyzing the different strategies and choosing the best one for this application.

It is also shown that closed loop control during the closing is difficult to implement because the control perturbs the scan signal. But a really efficient open loop control will be demonstrated with the possibility to adapt the voltage reference to ensure, during the life time of the device, a speed corresponding to the reference.

2 Design of the electromechanical actuator for its sensorless speed control

2.1 Introduction

The scope of this chapter is to propose a method that enables the optimization of a linear electromechanical actuator that takes into account constraints and dynamical transients. The optimization is needed to design an actuator that allows the best sensorless position detection. The method consists in sampling the dynamical transient profile in several different points in which the Newton equation $mw = \Sigma F$ is respected. It means that it is possible to transform a dynamic problem in several static ones with the advantage to reduce significantly the optimization time consumption. The first part of the chapter deals with the algorithms of the optimization and is based on a theoretical actuator where the only objective is to minimize the mass. It allows to introduce concepts like gradient-based and stochastic optimization, genetic algorithm and sampling of transient profile in order to perform only static optimizations.

In the second part of the chapter we will present the position detection optimization. As we will see in chapter 3, the difference of inductance between two positions of interest during the closing of the actuator is the parameter to optimize. We will see how to choose the basic configuration and how to optimize its parameters, which leads to a prototype. The measurements on the prototype that verify if it fulfills the objectives will be done at the end of the thesis, in the chapter 5.

2.2 State of the art

The dynamic of linear actuators has been studied in the literature and it is a challenging problem. Various authors present their solutions using analytical model of actuators.

[19] by doing several assumptions developed a mathematical model of a high-speed solenoid valve that allows fast switching time. The objective is to develop a method for fast switching by examining the parameters such as the dimensions of the actuator and winding or the number of winding turns and their effects on the dynamic of the mover. By doing this, the author conclude

with different statements on the applied voltage, the magnetic materials, the magnetic path length. The method does not result in an optimized solution but gives indications how to improve the existing system.

[4] studies the dynamic of linear actuators and handles the motion of the mover by using FEM and by combining it with boundary element methods. The method is based on an analytical model in which the author couples the electromagnetic, the external circuit and the mechanical models. This advanced model is applied to different electromechanical devices and allows the study of the influence of electrical, magnetic and mechanical parameters. [49] has developed a dynamic simulator which allows the analysis of various dynamic transients of electromagnetic actuators. It replaces the finite element method simulations by a fast calculation model where the electromagnetic circuit and the mechanical system are described by differential equations. These equations are solved by the Runge-Kutta method. In both articles, the configuration is relatively simple and the model is complicated. There is no evidence by optimizing and thus changing the configuration that the models are accurate enough to ensure the dynamic required by the specifications of the present thesis.

[16] combines genetic algorithm with finite element method for the cost minimization of a transformer. First, a novel external elitism strategy of the genetic algorithm associated with variable crossover and mutation rates is introduced in order to improve the algorithm. Then, two different models of transformers are described to finally obtain a global GA-FEM model that finds the global optimum. The author has applied his method on various transformer designs and has compared the results with those of deterministic optimizations. The conclusion is that the GA-FEM converges to global optimum while the deterministic ones tend to get stuck in local optima.

[8] uses deterministic methods with static and dynamic finite element simulations to optimize the torque of a switched reluctance motor. The shape of the motor is firstly experimentally designed. Then, deterministic methods are applied to obtain the optimal solution. The motor is characterized by 2 parameters that are the rotor and stator pole arcs. First, the saturation is not taken into account as the material is considered linear and the lateral flux leakages are neglected in order to obtain the experimental design. Then, saturation and lateral flux leakages are taken into account in the finite element simulations that compute the objective function. The method is adapted to improve an already good configuration that is characterized by a small number of parameters. The final configuration to optimize in our case is characterized by 9 parameters and during the thesis we have worked with configurations characterized by more than 30 parameters. Consequently the method is not applicable in our case.

[17] presented in 2010 the coupling of finite element method (FEM) with the Genetic Algorithm in order to maximize the torque on an angular range from 0° to 100° of a limited-motion actuator dedicated to the air flow regulation of an internal combustion engine. As in a similar paper presented at IEMDC 2009 [30], the author uses Matlab and the free software FEMM to optimize the motor. The method is different than ours because the GA is applied to an analytical model

and after a first optimization a FEMM model is created and used in an optimization based on a gradient-based algorithm in order to find a better solution. It is not very clear why the second optimization with FEMM is necessary, apart from validating the analytical optimization especially since the author speaks about global optimum after the GA optimization. The optimization is completely static; the influence of the dynamic simulations to the design is considered in the conclusion.

We tried to develop an analytical model in order to perform a gradient-based optimization. Indeed the combination gradient-based optimization with FEM is difficult to perform because in order to perform the derivation, simulations have to be done after slightly varying each parameters and this induces numerical noise. [8] could manage the derivation on two parameters but, in our case, because of the high number of parameters, between 9 and 31, it is absolutely not possible, therefore the combination of deterministic optimization and finite element method is not conceivable. As the analytical model was not possible to generate, we decided to combine finite element method with a stochastic algorithm. Genetic algorithm has been well studied in the laboratory during the past years, as it is described in the second part of the section 2.3.6, and we naturally decided to use this algorithm to optimize the linear actuator.

The first scientific contribution that is presented in this chapter is the use of multiple static simulations at chosen values of airgap that allows the optimization taking into account the required dynamic transient. Indeed, the use of 5 static simulations instead of 1 dynamic simulation saves a lot of calculation time.

The second contribution is the addition of penalties on the objective that allows taking into account out-constraints simulations and thus allows better convergence to the optimal configuration. The last contribution is the use of the optimization method to perform “Design for selfsensing”. Indeed, as the objective of the thesis is to describe a method for design, optimization and sensorless control of a linear actuator, the optimization has to improve the position detection of the actuator. The mass and then the material cost that are the main objectives at the beginning of the chapter, become constraints for the final optimization. Experimental results on the prototype of the optimal configuration show that the position is better detected with the new configuration than with the industrial one.

2.3 Introduction to optimization for dynamical transient

2.3.1 Problem definition

The theoretical electromechanical linear actuator that will be studied in the first part of this chapter consists of a copper winding and two ferromagnetic parts. The winding and the U-shaped ferromagnetic part form the stator (fixed part) and the other ferromagnetic part is the mover (Figs. 2.1 and 2.2). The current in the winding generates a flux in the iron which creates a force F_{em} that tends to bring closer the stator and the mover (and to close the actuator). A mechanical load

F_L (which is created by a spring) counters F_{em} and tends to open the actuator. The airgap value x varies between 1 mm (position closed) and 11 mm (position open). J is the current density in the winding.

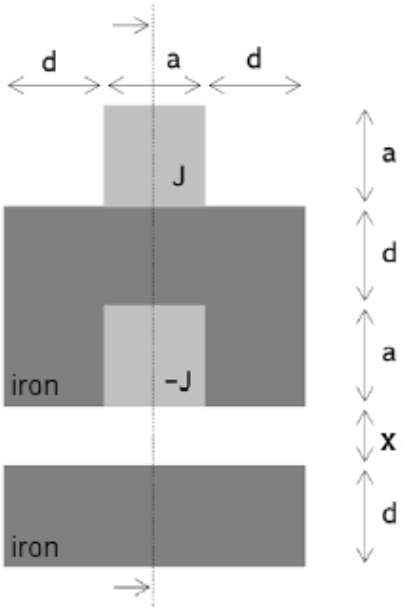

Figure 2.1: Linear actuator - face view

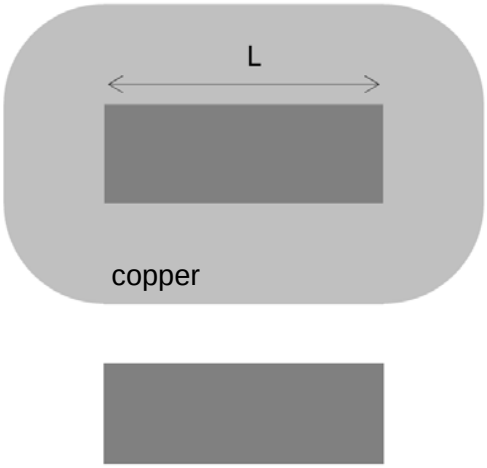

Figure 2.2: Linear actuator - side view

a, d, J and L are the free parameters. The densities of copper and iron are respectively 7700 kg/m^3 and 8900 kg/m^3. The iron is ideal. In order not to saturate the magnetic circuit, the flux density B is limited to 1 T. For modeling and construction reasons, minimal value of parameters a, d and L is 5 mm. For thermal reasons, the maximal current density J_{max} is 15 A/mm^2.

The objective is to minimize the actuator mass. The position profile ($x(t)$ in m) desired during the closing of the actuator (Fig. 2.3) is given by:

$$x = 0.006 + 0.005 \cos \frac{\pi}{T} t \tag{2.1}$$

with $T = 10$ ms. The mechanical load F_L in N in function of x (Fig. 2.4) is given by:

$$F_L = 12 \cdot 10^7 x^3 - 2 \cdot 10^6 x^2 + 2 \cdot 10^3 x + 80 \tag{2.2}$$

Those functions are arbitrarily defined; the goal is just to present the concept.

The mover speed v is given by:

$$v = -\frac{dx}{dt} = \frac{0.005\pi}{T} \cos \frac{\pi}{T} t \tag{2.3}$$

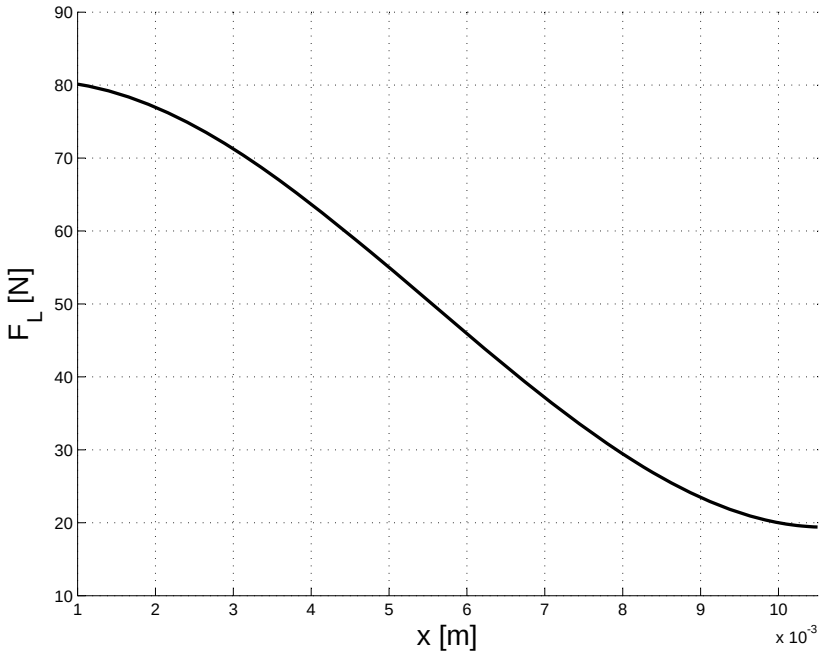

Figure 2.3: Airgap value versus time

and its acceleration w is:

$$w = \frac{dv}{dt} = \frac{0.005\pi^2}{T^2} \sin \frac{\pi}{T} t \tag{2.4}$$

2.3.2 Optimization problem: definition

The optimization problem is mathematically defined as follows. The global optimum of the objective function $f(x_1, x_2, \ldots, x_m)$ is to be determined, respecting:

- The free parameters limits (LU): $x_{1L} \leq x_1 \leq x_{1U} \ldots x_{mL} \leq x_m \leq x_{mU}$
- The equality constraints (CE): $h_k(x_1, x_2, \ldots, x_m) = 0$ with $k = 1, 2, \ldots, n$
- The inequality constraints (CN): $g_l(x_1, x_2, \ldots, x_m) = 0$ with $l = 1, 2, \ldots, o$

The limits LU and constraints CE and CN define a domain D in the space $(x_1, \ldots, x_m)$. The objective is to determine the global optimum of the function f on the domain D. In the case of two variables, the LU define a rectangle, the CE define a line and the CN define a half-plane bounded by a line.

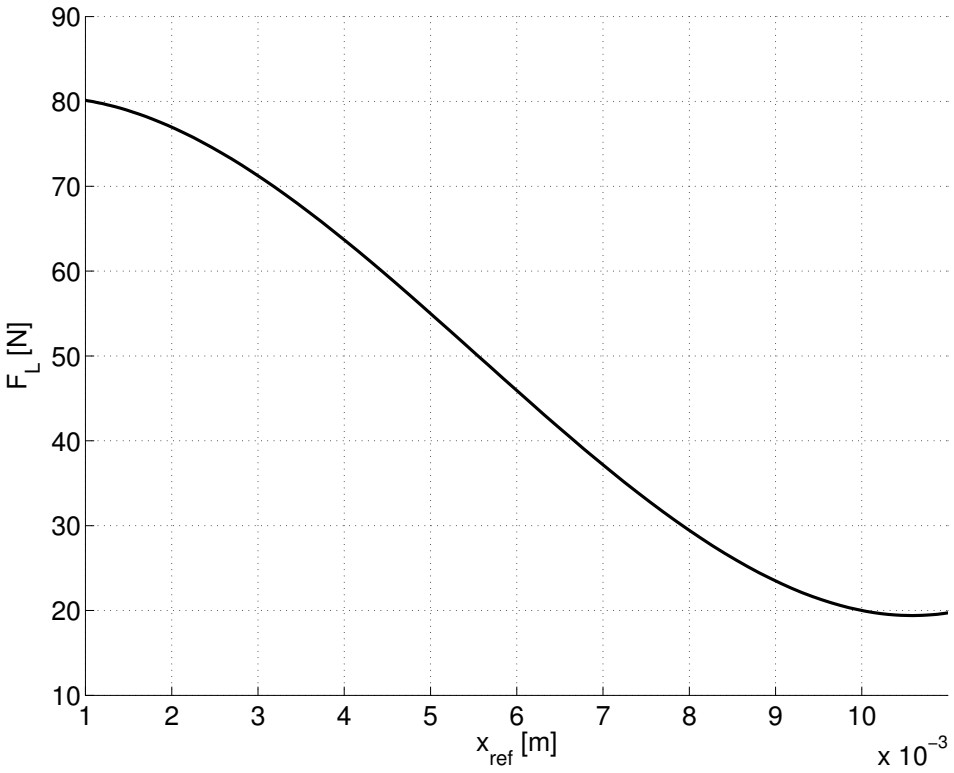

Figure 2.4: Mechanical load versus airgap value

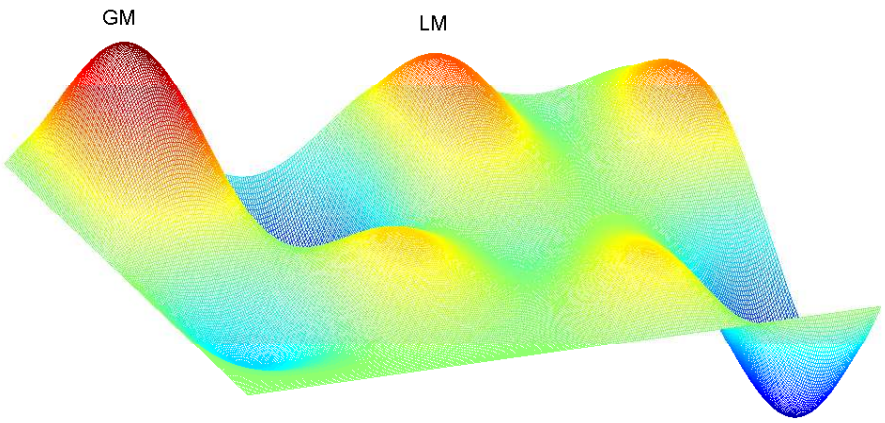

Figure 2.5: A function f of two variables with its global maximum (GM) and local maximum (LM)

The goal is to determine the global maximum GM (the maximal absolute value) of function f on the domain D. Local maxima LM are not important. We can say that a point $(x'_1,\ldots,x'_m)$ is a local maximum if there exists a neighbourhood of this point, which is located in the domain D, in which $f(x'_1,\ldots,x'_m) > f(x_1,\ldots,x_m)$ for all points $(x_1,\ldots,x_m)$.

2.3.3 Simultaneous optimization for different values of air gap

As the optimizer has to take into account the dynamic transient during closing and not only at one unique point, simultaneous optimization has to be done on several sampling points. In this example, the mover trajectory is sampled between 0 and 10 ms with steps of 2 ms. It means that there are 6 different values of airgap for which the actuator has to be optimized: sampled accelerations w_1 to w_6 and the mechanical loads F_{L1} to F_{L6} are presented in Table 2.1.

Table 2.1: Sampled position, acceleration and mechanical load

t[s]	0	0.002	0.004	0.006	0.008	0.010
e[mm]	11	10.05	7.55	4.45	1.95	1
w[m/s^2]	493.5	399.2	152.5	-152.5	-399.2	-493.5
F_L[N]	19.72	19.91	32.78	59.83	77.16	80.12

2.3.4 Optimization methods

There are 2 kinds of optimization algorithms to optimize the actuator, the deterministic and the stochastic optimization. Among the deterministic optimizations, there is the gradient-based method, which is generally the most efficient method because the partial derivations of the function f to optimize are analytically determined and the local maximum where $\bigtriangledown f = 0$ is directly found. Other deterministic optimizations such as the simplex method have not been analyzed.

There are two main problems with the gradient-based optimization. First, the determined maximum is local and not global, and the user will have to vary the initial conditions in order to try to find the global optimum. Second, if the analytical model cannot be generated, the method is difficult to use because all the parameters have to be derived numerically with FEM simulations. These derivations introduce noise and it becomes almost impossible to avoid this noise when dealinqg with a lot of parmeters which is our case (9 free parameters).

The other method is the stochastic one. There exist many stochastic optimization methods but in this thesis the only one that is studied and used is the genetic algorithm (GA) because it is the most convenient and intuitive. The genetic algorithm imitates the natural evolution: from a randomly generated population of individuals, it creates successive generations by cross-overing and mutating the chosen group of the best individuals. The basic GA is changed and improved, as it will be explained in section 2.3.6.

With stochastic optimization, the problem of local versus global optimum does not exist anymore, but the global one may or may not be reached. There are different termination conditions that stop the optimization process. In our case, it stops when a fixed number of generations is reached. This termination condition has the advantage to control the computation time, but generates a

risk that the global optimum is not found. The advantage with GA and stochastic algorithms in general is that it is possible to avoid analytical model by using finite element methods model.

2.3.5 Gradient-based method

Analytical model and constraints

One of the best gradient-based optimization software is ProDesign [10], which performs optimization based on analytical model by automatic and symbolic treatment. The user provides as inputs: the analytical model, the limits LU and constraints CE and CN, and also defines the objective function. To begin the process of optimization, ProDesign also requires the initial values of the free parameters.

The actuator analytical model, with the hypothesis described in section 2.3.1, is defined by the following equations at the 6 different values of airgap ($x = 1, 2, \ldots, 6$):

$$B_x = \frac{\mu_0 \, J_x \, a^2}{2 \, e_x} \tag{2.5}$$

$$F_{em,x} = \frac{B_x^2}{\mu_0} \, d \, L \tag{2.6}$$

$$m_{ir} = 4 \, d_{ir} \, L \, d \, (a + d) \tag{2.7}$$

$$m_{co} = d_{co} \, a^2 \, (2 \, L + 2 \, d + a \, \pi) \tag{2.8}$$

$$m_{mob} = d_{ir} \, L \, d \, (a + 2 \, d) \tag{2.9}$$

where:

- B: the magnetic flux density [T]
- F_{em}: the electromechanical force [N]
- J: the current density [A/m^2]
- m_{ir}, m_{co}: the mass of iron, copper parts [kg]
- d_{ir}, d_{co}: the density of iron, copper [kg/m^3]

The parameter limits (LU) are:

$$5 \cdot 10^3 < a < 30 \cdot 10^3 \tag{2.10}$$
$$5 \cdot 10^3 < d < 30 \cdot 10^3 \tag{2.11}$$
$$1 \cdot 10^6 < J < 15 \cdot 10^6 \tag{2.12}$$
$$5 \cdot 10^3 < L < 30 \cdot 10^3 \tag{2.13}$$

The inequality constraint (CN) is:

$$B_x < 1\,\mathrm{T} \tag{2.14}$$

and the equality constraint (CE) is:

$$F_{emx} = m_{mob} w_x + F_{Lx} \tag{2.15}$$

The initial values for the input parameters are arbitrarily chosen as:

$$a = 25 \cdot 10^{-3}\ \mathrm{m} \tag{2.16}$$
$$d = 20 \cdot 10^{-3}\ \mathrm{m} \tag{2.17}$$
$$L = 20 \cdot 10^{-3}\ \mathrm{m} \tag{2.18}$$
$$J_x = J_{max} = 15 \cdot 10^6\ \mathrm{A/m^2} \tag{2.19}$$

The objective function is the actuator mass m which has to be minimized:

$$m = m_{ir} + m_{co} \tag{2.20}$$

Results

Table 2.2 shows the parameters of the optimal actuator configuration. It is possible to see that the first value of airgap (x = 11 mm) is the critical one because it is the one where the maximal density constrain J_{max} is reached. The minimal mass is 1.01 kg.

Table 2.2: Optimal actuator configuration

a [mm]	d [mm]	L [mm]	J_1 [A/mm^2]	J_2	J_3	J_4	J_5	J_6	m [kg]
27.33	6.91	16.82	15	13.1	10.36	7.26	3.42	1.74	1.01

2.3.6 Stochastic method

Introduction to genetic algorithm

Among many stochastic optimization methods, it is the optimization with genetic algorithm (GA) which is the most convenient and intuitive. Optimization with GA is based on the principles of natural selection (biological evolution from one generation to another according to certain rules inspired by natural evolution).

Genetic algorithms (GA) start with a randomly created generation of individuals and evaluates the fitness of each of them. After various tests, we have decided to work with 10 different individuals per generation and this allowed us to converge quickly to the optimal solution. In our case an individual is defined by the evolutionary parameters of the actuator (a, d, L and J) and corresponds to an actuator design. The fitness is the objective function, in this case the actuator mass, weighted with penalties due to the constraints. ProDesign knows how to automatically treat the constraints. In the case of GA, we should treat them in an artificial way, by penalizing the configurations that does not fit the specifications in term of forces or flux densities.

The GA generates children by using crossover and mutation on a group of the best individuals. These children, accompanied by the best parents, form the next generation. Over successive generations, the population converges to an optimal solution. There are two major problems: premature convergence, when the algorithm converges quickly to a local optimum without sweeping the entire domain, and the slow convergence when the algorithm needs too many generations to find the global optimum.

In order to illustrate GA, we take the same example but we only focus on one value of airgap $x = 6$ mm. Consequently, the only objective is to minimize mass of the actuator and the optimal actuator must have enough force F_{em} to counter an external load of $F_L = 40$ N at the value of airgap of $x = 6$ mm. In this small example, the flux density is set to its limit and consequently $J = J_{max}$. Finally, we will work with only 4 individuals per generation.

First, 4 individuals are randomly generated and Table 2.3 shows them:

Their force at $x = 6$ mm is calculated using the analytical model and they are penalized if the force F_{em} is inferior to $F_L = 40$ N. We will see exactly how to calculate these penalties in the optimization procedure section. The fitness, that is the mass, is also evaluated and finally the objective function O is the product of the fitness and the penalties. Then, we classify the

Table 2.3: Random 1^{st} generation

	a [mm]	d [mm]	L [mm]
individual 1	10.00	15.00	20.00
individual 2	15.00	25.00	30.00
individual 3	25.00	35.00	10.00
individual 4	30.00	10.00	15.00

individuals in function of O. Table 2.4 shows the individuals evaluated and classified.

Table 2.4: Evaluation and classification of the individuals

	a [mm]	d [mm]	L [mm]	m [kg]	F_{em} [N]	P_F [-]	O [-]
individual 2	15.00	25.00	30.00	1.24	74.55	1	1.24
individual 4	30.00	10.00	15.00	1.34	238.56	1	1.34
individual 3	25.00	35.00	10.00	1.58	268.44	1	1.58
individual 1	10.00	15.00	20.00	0.32	5.89	728.17	233.96

Each individual has a probability relative to its fitness to become parents of the next generation. In this example, we keep the two best (2 and 4). It is time for crossover and mutation operation for the creation of the next generation.

The first child will take 75% of individual 2 (because it is the best one) and 25% of individual 4. Each parameter that constitutes the individual is called “gene". For example, the gene a of child 1 is:

$$a_{ch1} = 0.75 \cdot a_{ind2} + 0.25 \cdot a_{ind4} = 0.75 \cdot 15 + 0.25 \cdot 30 \tag{2.21}$$

$$= 11.25 + 7.5 = 18.75 \tag{2.22}$$

The second child will take 50% of each individual. Table 2.5 shows the population after the crossover. We keep the parents in the population.

Then, we choose a probability of mutation of each gene of each individual, with the exception of the best one from the last generation (individual 2). This probability has to be relatively low and if it occurs, mutation must have high probability to be very small. As an example, a relatively small mutation occurs on the gene “L” of child 1 (26 becomes 25.5) and a quite big mutation on gene “a” of individual 4 (30 becomes 18). Table 2.6 shows the new generation which will be

Table 2.5: Best parents and children after crossover

	a [mm]	d [mm]	L [mm]
individual 2	15.00	25.00	30.00
individual 4	30.00	10.00	15.00
child 1	18.75	21.25	26.00
child 2	22.50	17.50	22.50

evaluated again and will pass through the same process (Fig. 2.6, in red the mutations):

Table 2.6: New generation after mutation and crossover

	a [mm]	d [mm]	L [mm]	m [kg]	F_{em} [N]	P_F [-]	O [-]
individual 2	15.00	25.00	30.00	1.24	74.55	1	1.24
individual 4'	18.00	10.00	15.00	0.44	30.92	52.56	22.96
child 1'	18.75	21.25	25.50	1.14	131.50	1	1.14
child 2	22.5	17.50	22.50	1.16	198.14	1	1.16

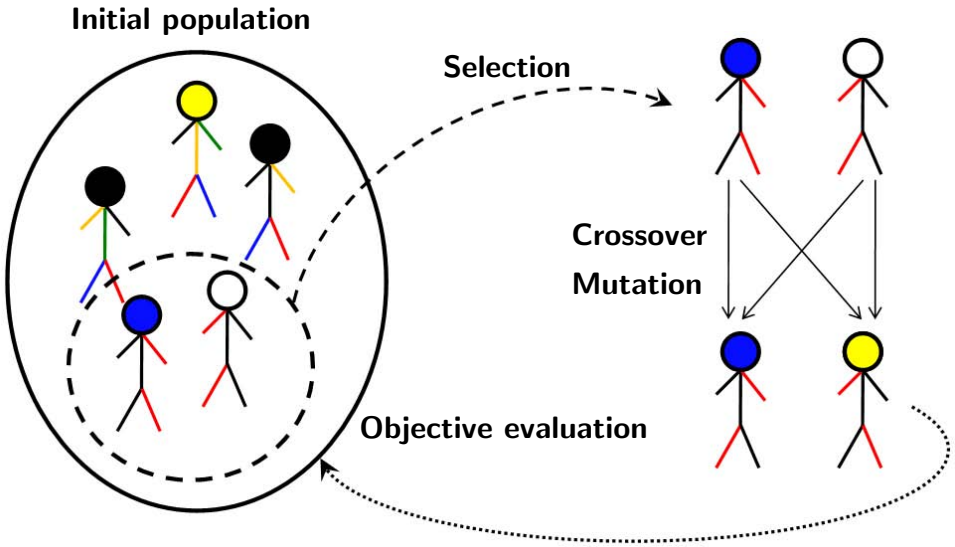

Figure 2.6: Genetic algorithm

Modification of the genetic algorithm

First, the Matlab function "ga.m" [54] was used, but the probabilities of mutation and crossover were difficult to choose and convergence was not acceptable. [40] and [6] have studied different methods to improve this algorithm and proposed two of them.

The first method uses "conditional genetic operators" [51], and avoids probabilistic parameters for operators of mutation and crossover. This method uses, instead of the operators conditioned by an objective, measurement of the population diversity.

The second method is based on [18] and [1], and concerns the crossover operator. It does not use two parents to produce a child but three. According to [18], this improvement allows a faster convergence without premature convergence problems. This method also relies on [34] and [47].

The combination of both methods, which is made in [40] and [6], allows good convergence without problems in determining the probabilities of mutation and crossover.

Optimization procedure

During the optimization, free parameters are limited by LUs. The constraints are taken into account as penalties of the fitness function f. In order to facilitate the optimization, the Newton equation $m_{mob}w_x = F_{em,x} - F_{Lx}$ is replaced by the inequality constraint $F_{em,x} > m_{mob}w_x + F_{Lx}$. Consequently, the penalties are set as:

$$P_F = \begin{cases} (1 + |\frac{F_{em}-F_L}{F_{em}}|)^2, & \text{if } F_{em} < F_L \\ 1, & \text{if } F_{em} > F_L \end{cases} \tag{2.23}$$

$$P_B = \begin{cases} (1 + |\frac{B-1}{B}|)^2, & \text{if } B > 1 \\ 1, & \text{if } B < 1 \end{cases} \tag{2.24}$$

where P_F and P_B are penalties due to force and flux constraints, F_{em} and B are force and flux density calculated, in this case, with the analytical model. If it is not available, it is possible to use finite element methods to calculate the forces and the flux as it will be shown in section 2.4.3.

For each value of airgap, there exists one force penalty P_F and one flux penalty P_B. As the objective function O is the fitness value f weighted by the constraint penalties, the fitness value f which is the mass m is multiplied by 12 penalties (P_{F1} to P_{F6} and P_{B1} to P_{B6}):

$$O = m \prod_{m=1}^{6} P_{Fm} \prod_{n=1}^{6} P_{Bn} \tag{2.25}$$

Results

The GA was started 3 times and Table 2.7 shows the results for these 3 different optimizations. Fig. 2.7 shows the evolution of parameters a, d and L during the optimization. These table and

figure show that the global optimum is not reached because none of the optimizations reaches the same point but rather a "zone" (red circle in Fig. 2.7) where the optimum parameters may be quite different ($L = 12.04$ in opt. 1 versus $L = 18.99$ in opt. 2), but the objectives (mass) are very close (~ 1 kg).

Table 2.7: Optimal configuration of the actuator for 3 optimizations

	a [mm]	d [mm]	L [mm]	m [kg]
opt. 1	28.11	8.12	12.04	1.01
opt. 2	26.66	7.09	18.99	1.00
opt. 3	27.29	6.89	16.50	1.00

Fig. 2.8 shows more schematically how the parameters a and d evolve during opt. 2. The red configuration is the optimal one for this optimization.

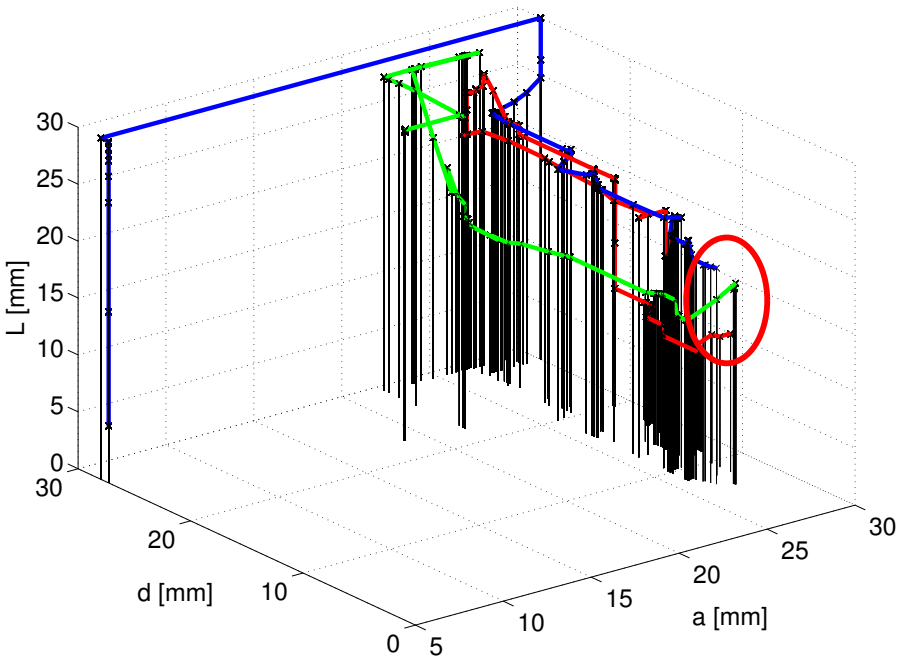

Figure 2.7: Evolution of the parameters during 3 different optimizations

2.3.7 Material cost optimization

In the precedent sections, in order to illustrate the optimization methods, the objective was to minimize the mass. But, actually, the mass is not an issue for our industrial partner but the cost of the actuator is far more interesting. As the fabrications cost are difficult to set, the study is only done on the cost of the material.

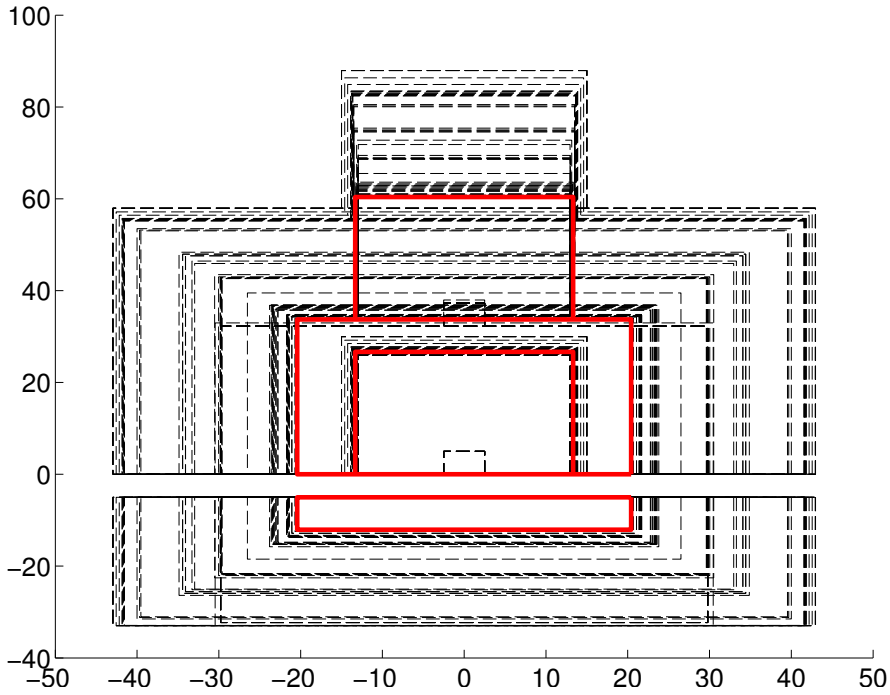

Figure 2.8: Evolution of the configuration during the optimization 2

Material cost optimization is exactly done as the mass optimization but the masses are multiplied by 1.43 €/kg for the iron and 5 €/kg for the copper (These amounts were given by our industrial partner in 2008).

$$c_{ir} = 1.43 \cdot m_{ir} \tag{2.26}$$

$$c_{co} = 5 \cdot m_{co} \tag{2.27}$$

$$c_{tot} = c_{ir} + c_{co} \tag{2.28}$$

And the objective function is now:

$$O = c_{tot} \prod_{m=1}^{6} P_{Fm} \prod_{n=1}^{6} P_{Bn} \tag{2.29}$$

Table 2.8 shows the parameters of the optimal actuator configuration. The minimal cost is 4.47 €.

For comparison, the material cost of the optimized actuator presented in Table 2.2 and the optim. 1 of Table 2.7 were respectively 4.61 and 4.68 €. This optimized actuator is 14 and 19 cents cheaper with a mass that is not significantly different (1.02 kg instead of 1.01 kg).

Table 2.8: Optimal actuator configuration for material cost optimization

a	d	L	J_1	J_2	J_3	J_4	J_5	J_6	m	c_{tot}
[mm]	[mm]	[mm]	[A/mm^2]	“	“	“	“	“	[kg]	[€]
26.30	8.61	18.61	15.00	14.71	14.97	8.73	3.48	1.64	1.02	4.47

In cases of mass optimization or material cost optimization, we do not take into account the position detection. In the next section, we will present the method of position detection based on the measurement of the amplitude of a scan signal.

2.4 Design for self-sensing

2.4.1 Introduction to the method

The final objective of the thesis is to perform sensorless speed control. Consequently, the actuator has to be designed in order to allow the best position detection.

In this section we continue the analysis with the example introduced in 2.3.1 and the industrial specifications will be described in subsection (2.4.2).

We will see in chapter 3 that the chosen method for position detection is based on the measurement of the amplitude of a scan signal that is superimposed to the main one. The amplitude of this signal is directly related to the inductance of the winding. If the inductance is more different from one position to another, then the position is easier to detect.

It means that the optimization has to be performed in order to maximize ΔL between 2 extreme values of the airgap. We will see later that the part of the trajectory where the speed has to be controlled is between the open position (x_{ref1} = 11 mm in our case) and the contact, which corresponds, in our example, to the fourth gap value (x_{ref4} = 4.45 mm).

The winding wire has a diameter arbitrarily set to d_w = 0.45 mm and the filling factor k_f is 60%. It means that the number of turns N is:

$$N = round(k_f \frac{a^2}{\pi(d_w/2)^2}) \tag{2.30}$$

and the inductance at the position x is:

$$L_x = N^2 \mu_0 \frac{2dL}{x_{refx}} \tag{2.31}$$

The difference of inductance ΔL to maximize is:

$$\Delta L = L_4 - L_1 \tag{2.32}$$

The mass and the material cost are no more objective functions. The material cost is taken into account as a constraint. Section 2.3.7 shows that the minimal cost c_{min} of the required actuator is 4.47 €. The material cost c_{tot} is constrained according to:

$$c_{tot} < 1.1 \cdot c_{min} = 4.92 \text{ €} \tag{2.33}$$

The idea is to keep the material cost no more than 10% higher than the minimal one (obtained as the result of material cost minimization) and to allow the optimizer to find a new configuration that maximizes ΔL. Fig. 2.9 shows the comparison between ΔL for material cost optimization and for ΔL optimization. The differences of inductance between the position open (x_{ref1} = 11 mm) and the contact (x_{ref4} = 4.45 mm) is ΔL = 302 mH when the mass is minimized, ΔL = 367 mH when the material cost is minimized and ΔL = 549 mH when ΔL is maximized and cost constrained.

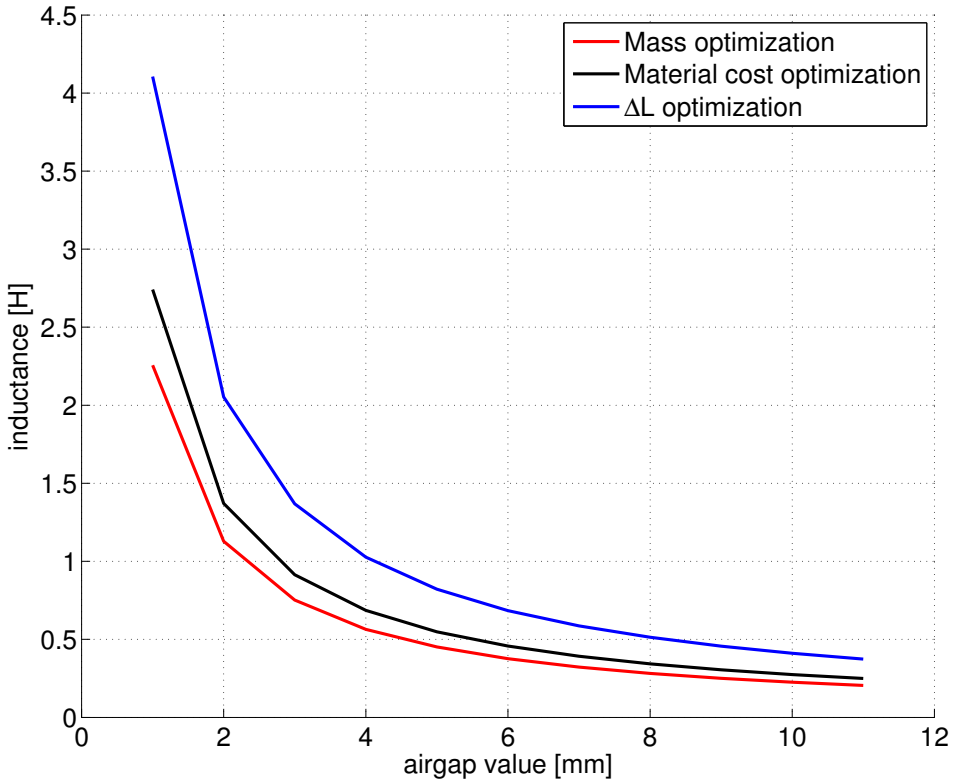

Figure 2.9: Comparison between ΔL for different optimizations

Table 2.9 shows the results for ΔL optimization and its comparison with the third configuration of mass minimization and the one when the material cost is minimized.

Table 2.9: Optimal configuration of the actuator

	a [mm]	d [mm]	L [mm]	m [kg]	c_{tot} [€]	ΔL [mH]
mass optim. 3	27.29	6.89	16.50	1.00	4.57	302
mat. cost	26.30	8.61	18.61	1.02	4.47	367
ΔL optim.	26.13	11.22	21.94	1.19	4.92	549

Table 2.9 shows that, by minimizing the cost, the actuator is 0.1 €cheaper than the one where the mass was minimized without increasing significantly the mass (1.02 kg instead of 1 kg). As it is also illustrated in Fig. 2.9, ΔL is 50 % and 80 % higher, when it is maximized, than for respectively the cost optimized and the mass minimized actuators, with a cost that is higher but within the constraint (10 %) and a mass 20 % heavier.

The example described in section 2.3.1 allowed us to study the different optimization in order to finally design the actuator with the best position detection. It is now time to apply the method to the real specifications given by our industrial partner.

2.4.2 Industrial actuator specifications

In the previous sections, we have presented a method to optimize an actuator configuration by taking into account its dynamical behavior during closing. It described a stochastic method of optimization (genetic algorithm), which is suitable when the analytical model is difficult to obtain (as for the configuration that we will present in this section). The optimized configuration was intended to allow position detection in order to perform the speed control.

The theoretical actuator was used only to show the concepts. At this stage, we show the configuration and specifications of the actuator to optimize, obtained from the industrial partner.

Fig. 2.10 shows the actuator with its stator and mover, and two springs. They have different force constants (K_1 and K_2). The contactor is open at the value of airgap x=10.5 mm and closed at x = 0.2 mm. At x = 4.9 mm, it is the intermediate position where the moving part touches the electrical contacts (Fig. 2.11).

The spring K_1 is much stronger than the spring K_2 and has two main purposes. First it absorbs the shock at the impact between the contacts at the closing and pushes the mover at the opening. The second spring serves to maintain the actuator open. It has to be weaker than the available force at the highest value of airgap to allow the closing. Consequently the mover, from the position "open" to the position "contact", only pushes the spring K_2. Then the contact is operated and the mover pushes the both springs

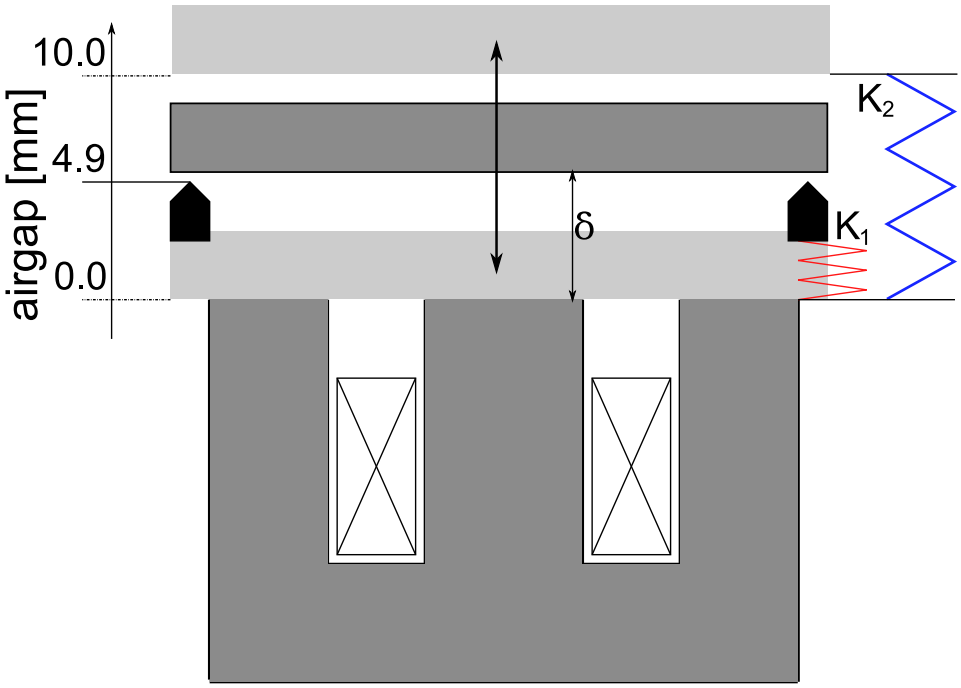

Figure 2.10: Mechanical scheme of the actuator

Table 2.10 shows the value of the force F_L due to the the springs.

Table 2.10: Load force due to the springs

x [mm]	0.0	0.2	4.9	5.0	10.5
F_L [N]	91.33	90.36	67.56	14.64	13.54

Our experience shows that at opening, the speed of the moving part is not an issue because the springs are strong enough to cause sufficient takeoff speed and thus to avoid unnecessary electrical arcs.

At closing, the speed is much more important because it is necessary to have the impact (position where the contacts touch each other) with an optimal speed of 0.4 m/s, fast enough to avoid unnecessary electrical arcs but not too fast in order to preserve the contacts at the impact and to avoid the rebounds. After impact, the speed is not an issue anymore. It means that we are mainly interested in the values of airgap between the open position and the contact one ($4.9 < x < 10.5$, Fig. 3.12).

Figs. 2.12 and 2.13 present the speed v_{ref} and acceleration w_{ref} references during the closing in function of the air gap x imposed by the industrial partner (zone of interest in grey).

In order to choose the configuration to optimize, we have studied different structures and two of

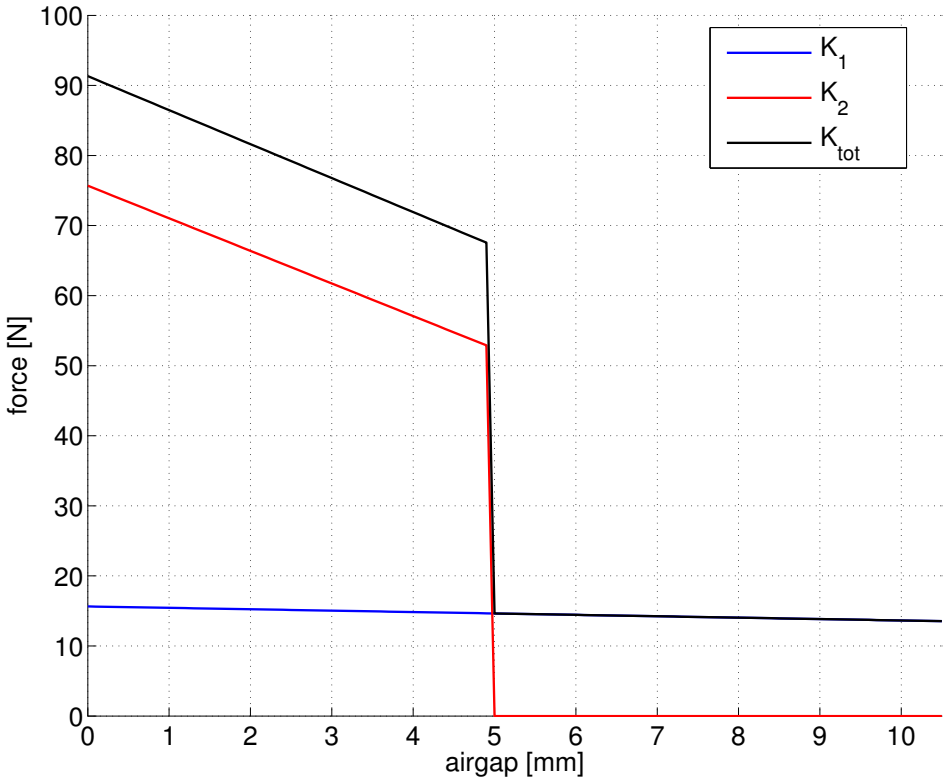

Figure 2.11: Springs resistance force versus the air gap

them were interesting while minimizing the material cost. Two prototypes have been built [30] and are presented in the appendix A. But, as the cost is not the real objective of the optimization, it is now decided to change the structure in order to have the best position detection and thus the maximum ΔL between positions $x = 10.5$ mm and $x = 4.9$ mm.

With a normal E-shaped reluctant configuration, the inductance has significant variations only for small values of the air gap, which is not interesting in our case. Consequently, to allow the optimizer to find the configuration which has important ΔL for higher values of air gap, we have modified the basic reluctant configuration in order to give the possibility to the mover to "enter" in the stator (Fig. 2.14). In addition, by introducing non-right angles, the idea is to allow the optimizer to have more degrees of freedom (more free parameters).

Geometry

The actuator has to be in a volume with the following maximal values:

- Maximum length, $le_{max} = 64.2$ mm
- Maximum width, $wi_{max} = 45$ mm

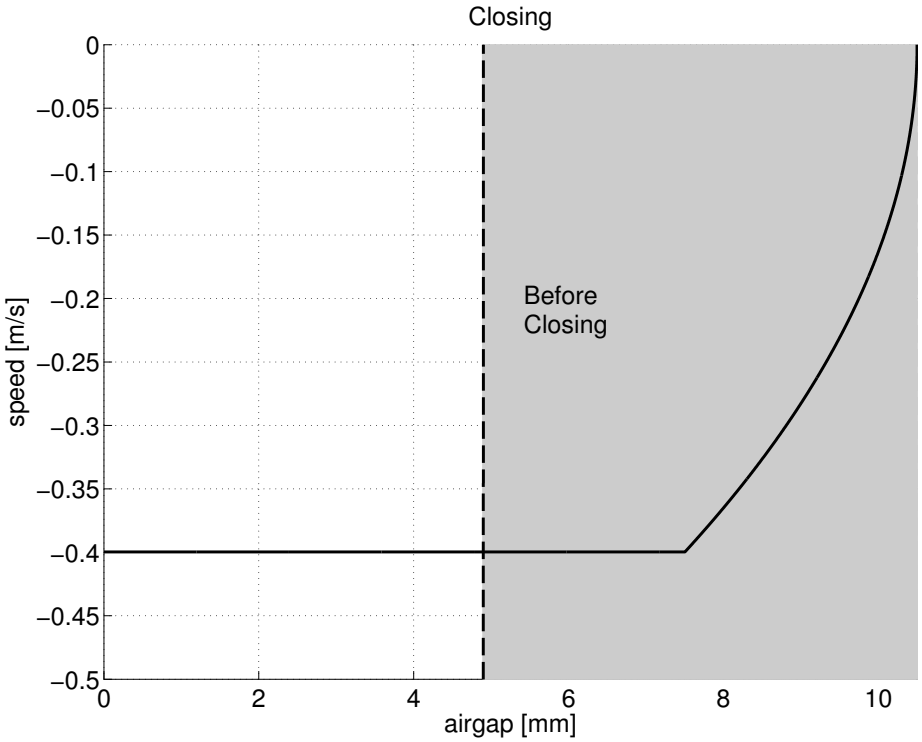

Figure 2.12: Speed reference versus the air gap

- Maximum height (actuator closed), he_{max} = 50.2 mm

These values have been given by the industrial partner and correspond to an existing contactor.

The free parameters limits (LU) are chosen as:

$$
\begin{array}{lcccl}
5\text{ mm} & < & a & < & 30\text{ mm} \\
5\text{ mm} & < & b & < & 30\text{ mm} \\
5\text{ mm} & < & c & < & 40\text{ mm} \\
7\text{ mm} & < & d & < & 30\text{ mm} \\
0\text{ mm} & < & hb & < & 20\text{ mm} \\
5\text{ mm} & < & L & < & 40\text{ mm} \\
0.5\text{ mm} & < & ds & < & 4\text{ mm} \\
0\text{ mm} & < & dda & < & 10\text{ mm} \\
0\text{ mm} & < & ddb & < & 10\text{ mm}
\end{array}
$$

k and ls are not free and are respectively set to 5 and 0.2 mm.

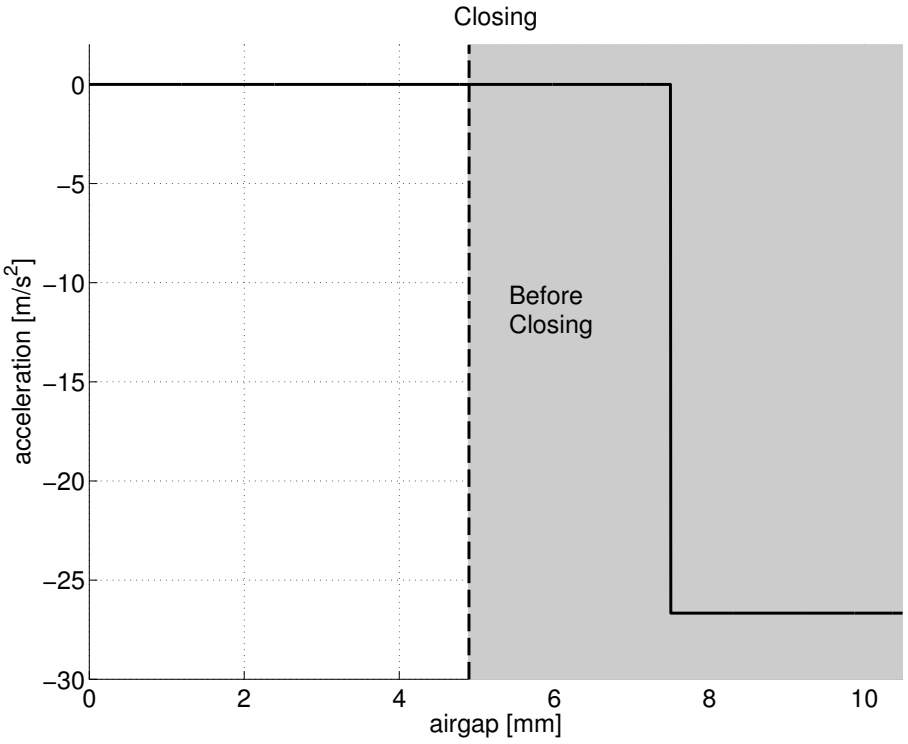

Figure 2.13: Acceleration reference versus the air gap

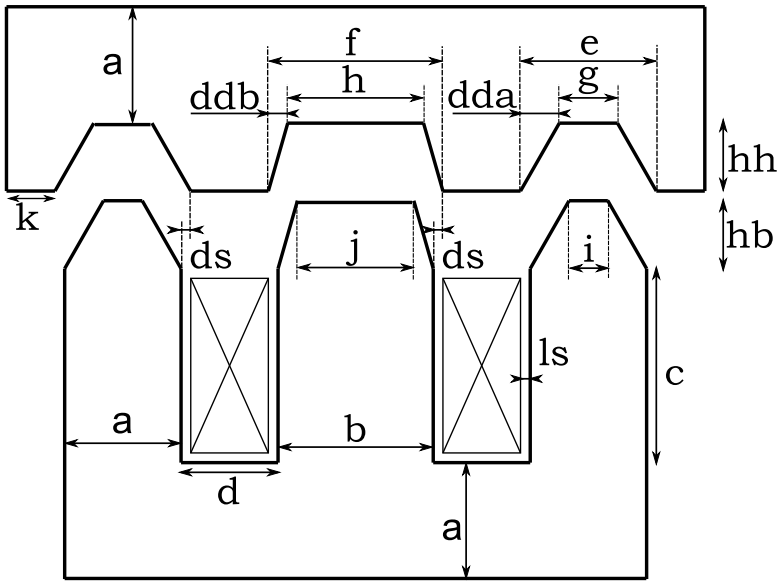

Figure 2.14: New configuration to optimize. The axial depth is L

Density of current and saturation

Experience shows that we can inject maximal current density constraint of $J_{max} = 40$ A/mm^2 (instead of $J_{max} = 30$ A/mm^2 in [27]).

We do not constrain the flux density B_{max} to 1 T anymore, but we use the real H-B curve of the Fe-Si given by our industrial partner (Fig. 2.15).

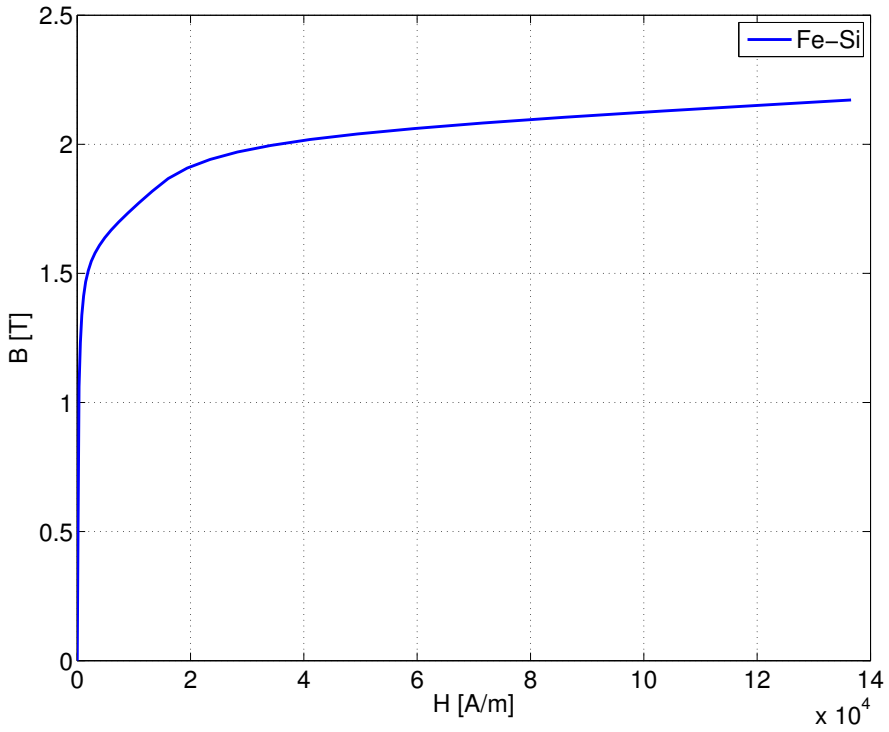

Figure 2.15: H-B curve of Fe-Si

It means that there does not exist any penalty on the flux density P_B and now the objective value is calculated as:

$$O = \Delta L \prod_{m=1}^{5} P_{Fm} \tag{2.34}$$

Consequently, the current densities J_x which were free parameters that have the objective to limit the saturation are now set to $J_{max} = 40$ A/mm^2. The idea is that if the actuator is able to close with this current, the user will be able to reduce it in order to perform the desired dynamics while respecting the specifications.

2.4.3 Finite element methods

In this case, the analytical model of the specified configuration is not easily feasible. Consequently, we have to use Finite Element Methods (FEM) in order to calculate forces and flux densities of the different configurations during the optimizations.

It is possible to combine a FEM model and a genetic algorithm (GA) in order to perform actuator optimization. We use the software FEMM [32] as it is very fast and communicates well with Matlab, where the GA is implemented. The code to build FEMM simulation is directly written in Matlab and with a Pentium 4 and a RAM memory of 3.4 GHz and 2 Go, a simulation for one value of the airgap lasts for 2.5 second in average.

In terms of simulations, we have 10 individuals that we simulate at 5 values of airgap of interest, that are:

- x = 0.2 mm (to be sure that the actuator closes properly)
- x = 4.9 and 5 mm (the two values of airgap that are important for the transition of springs, Fig. 2.11)
- x = 7.5 mm (to ensure the acceleration of the mover, Fig. 2.13)
- x = 10.5 mm (which is the open position)

It means that for each individual, the system performs 5 simulations and consequently there are 50 simulations for the first randomly built generation. Then, the algorithm only changes 2 individuals per generation (8 are kept unchanged for the next generation) and it converges usually after 2500 generations. So the algorithm performs:

$$5(10 + 2 \cdot 2499) = 25040 \quad \text{simulations} \tag{2.35}$$

It means that a complete optimization lasts for about 18 hours.

We understand now why it is important to work with static simulations which are faster to simulate than dynamical ones. First, it is not possible to use FEMM for dynamical simulations and we would have to use Flux, Ansys or other FEM software that are heavier and communicate less effectively with Matlab. For example, a static simulation on Flux does not take 2.5 seconds but around 10. And if we wanted to use dynamical ones, it is evident that we would not make 5 simulations per individual but one simulation would last for more than 1 hour. It means that we would multiply by more than 130 times the simulation time.

2.4.4 Design optimization

We first optimize the cost of the configuration and obtain a minimal material cost of C_{min} = 0.65 €. Then, during the optimization process of maximizing ΔL, the cost C is constrained according

to:

$$C < 1.1 \cdot C_{min} = 0.72 \text{ €} \tag{2.36}$$

Fig. 2.16 shows the evolution of the configuration during the optimization. The optimal solution uses the all the available space. The majority of the solutions are penalized either because of the dimensions, either because of the insufficient electromagnetic force.

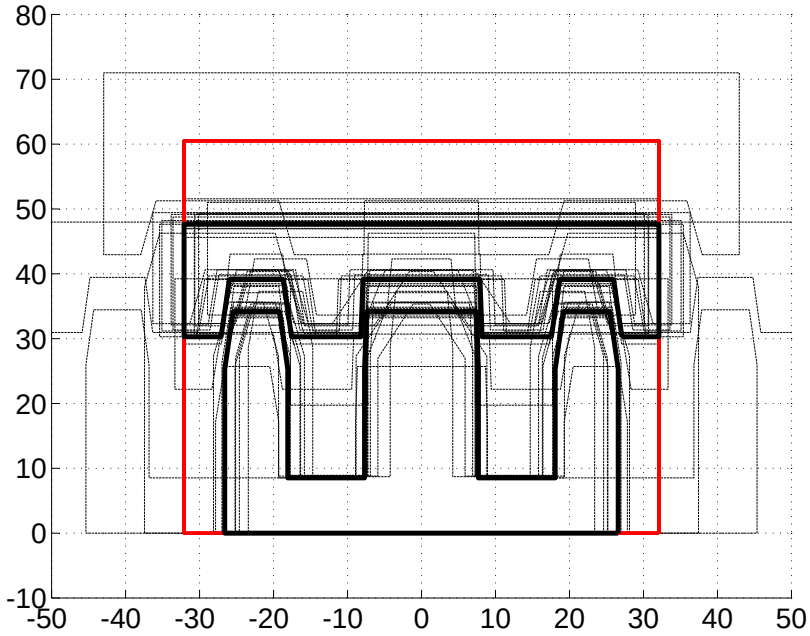

Figure 2.16: Evolution of the configuration during the optimization

After optimization, Table 2.11 shows the optimal configuration.

Fig. 2.17 shows the comparison between the winding inductance, simulated with the FEM software Flux 2D, for 4 different cases:

1. Industrial contactor (Telemecanique LC1D150).
2. Optimized configuration when the cost C is minimized without taking ΔL into account.
3. Optimized configuration when ΔL is maximized without taking the cost into account.
4. Optimized configuration when ΔL is maximized and the cost constraint is $1.1 \cdot C_{min}$ (Fig. 2.18).

Table 2.11: The optimal configuration

a	8.40 mm	b	14.90 mm
c	17.70 mm	d	9.50 mm
hb	9.50 mm	L	22.00 mm
ds	0.50 mm	dda	6.30 mm
ddb	0.30 mm	k	5.00 mm
ls	2.00 mm	$e = a + 2 \cdot ds$	9.40 mm
$f = b + 2 \cdot ds$	15.90 mm	$g = e - dda$	3.10 mm
$h = f - ddb$	15.60 mm	$i = g - 2 \cdot ds$	2.10 mm
$j = h - 2 \cdot ds$	14.60 mm	$hh = hb$	9.50 mm
V_{iron}	45.38 cm^3	V_{copper}	4.84 cm^3
M_{iron}	354.0 g	M_{copper}	43.1 g
M_{tot}		527.1 g	
C_{iron}	0.50 €	C_{copper}	0.22 €
C		0.72 €	

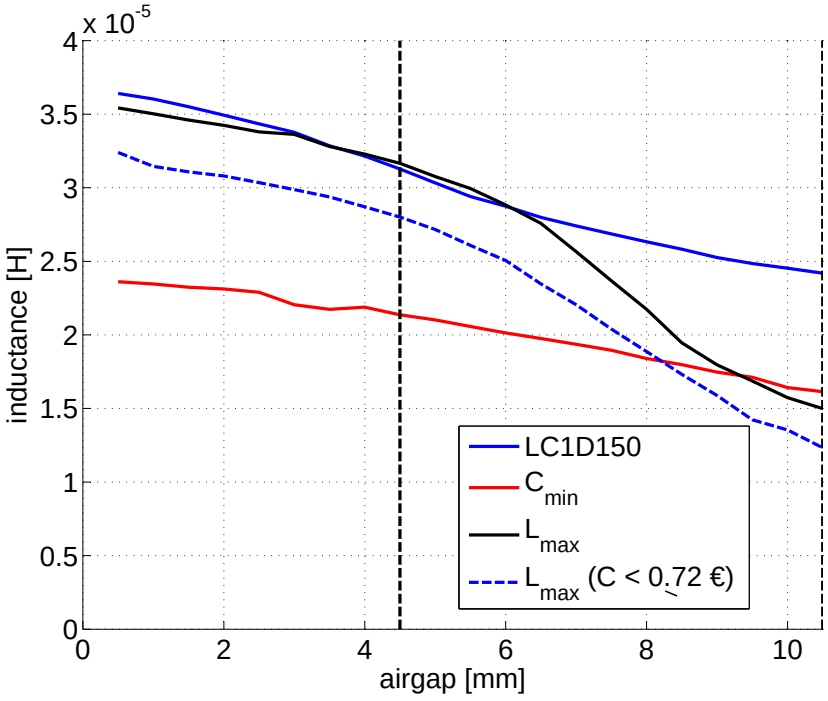

Figure 2.17: Winding inductance for four actuators

When ΔL is not taken into account, it remains relatively small: $\Delta L = 530$ μH for 1) and 700 μH for 2). Respectively, on the other side, configurations with ΔL optimization allow values of 1670 μH for 3) and 1570 μH for 4).

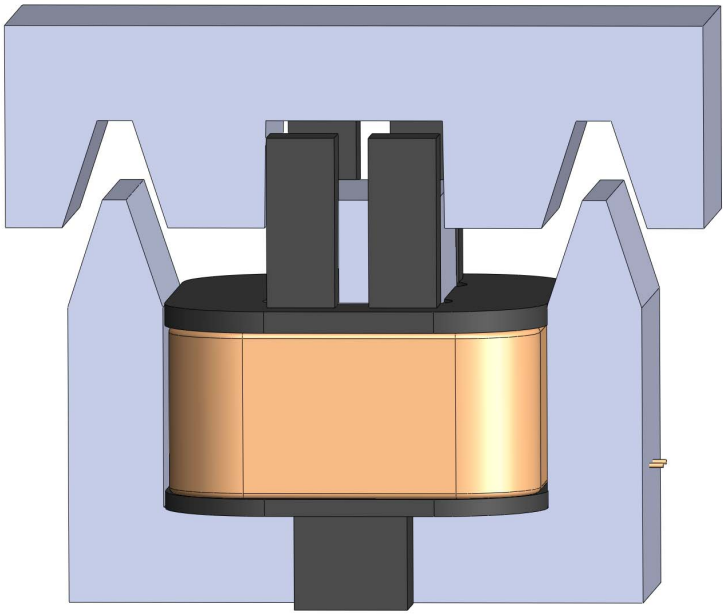

Figure 2.18: Solidwork model of the prototype

As expected, by optimizing ΔL, it is 2 to 3 times higher than for the industrial contactor or the cost optimized configuration. And, by constraining the cost to 10% higher than the one of the configuration with minimal cost, we only reduce ΔL of $\frac{1670-1570}{1670} = 6\%$ in comparison with the configuration with the best ΔL and the price is 10% higher than the cheapest actuator.

Fig. 2.19 shows the different optimizations (minimal cost, maximal ΔL and maximal ΔL with cost constraint). By optimizing the actuator with different constraints of cost (+ 2 %, + 4 %, + 6 %, ...) we could build the pareto curve but we already see that the 3 performed optimization are part of this curve.

2.4.5 Prototyping and inductance measurement

The configuration presented in the above section is built in EPFL's workshops and is shown in Fig. 2.20. The winding impedance versus the frequency is measured with the impedance analyzer Agilent and a comparison between the industrial contactor and this new prototype is presented in Fig. 2.21.

The scan signal, which will be used for the position detection, has a frequency range around 1 to 2 kHz and we can see in Fig. 2.22 that the inductance is more differentiable for the two positions of interest with the new prototype than with the industrial contactor.

In order to have comparable results, the measurements are made with the same winding (same wire and same number of turns) on both configurations.

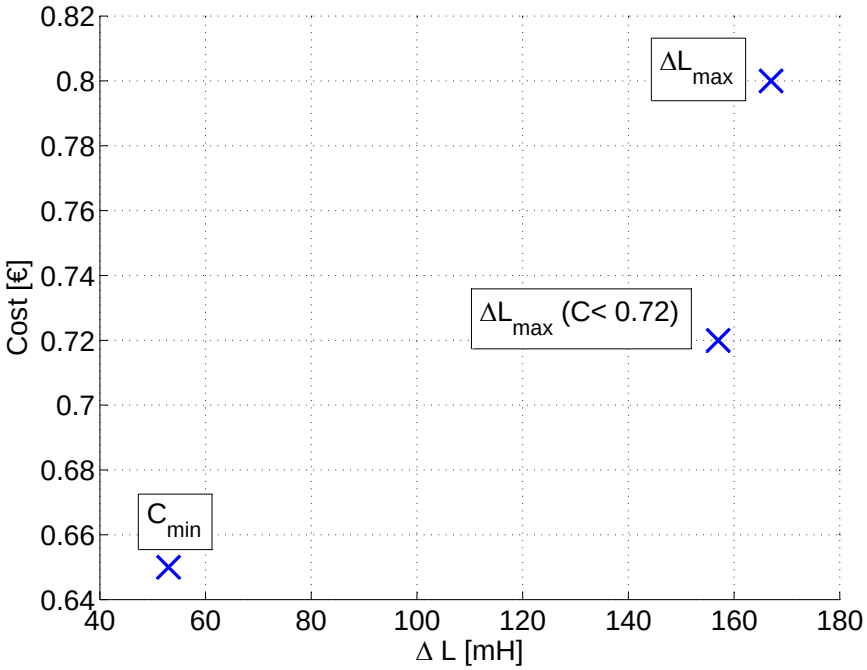

Figure 2.19: The different optimization on the paretto curve

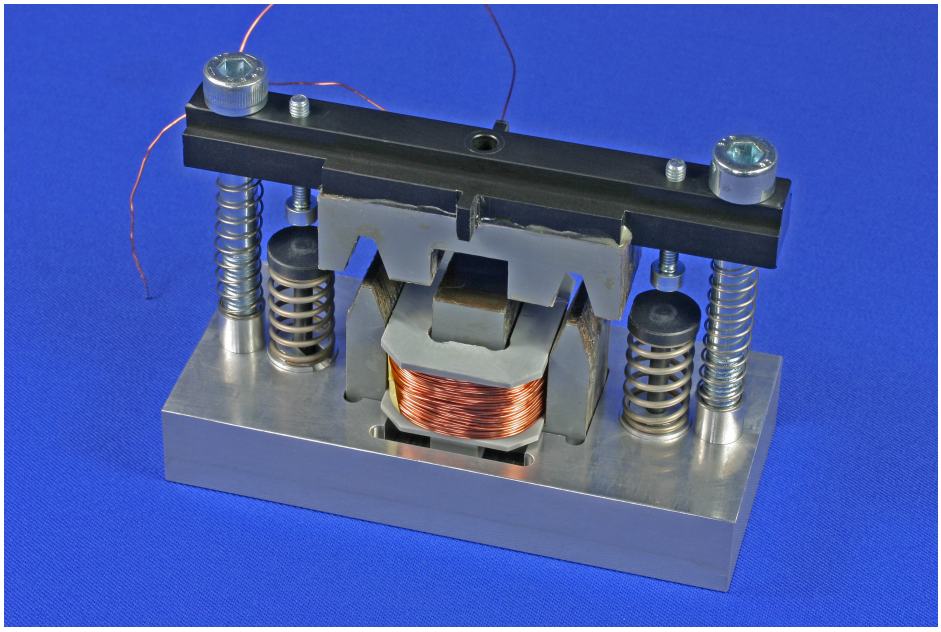

Figure 2.20: Optimal actuator prototype

2.5 Conclusion

The originality of this part of the thesis is to present a global way to optimize a contactor in order to perform its sensorless position and speed control (design for self-sensing).

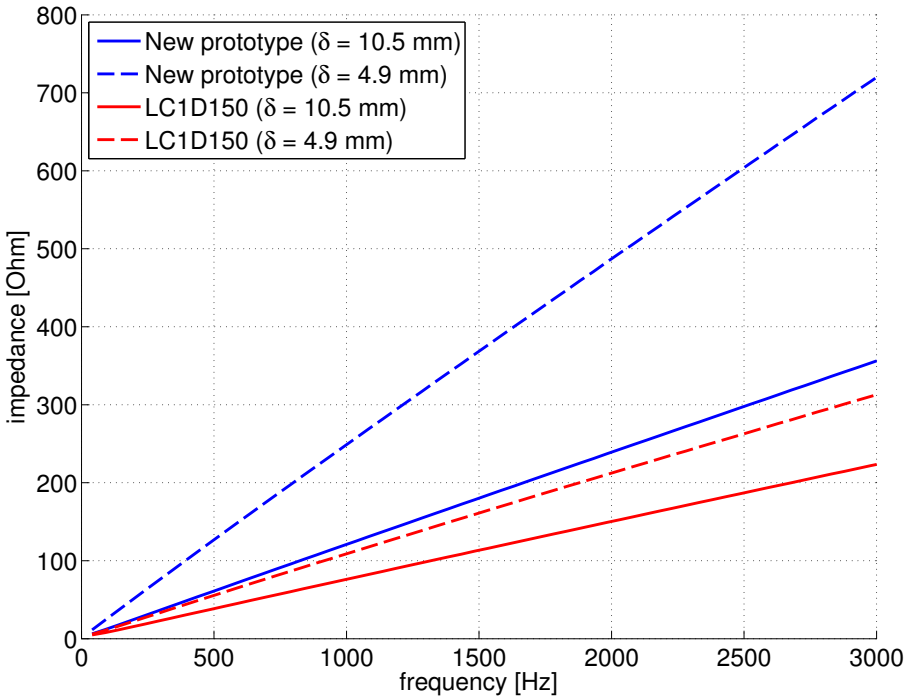

Figure 2.21: Comparison of impedance

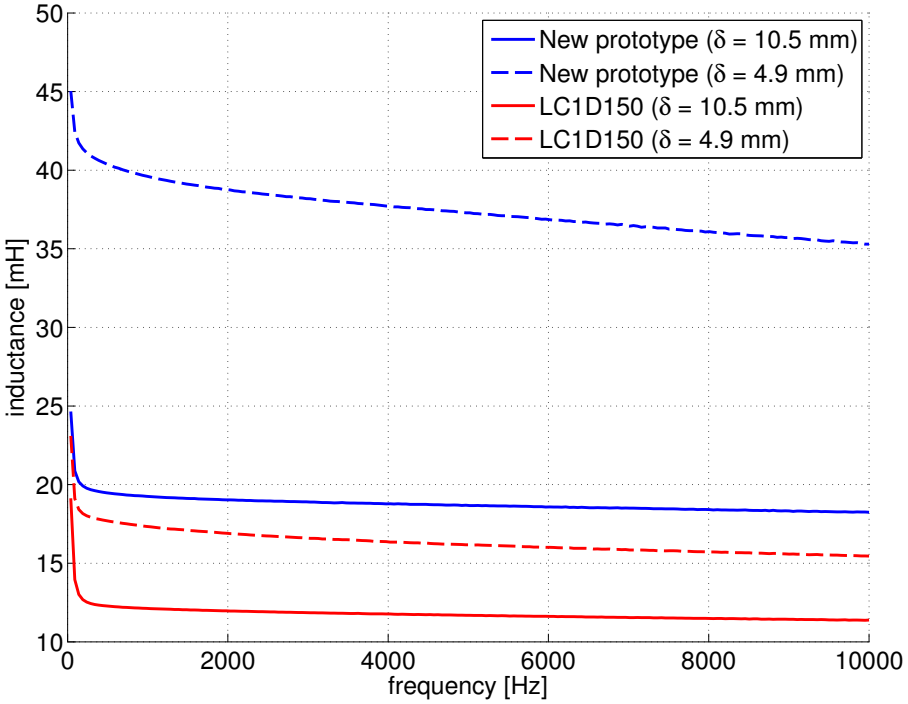

Figure 2.22: Comparison of inductance

Gradient-based and stochastic optimizations are based on multiple static optimization for different values of airgap and allow dynamical constraints. The gradient-based optimization requires an analytical model but is very quick and efficient if it is well defined.

The stochastic method is longer but allows to approach the global optimum and it can be applied to very complex actuator configurations and gives very good results.

At the end of the chapter, the actuator is designed in order to maximize the inductance difference ΔL for two extreme values of airgap that are relatively high ($x > 4.9$ mm) and allow the best position detection as it is shown in the next chapters.

3 Sensorless position estimation for the electromechanical actuator

3.1 Introduction

The objective of this chapter is to demonstrate a method to make sensorless position detection of a linear actuator's mover. The validation of the method is done on an industrial contactor (Schneider Electric - Telemecanique LC1D150, Fig. 3.1) and position detection is verified by displacing manually the mover and comparing its position with the one measured with an external sensor (Keyence laser). The method of position detection was done long before the design of the optimal prototype that is described in chapter 2 and that is why the demonstration of position detection is done with the industrial contactor. The method is also applied to the prototype and the results are presented in chapter 5 where the speed of the mover is estimated directly with the proposed method.

The actuator, that is part of the contactor, is formed with two E-shape ferromagnetic parts and a winding (Fig. 3.2). The ferromagnetic parts are made of laminations of Fe-Si of 0.5 mm. The BH curve of this metal is shown in Fig. 3.3.

The test bench and the electronic card are described in Appendix B.

3.2 State of the art

In the literature, concerning sensorless position estimation, the effort is mostly concentrated on rotating motors. LAI [39] has also heavily participated in the research in this field.

It is difficult to draw a parallel between principles of sensorless position detection of on rotating motors (first of all the BLDC ones) and that of linear actuators. The major differences are:

- The possibility to use the open motor phase as a sensor. The linear actuator is single-phase and consequently the same winding is used for drive and position detection.

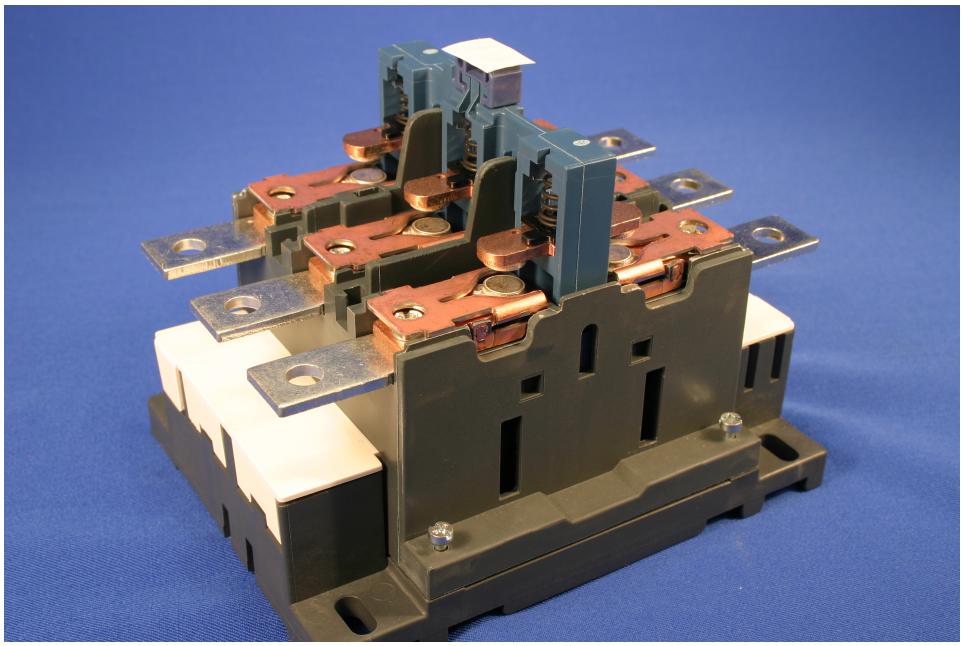

Figure 3.1: Industrial contactor - Telemecanique LC1D150

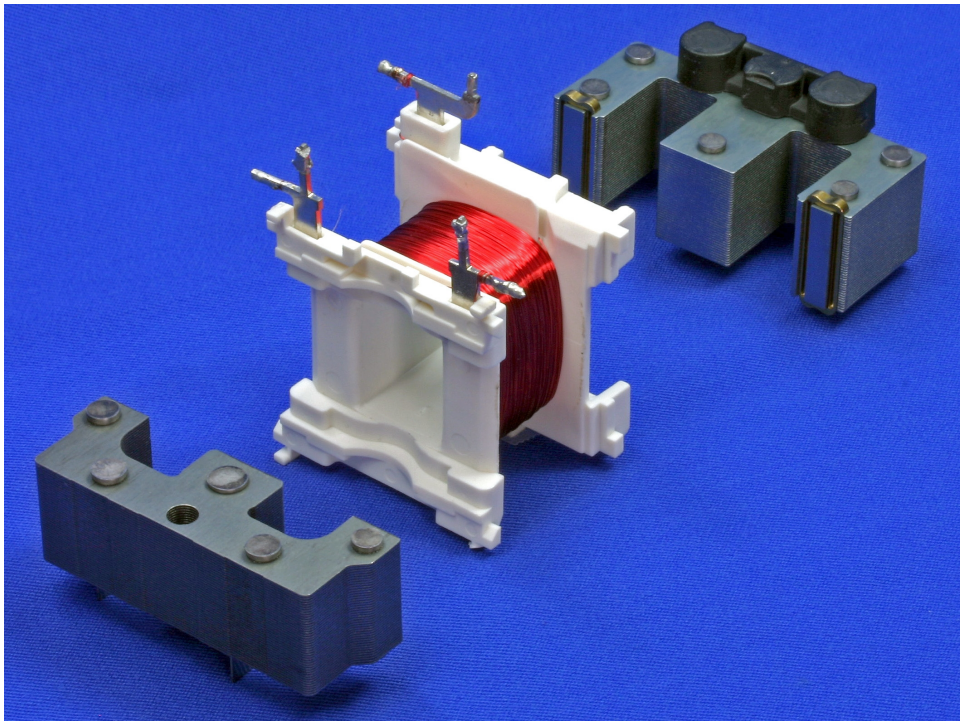

Figure 3.2: Linear actuator inside the contactor LC1D150

- The motor with non-salient rotor does not have a variable air gap, or at least it has not a great influence on the inductance as for a linear actuator.

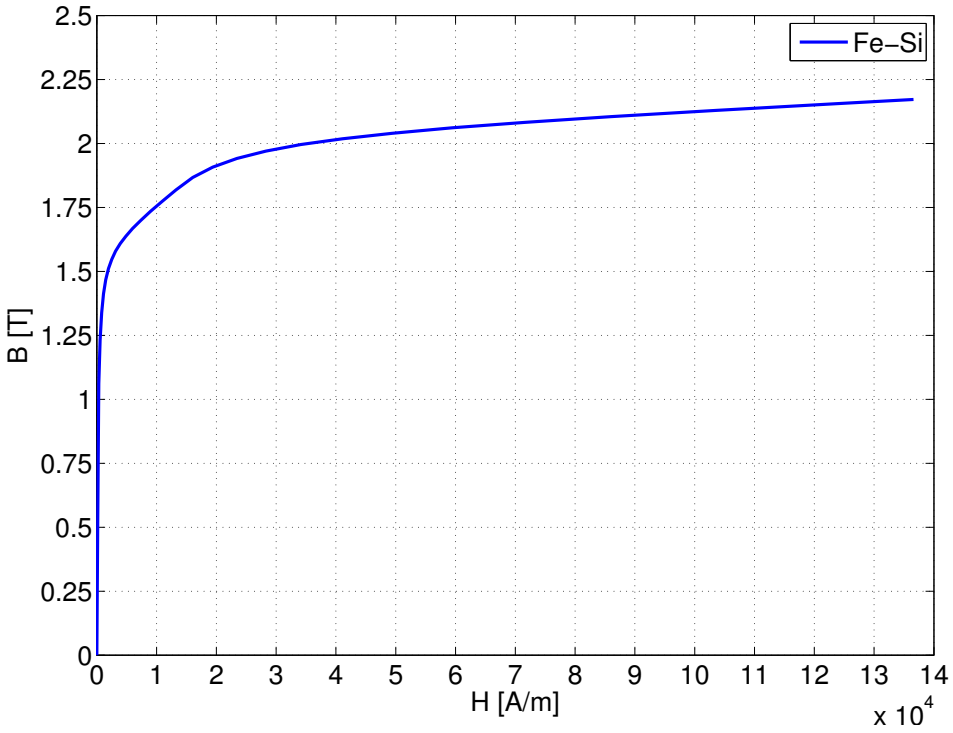

Figure 3.3: Fe-Si saturation curve

- For rotating motors in general, many articles focus on the position detection at standstill or at very low speeds. The problems are completely different in the case of linear actuators because the detection has to be done during a very short transient period.

The idea of sensorless position detection has been studied by various authors, most of them using the magnetic flux as the parameter of position detection.

[50] presents an approach of position detection, which is related to motors. The rotor position of a permanent magnet synchronous motor is directly determined by the shape of the current during the PWM. No prior knowledge of the machine parameters is needed and only the current ripple under conventional PWM modulation is measured to derive the back-EMF and the rotor position.

[33] uses an auxiliary winding to reconstruct the magnetic fluxes and proposes a control system architecture of a camless engine electromechanical actuator that allows the position detection knowing the trajectory reference. The results show limitation of the system but point the possibility to use the change of electromagnetic flux during the trajectory to detect the position.

[43] also uses a secondary winding for camless engine electromagnetic actuators and discusses the accuracy of position detection in relation with the system parameters tolerances. The position detection is performed for relatively small values of airgap (between 0 and 4 mm) because the studied application (camless engine electromagnetic valve) involves a contact between the mover

and the stator at the zero airgap.

[14] uses a nonlinear (sliding mode) estimator in order to avoid the bounces of the mover on the contacts by slowing the speed of the mover to 4 mm/s. The saturation in the ferromagnetic parts is neglected and the position and speed detection uses an analytical model which has been validated by Simulink simulations. The position is relatively well estimated and allows to control the slow speed of the mover but there are some delays which are too important (10 ms) to be usable with a mover at a speed of 400 mm/s, which is our case.

In 1996, Rahman [41] tried to eliminate the external position sensor to reach the same result. With this intention, the position is indirectly estimated thanks to the inductance of the winding. The value of inductance is obtained by measuring the current rise when it is modulated with a PWM. The method is suitable for any slow-moving single-phase variable reluctance motion device. The closing of the actuator lasts for 1 second and in our case the position detection has to work for closing of 15 to 20 ms, therefore 50-70 times quicker.

In 2002, Pawelczak [38] improved the concept develpped by[41] for a total control of the trajectory of the mover. The method is based on the voltage measurement on a shunt resistance at the beginning and at the end of each impulse of the PWM. It is possible to find a correlation between the difference in measured voltage and position.

[46] and proposes a hybrid structure which integrates a flux observer and a signal-injection techniques for the sensorless control of a surface-mount permanent-magnet (SMPM) machine. Although the SMPM machines have a low geometric saliency, the experimental results show a good detection of the position and speed of the rotor.

[56] improves the technique developped by [46] and have better dynamic behavior. But even if the authors explain that the technique is very performing for transient behavior, the change of speed is relatively slow (1 s). In addition, as explained before, the problem of weak saliency of the rotor, which is the main difficulty of the author, is not a problem in the case of a linear actuator where the airgap value and thus the inductance changes a lot during the closing.

[42] performs sensorless position detection of the mover of a switching solenoid by studying the steady state positions of the plunger. Experimental results highlight the relation between the current slope, the filtered input current and the mover position. The method is limited to the cases, in which the response speed is not the critical performance. Indeed, the experimental results show a closing of 3 mm in about 100 ms which is very slow.

[25] describes a method in which the inductance is directly calculated from the differentiation of sampled values of current. As the inductance is inversely proportional to the derivative of current, if ΔI is very small, the inductance becomes very large. Therefore, the author introduces a system of threshold, inside of which small values of ΔI do not generate new values of inductance. But even for a closing of the actuator that takes 100 ms, the position is not accurate enough to allow speed estimation.

Espinosa [13] improved the control of the actuator from [41] by applying fuzzy logic. It is not clear how he manages to detect the position without sensors but he uses it to control the speed at the closing of a contactor in order to minimize the wear of the contacts.

[12] describes an algorithm for closed-loop sensorless control of linear electromagnetic devices. The objective is achieved by applying fuzzy logic that takes care of the position and speed of the mover. The position detection is difficult to understand, it is based on the calculation of the inductance from the current and voltage in the winding but without explaining how these signals are measured. It may be based on the same technique as in [25]. The analytical model of the actuator is corrected by a constant factor to introduce the fringing flux in the calculation. Our experience shows that this strategy may be possible for small values of airgap but it is difficult to understand that the calculation is still accurate for high values of airgap. In addition the author shows a figure at the beginning where the calculated inductance does not vary significantly during the first millimeters of the closing it is shown by our experience.

The solution that has been chosen to fulfill the objective of the thesis consists in superimposing a scan signal on the main one and allows the position detection during the closing that lasts between 15 and 20 ms. Indeed, the frequency of the PWM does not have any influence on the position detection and can be high enough to have a good dynamic. The frequency of the scan signal depends on the resonant frequency of the winding and on the calculation time of the DSP. The presented solution is tested experimentally and is adapted to the objective of sensorless speed control of the actuator.

The state of the art highlights several phenomena that may be useful for sensorless position detection.

3.3 Phenomena relevant to position detection

The solution has to be sensorless, consequently the only signals available to estimate the position are current i and voltage supply u of the actuator winding.

The general equation for the winding voltage for a linear actuator is (assuming no saturation effect):

$$u = R \cdot i + \frac{d\Psi}{dt} = R \cdot i + \frac{d}{dt}(L \cdot i + \Psi_a) \tag{3.1}$$

$$u = R \cdot i + L \cdot \frac{di}{dt} + i \cdot \frac{dL}{dt} + \frac{d\Psi_a}{dt} = R \cdot i + L \cdot \frac{di}{dt} + i \cdot v \cdot \frac{dL}{dx} + v \cdot \frac{d\Psi_a}{dx} \tag{3.2}$$

The 4^{th} term in (3.2) has been little studied in the literature because the state of the art concerns

R	:	Winding resistance
$L = L(x)$	:	Winding self inductance
$\Psi_a = \Psi_a(x)$	:	Mutual flux due to magnet in the winding
Ψ	:	Total flux

principally actuators without magnet. This term is actually an induced voltage, also influenced by the position x and speed v:

$$e_v(x, v) = v \cdot \frac{d\Psi_a}{dx} \tag{3.3}$$

These term has been studied during the industrial collaboration because the first prototype included magnets (Appendix A). But in the present case, as the actuator is reluctant, the equation (3.2) is reduced to:

$$u = R \cdot i + L \cdot \frac{di}{dt} + i \cdot v \cdot \frac{dL}{dx} \tag{3.4}$$

There are hence 3 terms that influence the shape of rising and falling of the current.

Rahman [41] neglects the 3^{rd} term without justification. This term can be interpreted as an additional resistance $R_v(x, v)$ multiplied by the current i:

$$R_v(x, v) = v \cdot \frac{dL}{dx} \tag{3.5}$$

Fig. 3.4 shows the decomposition of the typical voltage profile for the closing of the industrial contactor. We can see that $R_v \cdot i$ is negligible in comparison with $R \cdot i$ and $L \cdot di/dt$. This conclusion cannot be generalized and has to be ensured with other applications.

Thus, the voltage u is reduced to:

$$u = R \cdot i + L \cdot \frac{di}{dt} \tag{3.6}$$

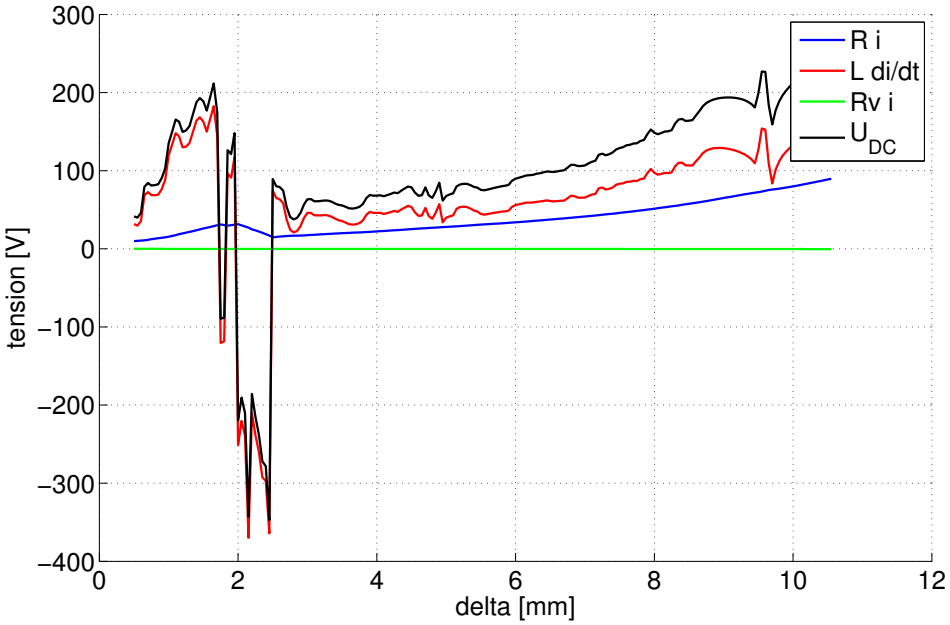

Figure 3.4: Justification of the negligible impact of R_v

And consequently, for the analysis of transient dynamics for a voltage step from 0 to U_{DC}, the difference of current Δi during the time Δt is:

$$\Delta i = \frac{U_{DC}}{R}(1 - e^{\frac{-\Delta t}{\tau_{el}}}) \tag{3.7}$$

where:

$$\tau_{el} = \frac{L}{R} \tag{3.8}$$

The electrical time constant is critical because the time of closing the actuator is very short.

3.3.1 Saturation

It can be shown mathematically that the winding inductance and the flux are directly influenced by the slope of the BH curve. If the airgap value is sufficiently large, the actuator magnetic circuit is not saturated (points 1 and 2 in Figs. 3.5 and 3.6) and the inductance is low. If the airgap value is small, in the ideal case when the ferromagnetic material is linear (point 3), the winding

inductance is high. However, as the ferromagnetic material is saturated, the inductance is smaller (point 3'). The reasoning is the same for the flux, therefore saturation reduces the ΔL ($\Delta L > \Delta L'$ in Fig. 3.6) and $\Delta\Psi$ which have a strong influence on the Δi, which is important for sensorless position detection.

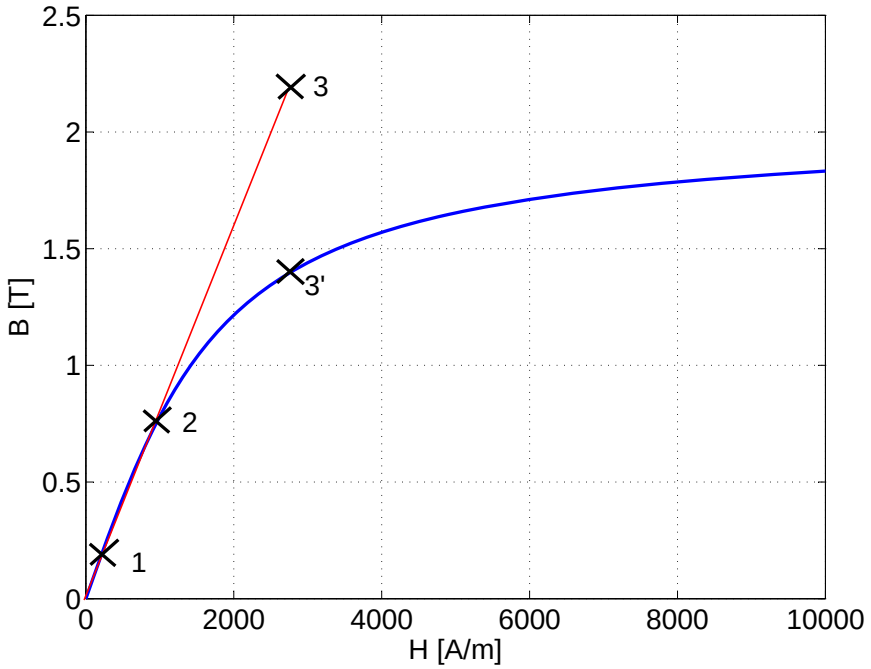

Figure 3.5: BH curve and saturation consequences

In all cases, saturation tends to reduce the inductance and thus its influence for different values of the air gap will be reduced. It is therefore unnecessary in our case to use the saturation as a source of information on the position and this method is consequently abandoned: the position will be detected the most easily if the magnetic circuit always stays linear.

3.3.2 Eddy currents

Another possibility would be to use an eddy current inductive sensor to detect the position. This sensor is a coil that produces an oscillating magnetic field. When the mover of the actuator enters this field, eddy currents are generated, and according to Lenz's law, they always oppose to the motion or change causing it. It is therefore possible to relate the coil inductance attenuation to the position of the mover.

In our case, it is not possible to use an external sensor, as only the actuator signals (current and voltage) should be used to detect the effects of eddy currents and consequently to detect the position. The difficulty is that eddy currents tend to increase when the airgap value decreases, thus to reduce the flux and, consequently, to reduce the $\Delta L/\Delta x$ which allows finally to detect

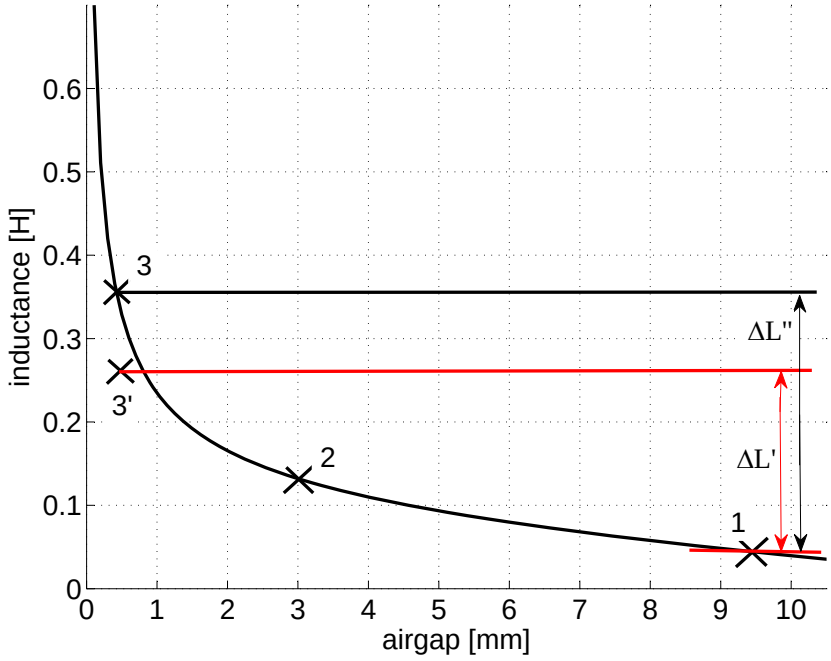

Figure 3.6: Inductance versus airgap value and saturation consequences

position. Fig. 3.7 shows that the measured inductance difference with eddy currents ($\Delta L''$) is smaller than this difference without eddy currents (ΔL).

The possibility of introducing a conductive piece on the mover has also been considered in order to excite eddy currents with a very high frequency signal. The problem, as described above, is that the eddy currents still tend to decrease the inductance differentiation versus the position.

The presence of eddy currents increases the measured winding resistance. This increase should 'cover' the losses generated by the eddy currents and another possibility to use the eddy current could be to use the resistance difference versus the value of airgap to determine the position if the term $R\ i$ of equation (3.6) was strongly dominant compared to $L \cdot \frac{di}{dt}$. Fig. 3.8 shows that these two terms are similar.

Finally, as the eddy currents tend to oppose themselves to flux changes, they will counter the main current changes necessary for the actuator dynamic during speed regulation.

Consequently, eddy currents are minimized by laminating the ferromagnetic parts.

3.3.3 PWM and inductive sensor

The only way to control the voltage that drives the actuator is to use a PWM.

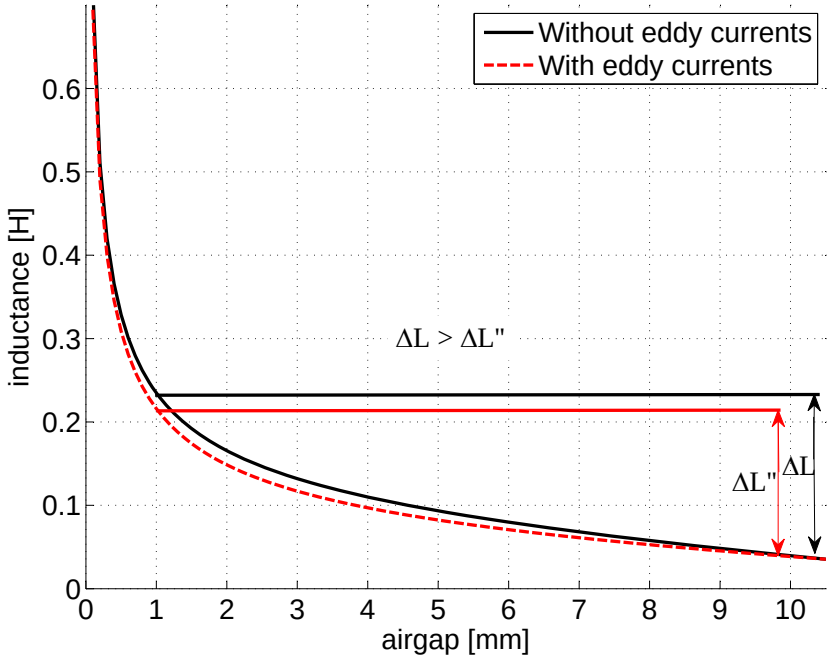

Figure 3.7: Eddy current influence on the inductance

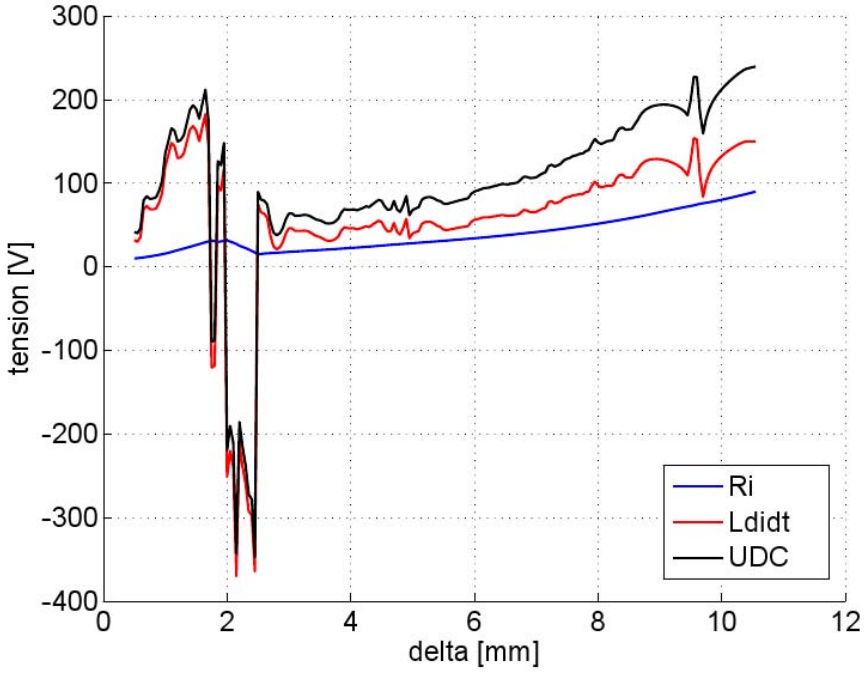

Figure 3.8: $R\ i$ and $L \cdot \frac{di}{dt}$ versus position

The inductance of the coil varies with the value of the airgap and if it is possible to measure the inductance, it is possible to evaluate the value of the airgap and therefore to know the position of the mover. The coil is used as a sensor.

Fig. 3.9 presents the principle of position detection. During the PWM, the circuit measures the rise or fall of current Δi depending on which one is longer (duty cycle of 50% is the worst case). By combining this value with the precedent one, the system is able to evaluate the speed.

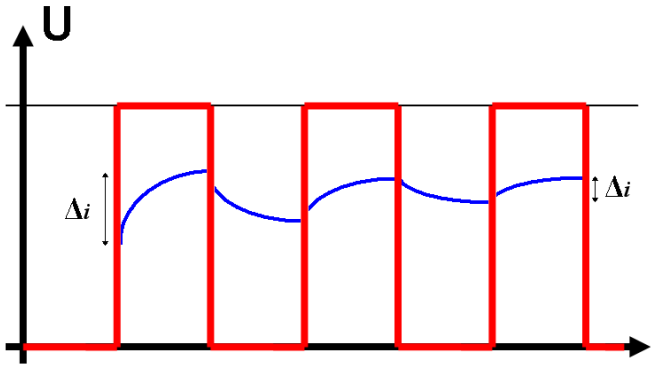

Figure 3.9: Influence of inductance on the current rise and fall in a PWM

Measurements on an existing prototype show that for actuator designed for contactors, the electrical time constant is comparable to the time of closing the actuator, and consequently that the dynamic is a crucial point. For example, with the winding for U_{DC} = 110 V (LX1-D8 F7), which has a diameter of 0.28 mm and 1079 turns, the resistance and inductance are:

- R: 30 Ω
- L ∈ [0.3,0.9] H (actuator open, closed)

τ_{el}, the electrical time constant of the system:

$$\tau_{el} = \frac{L}{R} \in [10,30] \text{ ms} \tag{3.9}$$

The specifications of contactor require the closing time between 30 and 50 ms:

$$\tau_{mec} \in [30, 50] \text{ ms} \tag{3.10}$$

At a PWM frequency of 40 kHz, that is suitable to have a good driving dynamic, considering that the worst case is duty cycle of 50%, τ_{el} = 10 ms when the actuator is open and consequently the equation 3.12 becomes:

$$\Delta i = \frac{110}{30}(1 - e^{\frac{-50\%/40 \cdot 10^3}{5 \cdot 10^{-3}}}) \tag{3.11}$$

$$\Delta i = 4.6 \text{ mA} \tag{3.12}$$

Δi is small. Fig. 3.10 shows the noise due to the electronic circuit in the current at the input of the actuator. We can see that Δi is comparable to the noise and consequently difficult to measure.

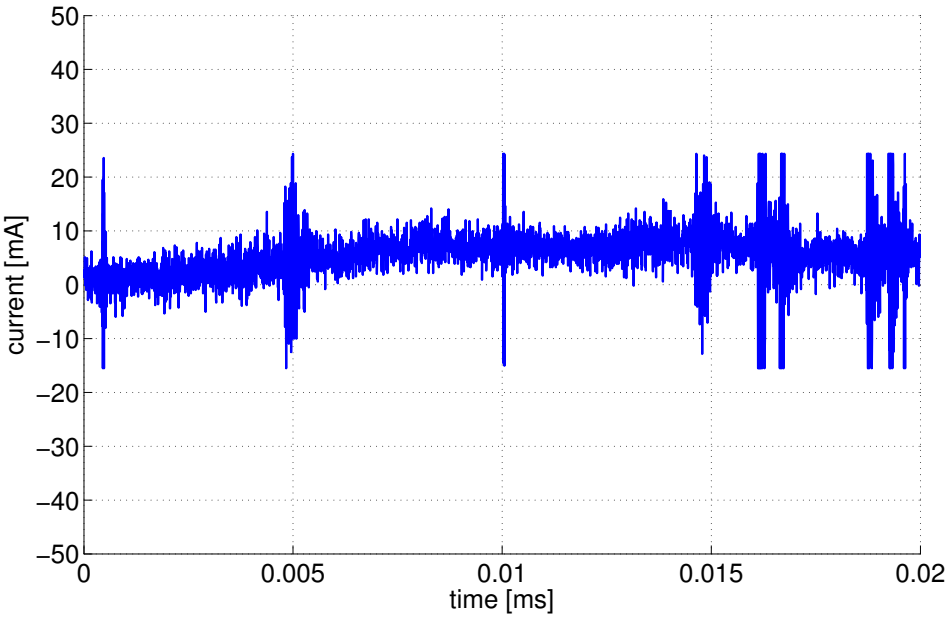

Figure 3.10: Electronic noise in the current at the actuator's input

The method of section 3.3.4 uses the same principle, but the sampling period does not affect the results of position estimation.

3.3.4 Injection of a scan signal in the winding

The method is based on injecting a scan sinusoidal voltage in the winding and detecting the amplitude of the scan current that is position-dependent. The scan voltage is superimposed to the main voltage which drives the actuator.

Fig. 3.11 shows the superimposition of the scan signal and the main signal. The total current is the addition of the drive current (main current) and the scan current.

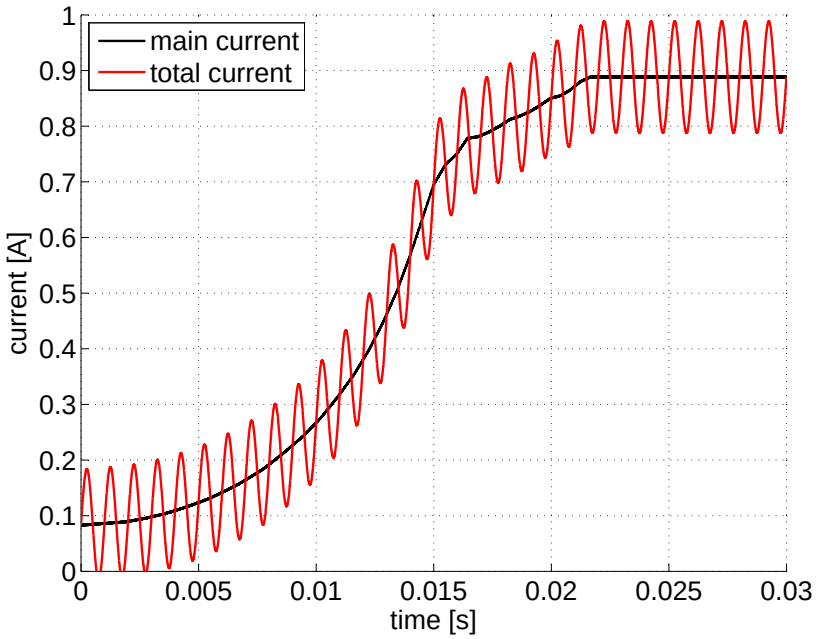

Figure 3.11: superimposition of main and scan signals

The scan current is filtered and its amplitude is directly related to the position of the mover.

This method is used in patent [21] to estimate the static position of an hydraulic valve. Here, the application is different because in this case, the detection must be done on a moving object in order to regulate its speed.

The method is applied to the industrial contactor and presented in the following sections (3.4 - 3.6). The value of airgap δ (which is also the position the mover) is between 0.2 mm when the contactor is closed and 10.5 mm when it is open (Fig. 3.12).

During the closing, the important part of the trajectory to control is between 10.5 mm and 4.9 mm, since for values of airgap smaller than 4.9 mm, the contacts are closed and the speed is not critical anymore.

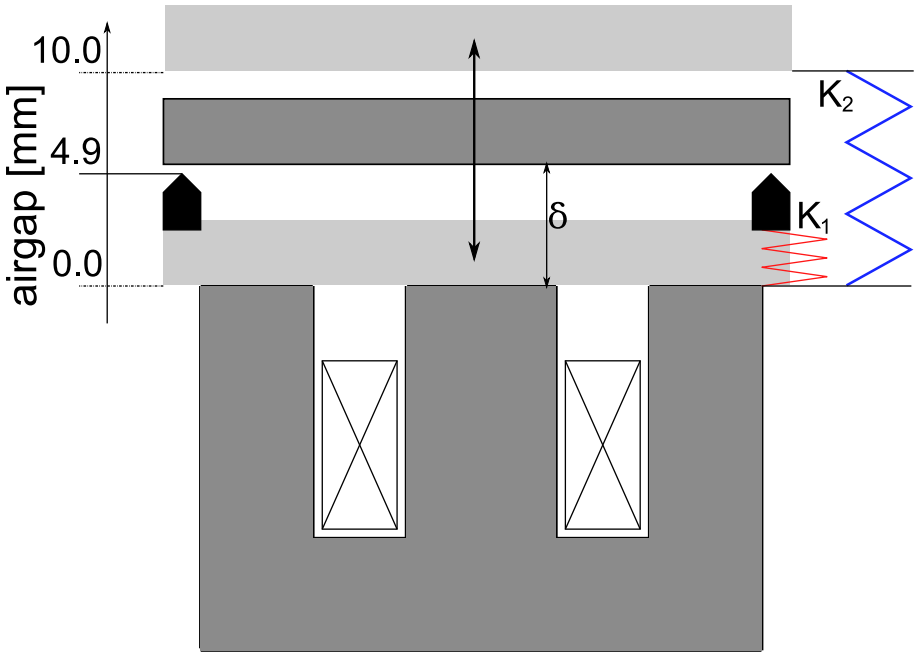

Figure 3.12: Mechanical diagram of the actuator

3.4 Determination of the scan voltage frequency

When we wanted to determine the scan voltage frequency, we were working with industrial windings that are actually composed by two separate windings. Indeed, there is a hold-in winding, which has very thin wire and a lot of turns. It is only used to maintain closed the actuator with a small current.

We decided to open this hold-in winding and not to take it into account. But even open, this winding operates as a parasite capacitance and changes a lot the resonant frequency of the main winding.

In subsection 3.4.1, we explain how the scan voltage frequency is chosen with both windings and, in subsection 3.4.2, we show why this frequency is kept unchanged when the hold-in winding is removed.

3.4.1 Determination of the scan voltage frequency with the hold-in winding

Fig. 3.13 shows the main winding input impedance Z in function of the frequency. By taking the contactor LC1D150 and the winding LX1-D8 E7, which has a diameter of wire of 0.45 mm and is predicted for a voltage of 48 V, it can be seen in Fig. 3.13 that the impedance is different for δ = 4.9 mm and δ = 10.5 mm that are the two extreme positions of interest. The amplitude of the scan current gives the position of the mover and Fig. 3.14 shows the relative difference of current $\Delta i/i$ versus the frequency of the scan current. $\Delta i/i$ is in percents and is calculated as following:

$$\frac{\Delta i}{I} = 100\frac{abs(I_{op} - I_{co})}{I_{op}} \tag{3.13}$$

where I_{op} and I_{co} are respectively the current when the actuator is open (δ = 10.5 mm) and when the contact is made (δ = 4.9 mm).

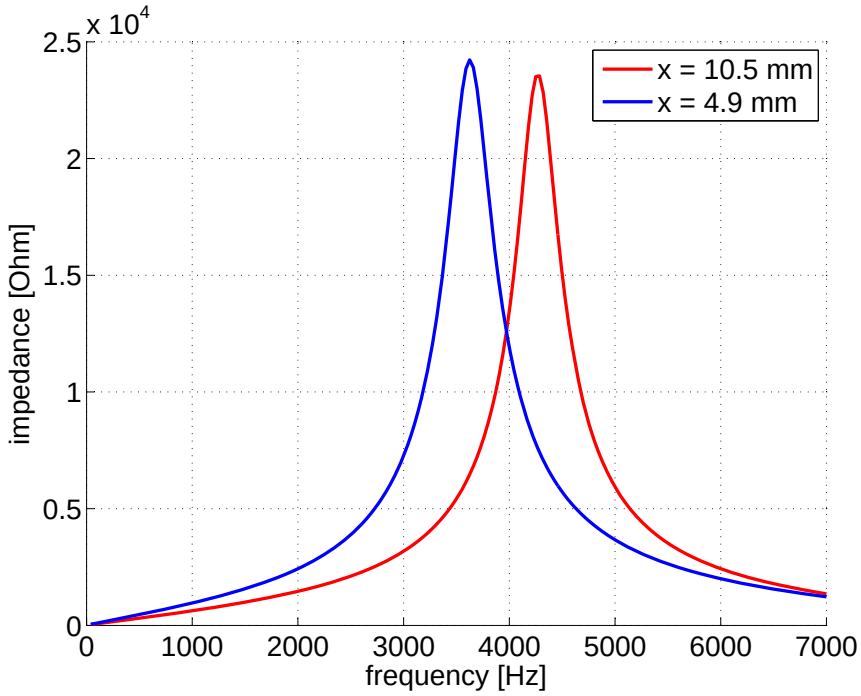

Figure 3.13: Winding impedance Z versus the frequency f

This form of $Z(f)$ is a consequence of an important value of capacitance between the winding conductors which causes that the winding should be regarded as a RLC circuit starting from the low frequencies.

Theoretically, the scan frequency has to be the highest possible in order to increase the frequency of position detection, but also a compromise should be made between the absolute value of current I (Fig. 3.15), which has to be high enough not to be disturbed by the noise, and the relative difference of current amplitude $\Delta i/i$ (Fig. 3.14).

The DSP works at a frequency clock of 100 MHz. A frequency of PWM of 40 kHz allows just enough code lines to perform position detection and filter of position and speed (Chapter 4). We decided to work with a scan signal frequency of 1250 Hz because it is equal to 40000/32 and the division by 32 in the DSP is simple because it is a power of 2 ($2^5 = 32$). Actually, a division by a

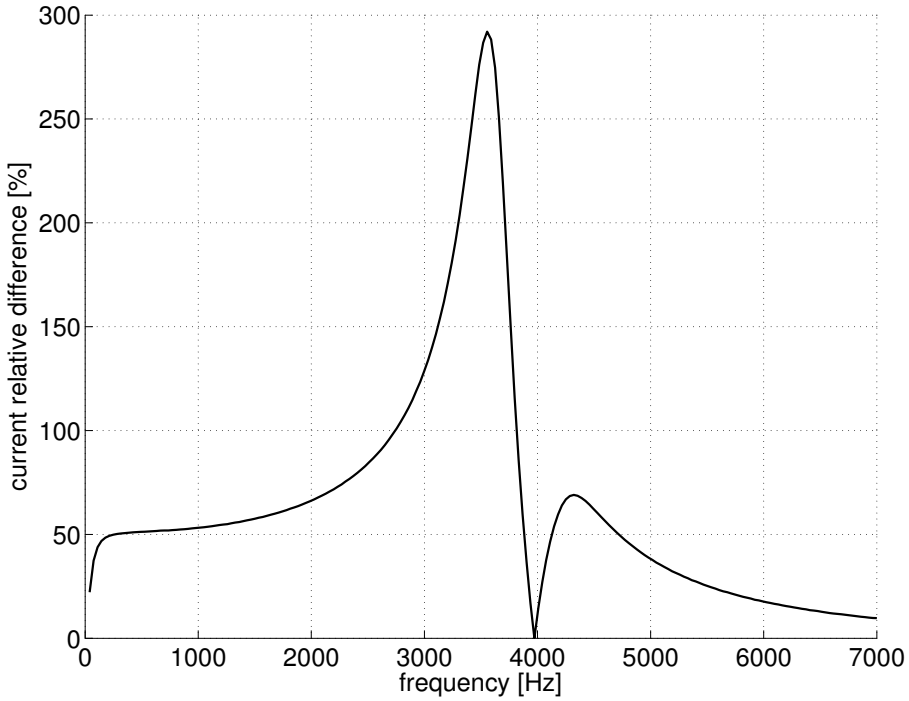

Figure 3.14: Relative difference of current versus the frequency for two extreme positions

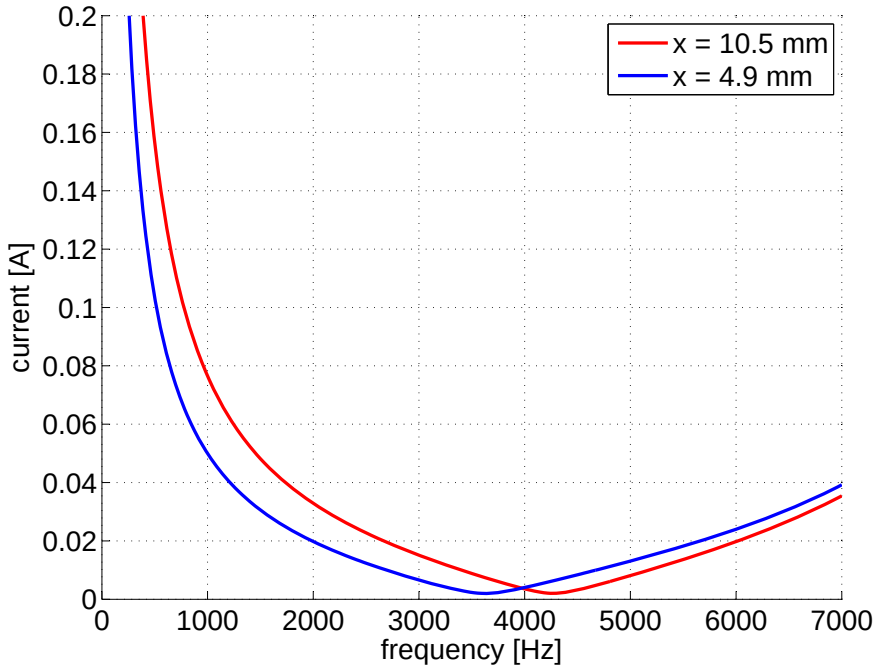

Figure 3.15: Current at extreme positions versus the frequency

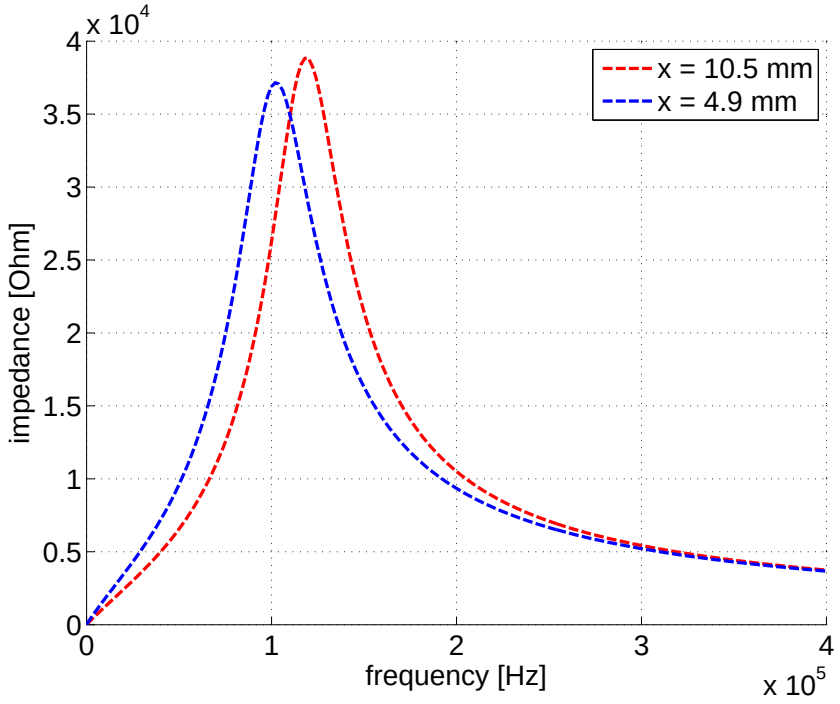

Figure 3.16: Winding impedance Z versus the frequency f

power of 2 takes only one line of code while another division may take up to 100 lines.

3.4.2 Determination of the scan voltage frequency without the hold-in winding

But, as the specifications enables only one winding, we had to find a way to do the same without the hold-in winding. Fig. 3.16 shows the impedance of the same winding of Fig. 3.13 but without the hold-in one. We can see that the resonant frequency is much higher than before (120 kHz against 4240 Hz when the actuator is open). The first idea was to displace the resonant frequency by adding RLC circuits in parallel and in series with the actuator. We optimized the values of R, L and C in order to have the best relative difference of current amplitude $\Delta i/i$ at the frequency of 1250 Hz, but the result is that all the additional components tend to decrease $\Delta i/i$. It means that, finally, no additionnal circuit is implemented.

We can see in Fig. 3.17 that the current for both configurations, with and without the hold-in winding, are not very different at the chosen frequency of 1250 Hz.

With the seocndary winding: $\Delta i/i = 35.6\ \%$

Without the hold-in winding: $\Delta i/i = 33.9\ \%$

Consequently the scan current frequency of 1250 Hz has been kept because it is very convenient for the calculation and gives very accurate results. All the following measurements have been

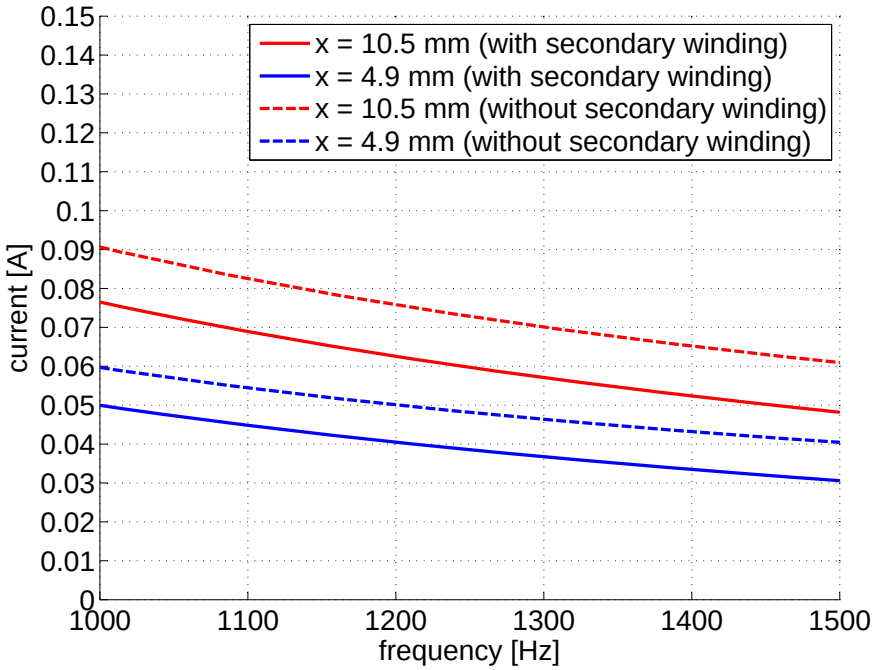

Figure 3.17: Winding current i versus the frequency f

done on contactors without the hold-in winding.

3.5 Injection of the scan signal only

The scan signal is generated by a DSP (TI-TMS320C2000, Piccolo) with a PWM frequency of 40 kHz and a H-bridge with power transistors A and B (Fig. 3.18).

3.5.1 Power source and power electronic circuit

We decide to use a Continuous Mode PWM, in order to have a simple switch control. For closing the actuator contacts, a high current is needed (typically 1.5 A). This implies the high voltage and accordingly high power value at the actuator terminals. Thus, output of the DSP needs to drive the power amplification circuit. The use of an H-bridge is an efficient way to implement power amplification. The main issue when using the H-bridge is that it has to be able to provide the necessary power needed by the actuator. That means that it has to be able to supply around 1.5 A, at the voltage values between 100 V and 200 V.

In this chapter, the bridge is supplied by a DC-source of 30 V. The contactor is connected between the two branches of the bridge (② in Fig. 3.18). Fig. 3.19 shows the current measured at the input of the contactor.

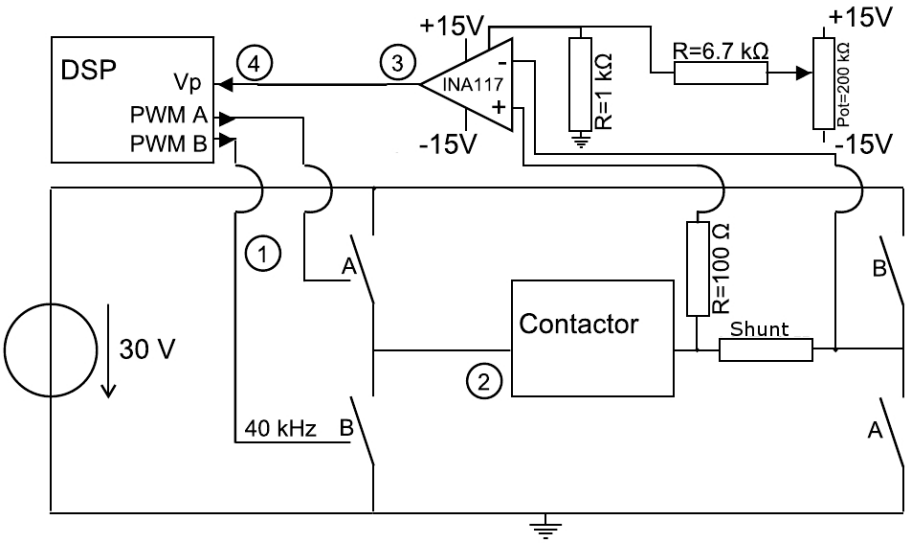

Figure 3.18: Position detection electronic circuit (for scan current only)

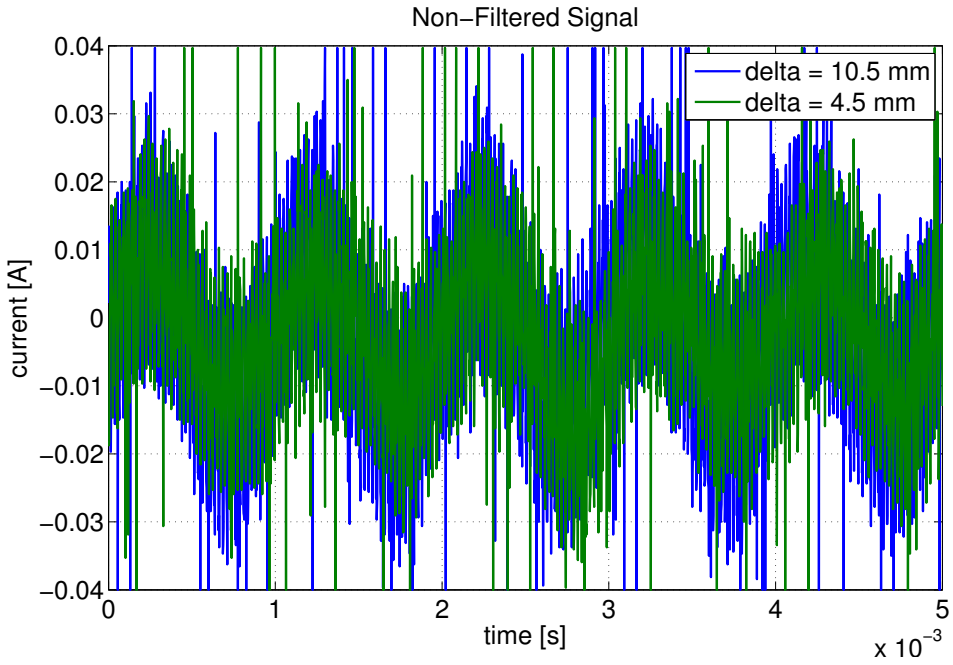

Figure 3.19: Scan current for two extreme positions

3.5.2 DSP switching logic

The DSP generates two PWM signals (PWM A and PWM B) at the frequency of 40 kHz (① in Fig. 3.18), that are opposed and with a duty cycle that changes periodically at 1.25 kHz (Fig. 3.20). Because of the Continuous Mode, we have to introduce a band gap, visible in Fig. 3.21, that does not allow both transistors of the same branch to conduct.

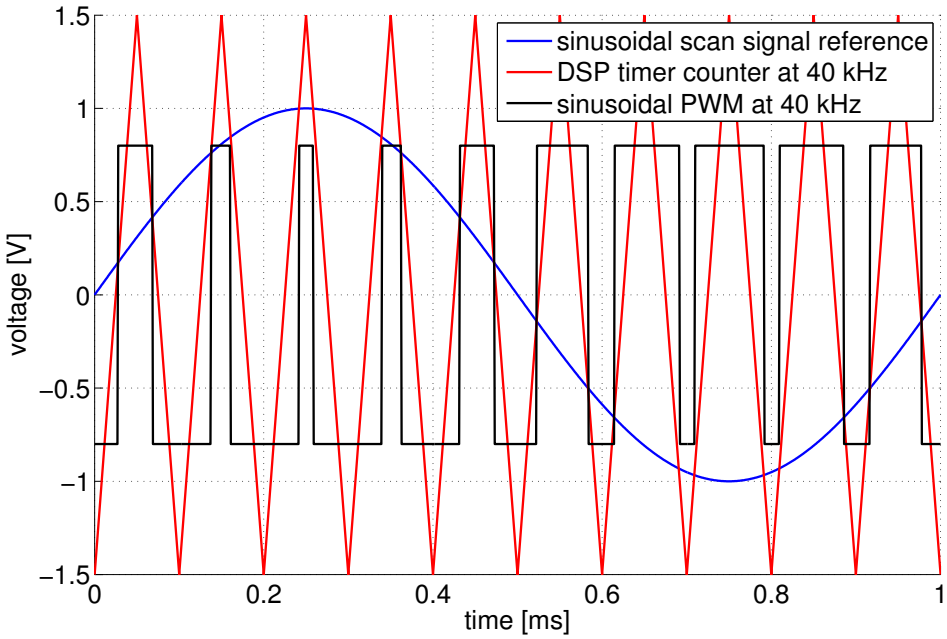

Figure 3.20: Principle of PWM generation

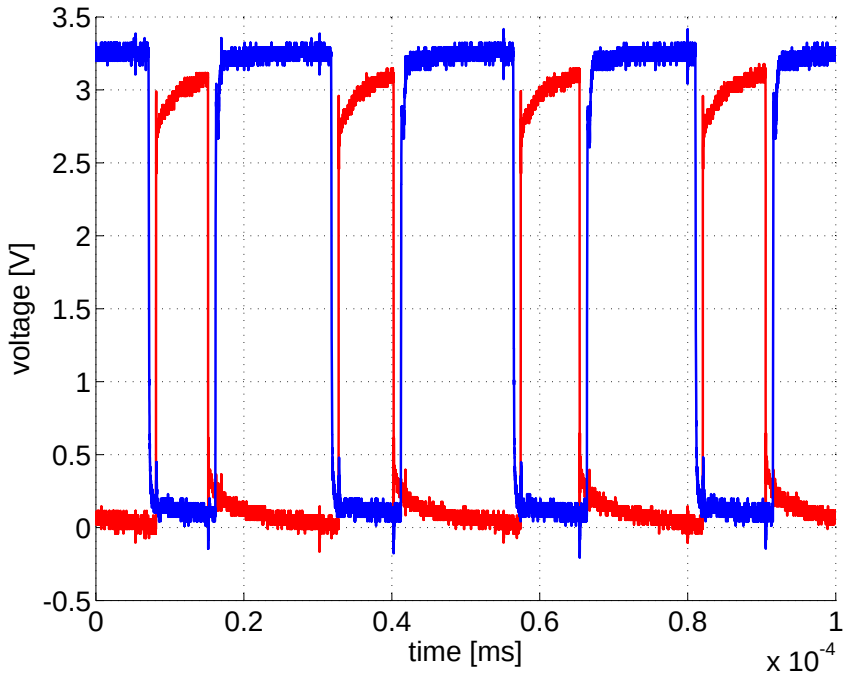

Figure 3.21: Two inversed sinusoidal PWM with a band-gap

Furthermore, to avoid additional circuitry, both of PWM signals are generated by using two output pins of the DSP's PWM module, inverted in respect to each other, with the same duty

cycle. Therefore, the pulse width (duty cycle) is modulated such that it provides both signals simultaneously, simplifying the hardware and slightly increasing complexity of the software.

3.5.3 Amplitude and offset adjustment circuit

The concept of sensorless control requires this system to be able to measure the current supplied to the actuator. As explained before, this current besides the function of controlling the actuator, is also the only information available on the position of the actuator's mover. Therefore, it is necessary to use this information in the closed-loop position control system. However, the current has to be measured without influencing the actuator impedance. In other words, it requires a high input resistance amplifier which will decouple the measuring circuit from the actuator winding. A resistance is placed in series with the contactor as it is shown in Fig. 3.18 (shunt) and the measurement of the current to estimate the position is performed on this resistance

Furthermore, what is even more important, the amplifier needs to have an extremely high Common Mode Input Voltage. This is due to the fact that the amplifier input will have to be connected to the actuator, which means high voltage of about ±200 V (even if in this case, we will only use a voltage source of 30 V). The amplifier that meets all the requirements is the Texas Instruments (BB - series), INA117 (③ in Fig. 3.18) difference amplifier with high common-mode input voltage. This amplifier is generally used for current sensing for a wide range of devices. There are numerous different configurations for implementing the current sensing circuitry by using it, and all are quite simple and efficient.

In order to measure the scan current directly with the same DSP, the measured voltage should be adapted to the DSP analog input, which is in the range between 0 and 3.3 V (④ in Fig. 3.18). For this purpose, we use a resistance that adjusts the amplitude and a circuit that adjusts the offset.

3.5.4 DSP acquisition

Fig. 3.22 shows the DSP value corresponding to the measured voltage (which is an image of the contactor current) versus the time for different values of δ. The curves are not filtered but have much less noise than in Fig. 3.19 because the DSP reads the values between the glitches and avoids the measurements in the instants of commutation. We see that the amplitude of the scan signal varies significantly in function of the position.

The method of measuring the difference between the maximum and the minimum of the scan signal in order to determine its amplitude and consequently the position is not the most appropriate for different reasons. First, it is not trivial to determine the minimal and maximal values. Second, only one determination of the position by period is possible, which means only 24 times for a closure of 30 ms at a scan signal's frequency of 1.25 kHz. Thirdly, the method is not robust because the result depends on the values measured at particular points, instead of using the complete measured signal.

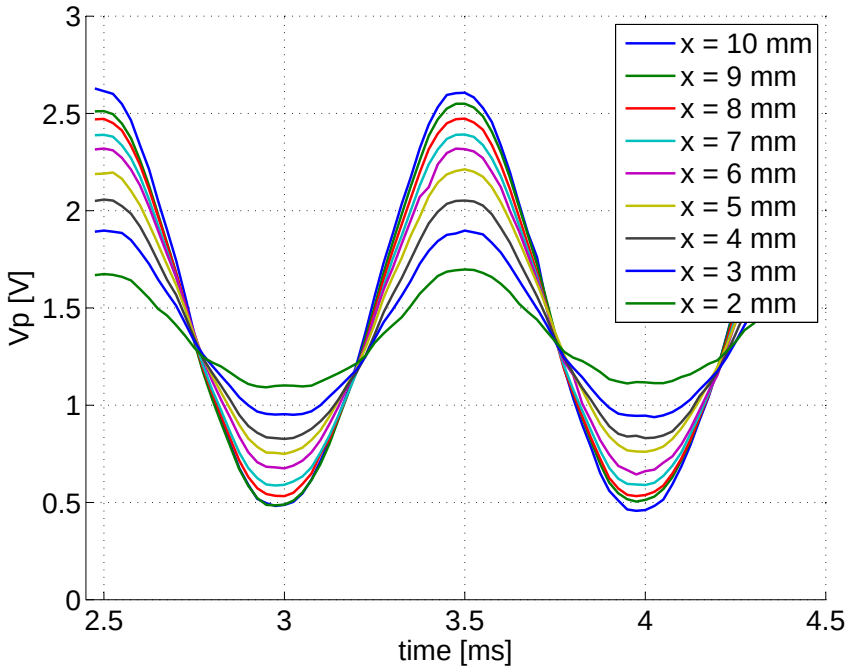

Figure 3.22: Scan current measured with the DSP (4096 = 3.3 V)

Consequently, we decided to work with a sliding window that is one period broad (Fig. 3.23). First, we calculate $\overline{V}_k$ the average value of V during the sliding period:

$$\overline{V}_k = \frac{1}{N} \sum_{i=k-N}^{i=k} V_i \tag{3.14}$$

Then, we calculate the sum of the square difference between V and $\overline{V}_k$, and divide the result by 2^{11} in order to have again a value S that is readable by the DSP:

$$S = \frac{1}{2^{11}} \sum_{i=k-N}^{i=k} (V_i - \overline{V_k})^2 \tag{3.15}$$

S is now the parameter that represents the position.

Fig. 3.23 shows four different positions of the sliding window. We can see in blue the V which has to be evaluated and its average value $\overline{V}_k$ (black line). In red is represented the square difference between V and $\overline{V}_k$. Finally, S is represented by the black dot at the end of the sliding window. The figure A shows the first evaluation ($k = 1$), the figure B shows the results for $k = 14$, the

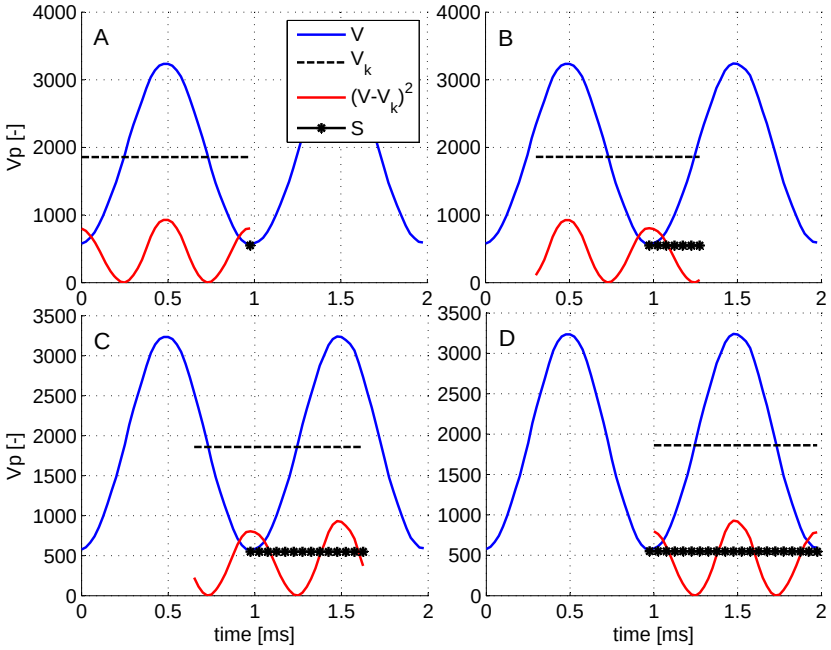

Figure 3.23: Sliding window and S calculation (δ = 10 mm)

figure C for $k = 28$ and the figure D for $k = 40$.

Finally we statically measured S for different values of the air gap in order to determine a look-up table that relates S to the position. During this measurement, the values of the air gap are measured using an external position sensor.

This look-up table is implemented in the DSP in order to determine the position without the external sensor. Fig 3.24 shows the value of the air gap δ versus the value of S.

3.5.5 Results

Fig. 3.25 shows dynamical results when we move manually the mover of the actuator. With the scan signal only, we can see that the method of position detection is accurate.

The speed expected by the specifications is not reached and this measurement only shows that the position is well detected at low speed without the main current.

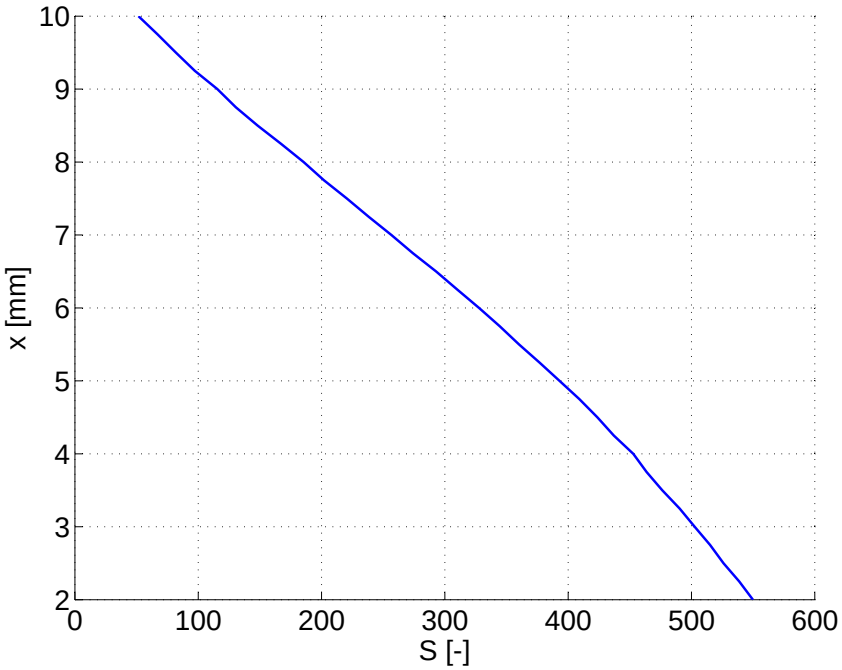

Figure 3.24: Sum of square difference to the average

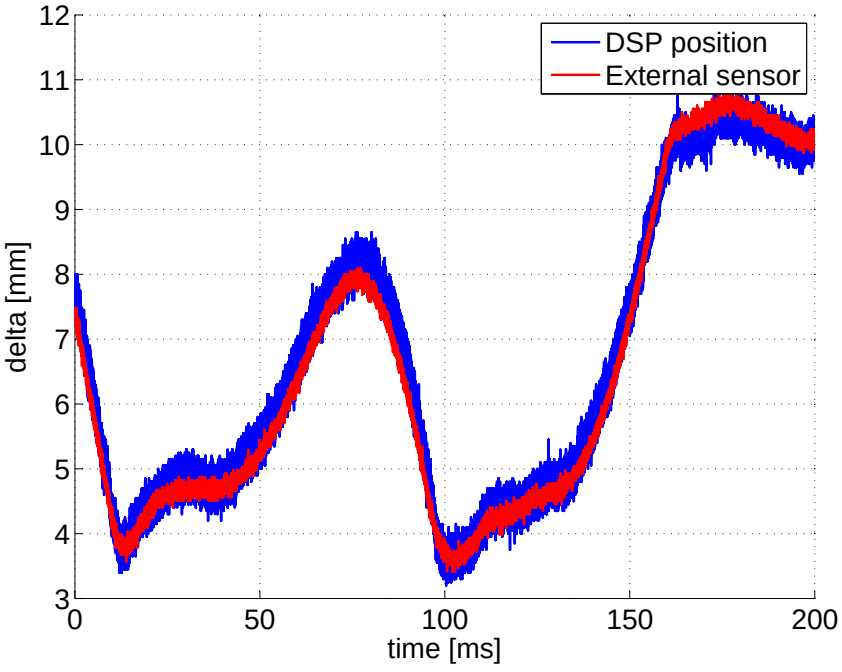

Figure 3.25: Comparison with an external sensor

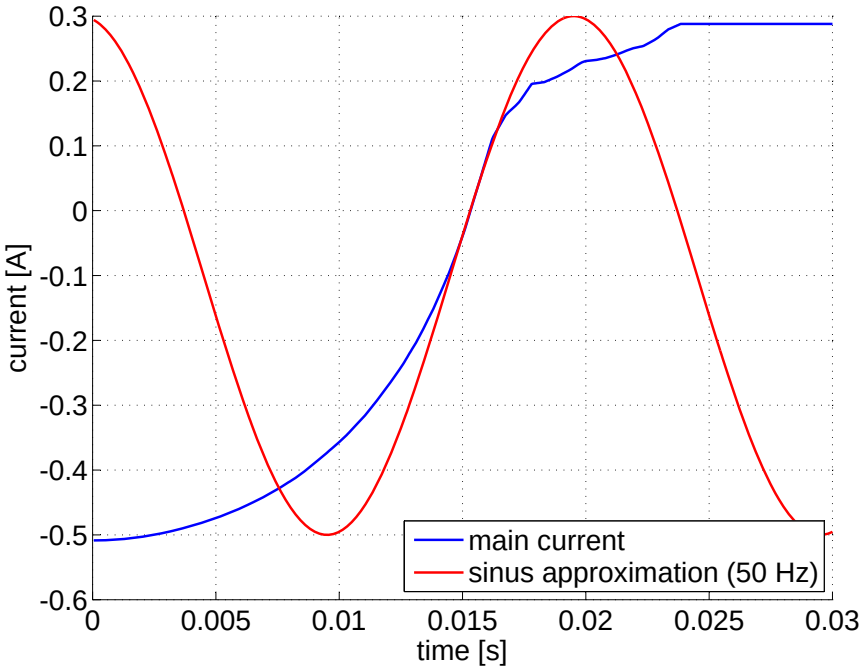

Figure 3.26: 50 Hz sinus approximation of the main current

3.6 Injection of the main current with the scan current

The next step is to introduce the main current, which can be regarded as a perturbation for the position measurement. In order to simulate a typical form of the main current, we used a sinus of 50 Hz, that allows to study the impact of the amplitude and the slope of the current (Fig. 3.26). The main current is injected using the same circuitry and the scan signal is simply superimposed to the main one.

Fig. 3.27 shows the actuator current built by the superimposition of both signals at 1250 and 50 Hz.

3.6.1 Pass-band filtering

In order to detect the position with the same method that is used with the scan signal only, the current must be filtered. The filter which is inserted between the points ③ and ④ of Fig. 3.18 is shown in Fig. 3.28.

The chosen filter is a second order Sallen-Key band-pass filter [26], [44] because it is simple to implement (Fig. 3.29). Its input impedance is practically infinite and its output one is practically 0. It allows low-pass, high-pass, or bandpass response with very high Q factor and passband gain without the use of inductors.

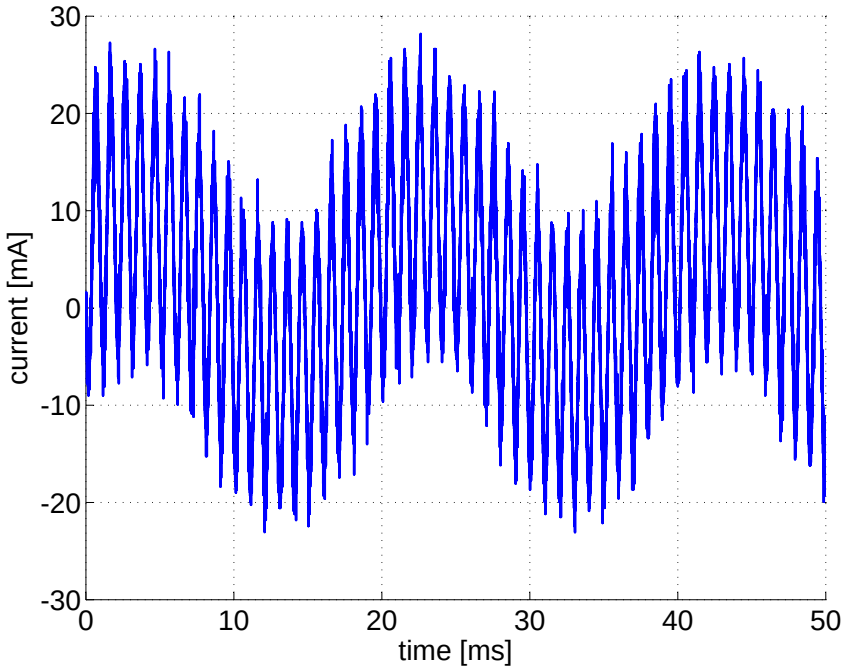

Figure 3.27: Current in the contactor with main signal

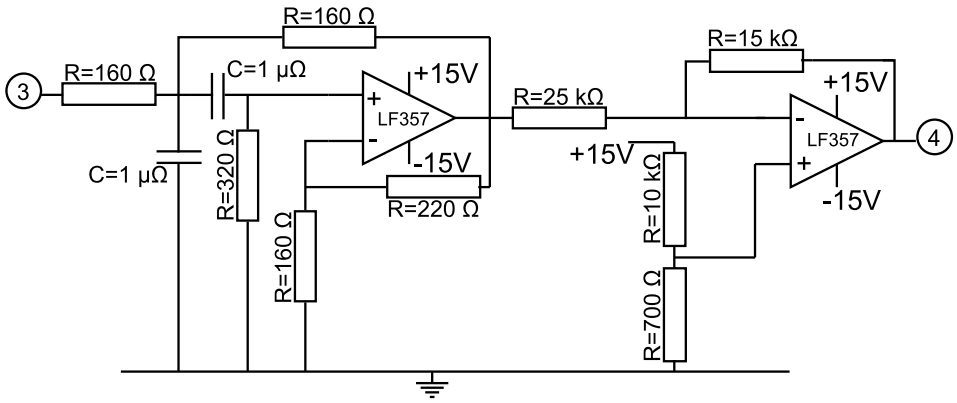

Figure 3.28: Filter with amplitude and offset adjustment circuit

Transfer function of the filter $A(s)$ is visible in Fig. 3.30 and its equation is:

$$A(s) = \frac{G\,R\,C\,s}{1 + R\,C\,(3-G)\,s + (R\,C\,s)^2} \tag{3.16}$$

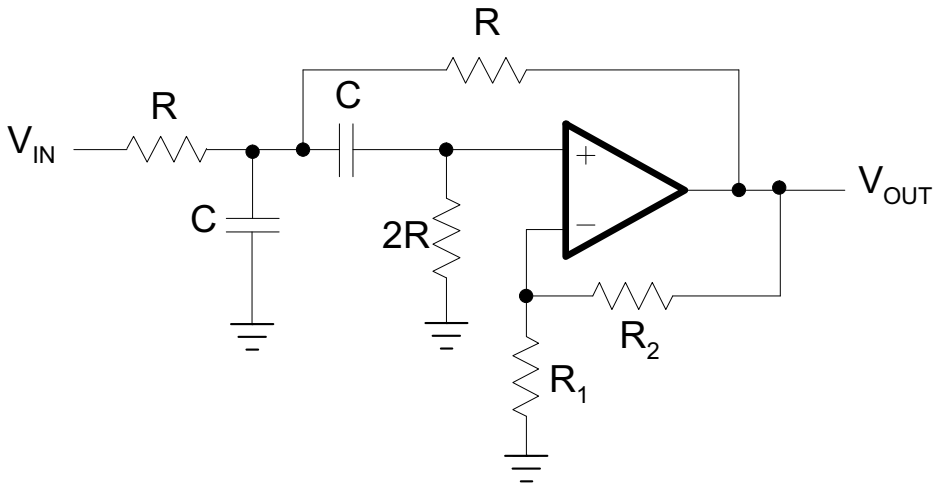

Figure 3.29: Sallen-Key band-pass filter

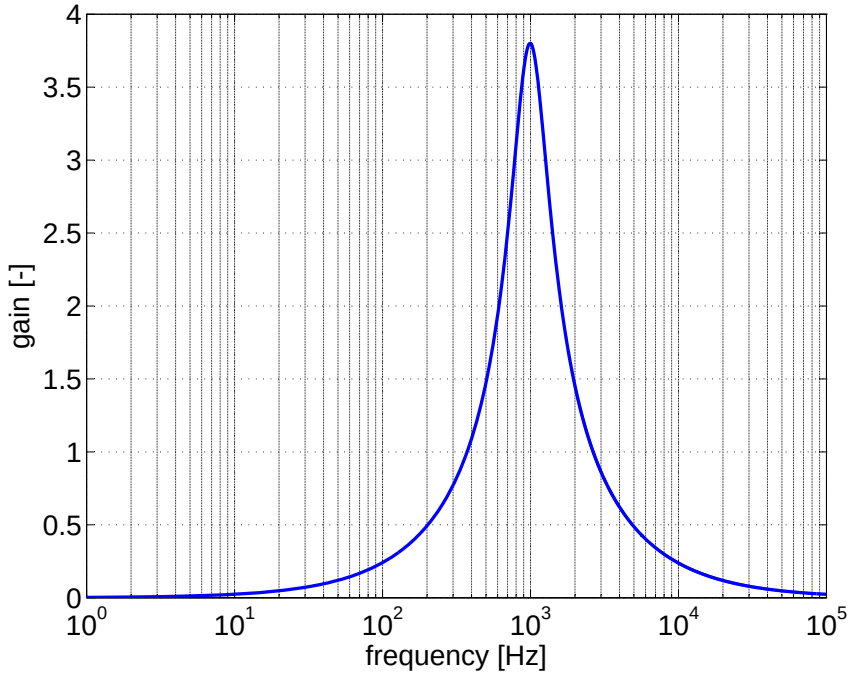

Figure 3.30: Transfer function of the filter

with the mid-frequency f_m:

$$f_m = \frac{1}{2\pi\ R\ C} \tag{3.17}$$

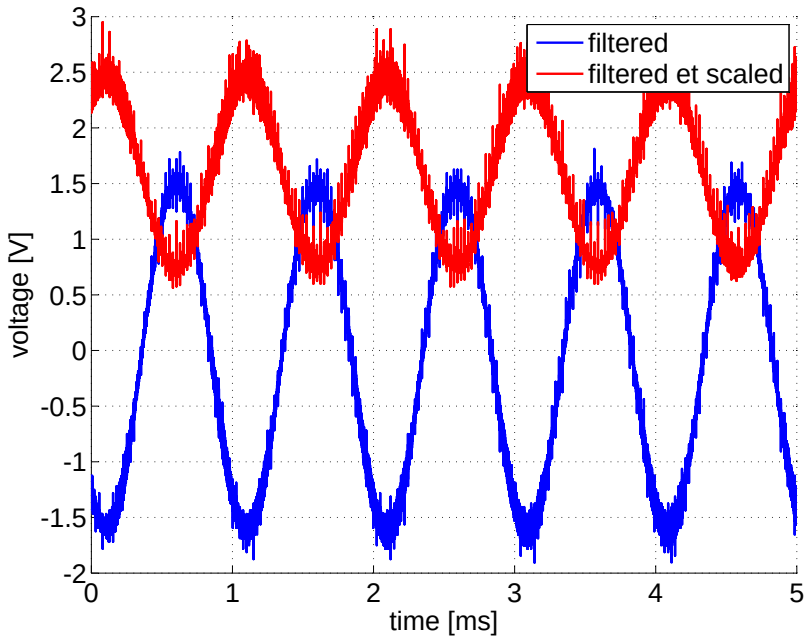

Figure 3.31: Visualization of amplitude and offset adjustment

and the inner gain, G:

$$G = 1 + \frac{R_1}{R_2} \tag{3.18}$$

3.6.2 Amplitude and offset adjustment circuit

As for the scan signal only, we have to adjust the amplitude and the offset of the scan current to obtain a signal in the range between 0 and 3.3 V. This adjustment circuit is placed just after the Sallen-Key filter as shown in Fig. 3.28 and the whole circuit is inserted between ③ and ④ in Fig. 3.18. The amplitude and offset adjustment performed by the INA117 is now redundant and could be removed, but is kept in order to have the possibility to treat the signal before the filtering.

Fig. 3.31 shows the filtered and scaled signals.

3.6.3 DSP acquisition

Fig. 3.32 shows the values of S for different values of the air gap δ. We see again that there is a good differentiation of the position in function of S. It is again possible to create a look-up table and implement it in the DSP in order to perform position detection. The values of S are not

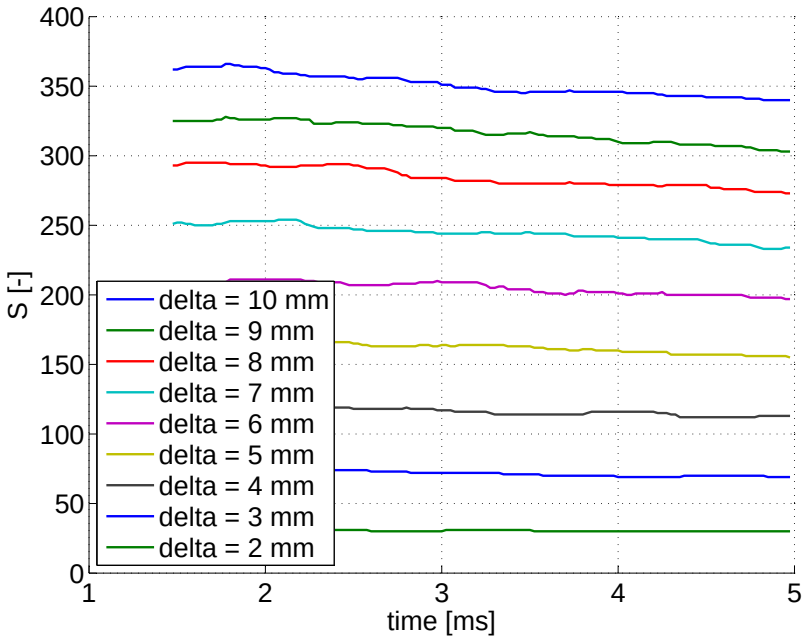

Figure 3.32: Sum of square difference to the average

completely constant due to the presence of the 50 Hz component, which means that the filtering should be improved. The final results on position and speed which can be seen in chapter 5 are analogically and digitally better filtered.

3.6.4 Results

When we move manually the mover, Fig. 3.33 shows dynamical results with both main and scan current. The method of position detection is still accurate even if we see in the figure that the position detection is less precise. The parameters of the filters and the adding of digital filters allow more precise results that are shown while speaking about filters and speed control of the prototype in chapters 4 and 5.

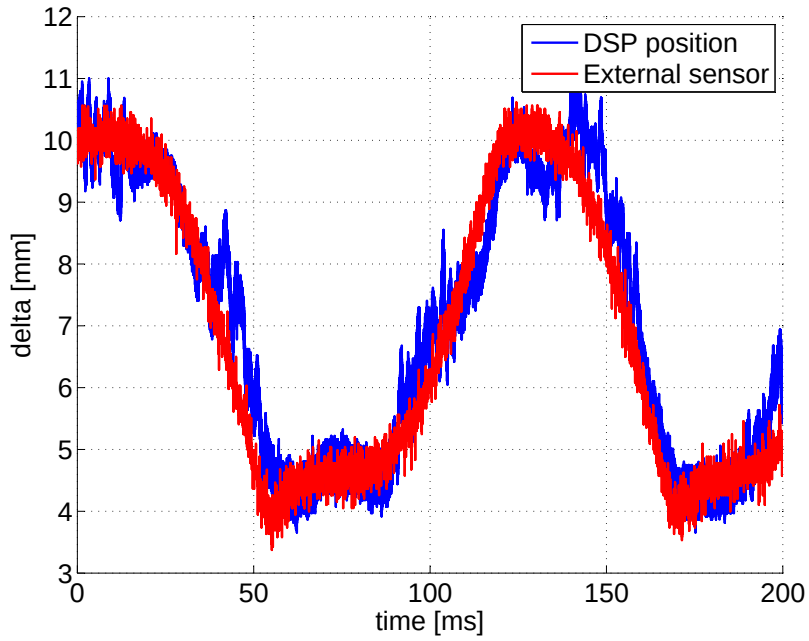

Figure 3.33: Comparison with an external sensor

4 Adapted Kalman filter for filtering noisy position and speed signals

4.1 Introduction

Position detection was presented in chapter 3. The measured position is contaminated by various noises and it is impossible to directly obtain the speed by deriving this position. Consequently, the position and the speed have to be filtered. The principle is: the measured position is filtered and derived to obtain the 'measured' speed; then, the speed (which is the signal to control) is also filtered in order to have an even cleaner measured signal at the end of the process.

Kalman filter algorithm can be very effective for filtering signal in order to regulate speed [5] but is difficult to implement in a DSP because of its relative complexity. This chapter presents a method to filter position and speed quickly and simply enough to be implemented in a DSP.

The originality of the chapter is an adaptation of Kalman filter for the case of time-limited computation. It also describes a method to determine the Kalman filter factors that allow the best filtering with the help of signal references (for position and speed).

4.2 State of the art

[53] uses an extended Kalman filter algorithm, which is a variation of the Kalman filter for application to solve non-linear problems, in order to filter the estimated position of the manipulator of a robot. The position is obtained from sensors that are placed at end-points. As the position is estimated at sample frequency of 61 Hz, the author can implement the extended Kalman filter algorithm without calculation lines problems. Indeed, with this sample frequency the calculation time between two samples is sufficiently long not to be a problem. Consequently a model is developed that relates feature point locations to the relative camera which is the external sensor. The problem is non-linear and, as Kalman filter requires a linear state space model, the output equations are linearized at each step of time. The noise has to be properly modeled by covariance matrices in the filter in order to have optimal estimation.

[20] develops a Kalman filtering method for estimating the position of fast-moving touch points in touch panels when the drawing mode is activated. The dynamic behavior is described by state equations. The position is first evaluated by an adaptative linear neural network (ALNN) but the Kalman filter allows more accurate results.

[45] applies the extended Kalman filter for sensorless speed direct-torque control (DTC) of induction motor drive system. The filter estimates the stator flux and the rotor speed in low-speed conditions. The covariance matrices of measurement and system noises are known and the filter is directly implemented on a DSP. The frequency of the PWM is not mentioned but as the objective is to accelerate the rotor from 0 to 10 rpm in 1 second, which is relatively slow, the implementation of the filter on the DSP does not generate a calculation lines problem.

[37] uses extended Kalman filter for the same application which is the sensorless DTC of induction motor for speed control. The author states that the extended Kalman filter improves the system performance at low speed but has to deal with bias problems when the stochastic noise used to calculate the error covariance does not match the real noise. The author only presents simulation results and they have to be validated by implementing the filter on a DSP and measuring the real speed on a test bench.

[57] also uses the extended Kalman filter to estimate the inverse rotor time constant (R_r/L_r) of an induction motor. The estimation is based on the stator voltages and currents and the rotor speed. A PWM drives the motor and simulation and experimental results show that the Kalman filter is capable to estimate the rotor time constant if the rotor speed is constant or time varying. The problem is that the extended Kalman filter takes a lot of calculation lines. The author explains that at each step of the filter, the DSP makes 700 multiplications and 600 additions, which is not a problem for this particular application but is impossible in our application to implement because we need computational space to perform the position estimation. We will see further in the chapter that for the adaptation of Kalman filter only 2 equations are needed and this represents 1 multiplication and 6 additions, which is obviously simpler to implement on the DSP.

[55] adopts the extended Kalman filter to estimate the position and speed of the rotor of a bearingless permanent magnet synchronous motor. The Kalman filter takes into account the system and measurement noise and gives high robustness against parameter variations. A simulation model of the motor has been developed on Matlab and, by detecting the stator voltages and currents, the rotor speed can be estimated accurately. Experimental measurements have still to be done.

[23] proposed a speed sensorless DTC control based on the extended Kalman filter for a surface permanent magnet synchronous motor (SPMSM). The Kalman algorithm in all the articles cited in the precedent paragraphs are relatively similar to this one. Their application change a little bit but all the authors agree to say that the Kalman filter is robust and accurate. In this particular article, the author notes some inaccuracies in the filter that causes delays in the speed and rotor angle and he needs to study further his method.

[2] compares its own Kalman filter called “Fingerprint Kalman Filter" (FKF) with other Kalman-type filters. Its definition for Kalman-type filters is filters that approximate and store only the current estimate and error covariance. The author shows by experimental results that the FKF is more effective than the conventional Kalman filter but even if the method is considered to require small computational and memory, it is still very complex and would be impossible to implement on a DSP for our application.

The literature shows that Kalman filter is widely used to filter noisy signals mainly because of its accuracy and of the fact that a memory is not needed. The objective of this chapter is to simplify the filter in order to be easily implemented on the DSP. We will see further in the chapter that by the adaptation of the Kalman filter, the error covariance is included inside the Kalman parameter K which is even simpler of the definition given in previous paragraph. Consequently, even if the term Kalman filter is uses toward the chapter, it may be fairer to speak about Kalman-inspired filter.

4.3 Kalman filter

4.3.1 Problem definition

The final objective is to control the speed of the mover. We saw in the chapter 3 the method to detect the position of the mover. In order to obtain its speed, this position has to be derived. But, as the measured position is noisy, the speed is impossible to determine without a filter.

The system has to filter only the noise without filtering the consequences of other disturbances like the wear of the contacts, a change of spring stiffness, or any other phenomenon that changes the speed of the mover and that the control system must detect. To illustrate the method, we work in this chapter with the speed reference v_{ref} described by the industrial specifications in section 2.4.2 with a speed of 0.4 m/s at the impact on the contacts. Consequently, in order to design the filter, the hypothesis is made that the mover has a speed v_{real} 10% higher than the speed reference (Fig. 4.1):

$$v_{real} = v_{ref} \cdot (1 + 0.1) \tag{4.1}$$

In general, the speed is supposed to always follow its reference; however in this case it is supposed that the control system did not achieve it. The reason to introduce this difference will be explained later. And consequently, in this case, the real position of the mover is:

$$x_{real} = \int v_{real} dt \tag{4.2}$$

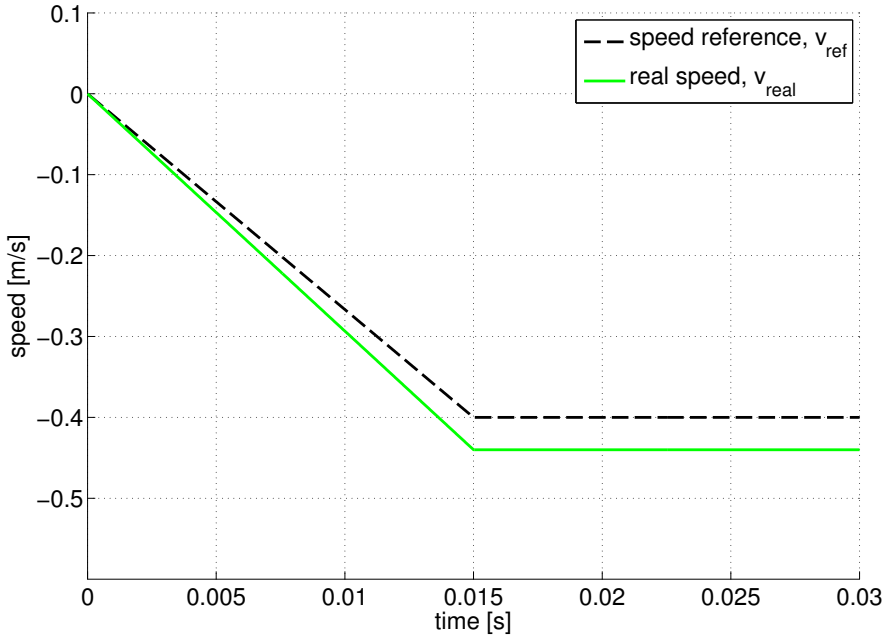

Figure 4.1: Comparison between the speed reference and the real speed

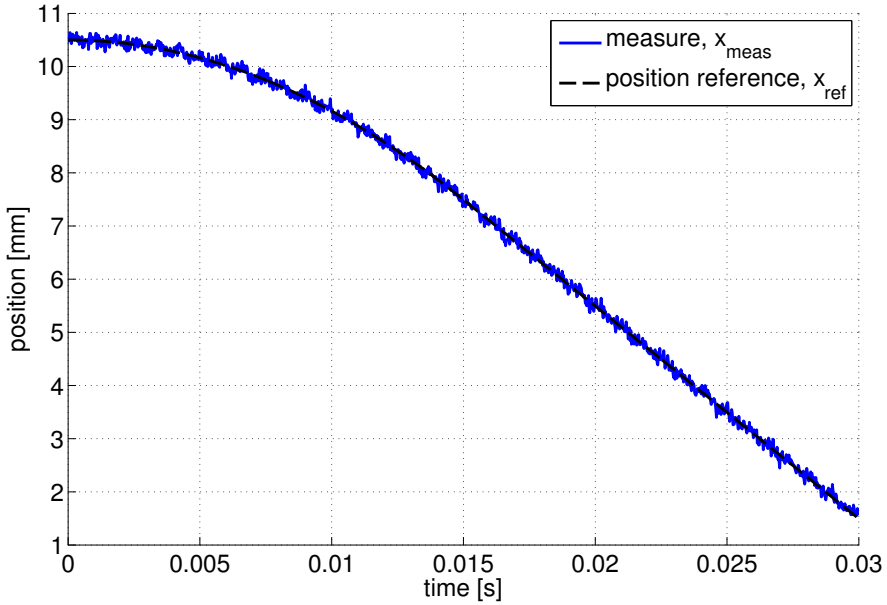

Figure 4.2: Noisy position of the mover versus time

Fig. 4.2 shows the measured position x_{meas} of the mover versus the time. A noise n is added artificially to the real position as:

$$x_{meas} = x_{real} + n \tag{4.3}$$

In order to have a noise that is close to reality, it is generated to correspond to the real noise measured on the test bench.

The noise is generated by the formula:

$$n = \epsilon((2R_1 - 1) + R_2 \sin(2\pi F_1 t) + R_3 \sin(2\pi F_2 t)) \tag{4.4}$$

ϵ is the amplitude of the noise. Here, $\epsilon = 10^{-5}$ m. R_1, R_2 and R_3 are random numbers between 0 and 1. F_1 and F_2 are frequencies of two sinusoidal components of noise. They can be varied in order to assess the impact of different noise frequencies. In this example, $F_1 = 1250$ Hz and $F_2 = 6250$ Hz. The noise has significant consequences on the calculation of the speed when it is derived. Fig. 4.3 shows the speed v_{meas} obtained by the direct derivation of x_{meas}. It is obviously unusable.

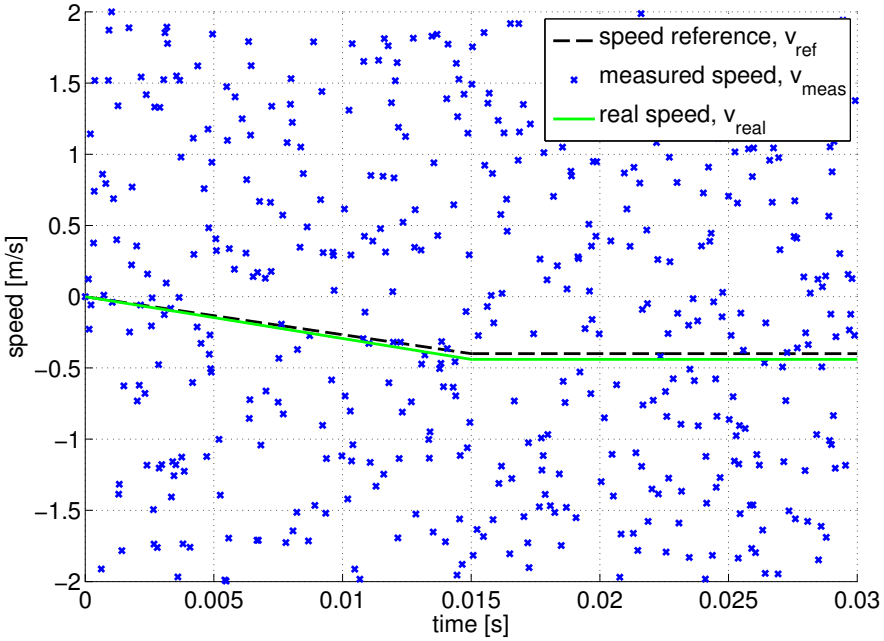

Figure 4.3: Speed after deriving the signal from Fig. 4.2

The filter should be able to obtain v_{real}. In other terms, the filter has to remove the noise while keeping the information on the disturbance due to "real" problems.

4.3.2 Discrete Kalman filter

The Kalman filter addresses the general problem of estimating the state $x \in \Re^n$ of a discrete-time controlled process that is governed by the linear stochastic difference equation:

$$x_k = Ax_{k-1} + Bu_{k-1} + w_{k-1} \tag{4.5}$$

with the measurement $z \in \Re^n$:

$$z_k = Hx_{k-1} + v_k \tag{4.6}$$

w_k and v_k represent the process and measurement noise (respectively). In our case, we assume that there is no noise during the process and $w_k = 0$.

The parameter A relates the actual state (x_k) to the precedent one (x_{k-1}) without any perturbation or noise. The parameter B relates the precedent control input u_{k-1} to the actual state. z_k is the actual measured signal and H relates the state to the measurement.

The discrete Kalman filter algorithm is described in [52]. Its time equations are:

$$\hat{x}_k^- = A\hat{x}_{k-1} + Bu_{k-1} \tag{4.7}$$
$$P_k^- = AP_{k-1}A^T + Q \tag{4.8}$$

and its update equations are:

$$K_k = P_k^- H^T (HP_k^- H^T + R)^{-1} \tag{4.9}$$
$$\hat{x}_k = \hat{x}_{k-1} + K_k(v_{meas,k} - H\hat{x}_{k-1}) \tag{4.10}$$
$$P_k = (1 - K_k H)P_k^- \tag{4.11}$$

Q and R are respectively the process noise covariance and the measurement noise covariance. The sign ˆ denotes estimation and the superscript $-$ denotes the a priori state estimation.

$\hat{x}_k^-$ is the a priori state estimation and $\hat{x}_k$ the a posteriori state estimation. P_k^- and P_k are respectively the a priori and a posteriori estimate error covariance. K is the gain that minimizes the errors between the real state x_k and the estimated states $\hat{x}_k^-$ and $\hat{x}_k$.

We will see in the next sections (4.3.3 - 4.3.8) that we adapt the Kalman filter in order to minimize the calculation time of the algorithm. Consequently, H is equal to 1 because the state is directly measured. In addition, P, R and Q desappear in the final algorithm because in this case K is constant. As we assume there is no control at this level of filtering, B is set to 0.

4.3.3 Adapted Kalman filter applied to a random constant

It is difficult to implement these equations in the DSP, because they are too time consuming for our application. At this stage, the Kalman filter is adapted in order to filter a random constant

[52]. In this case, (4.7)-(4.11) become:

$$\hat{x}_k^- = \hat{x}_{k-1} \tag{4.12}$$
$$P_k^- = P_{k-1} + Q \tag{4.13}$$
$$K_k = \frac{P_k^-}{P_k^- + R} \tag{4.14}$$
$$\hat{x}_k = \hat{x}_{k-1} + K_k(v_{meas,k} - \hat{x}_{k-1}) \tag{4.15}$$
$$P_k = (1 - K_k)P_k^- \tag{4.16}$$

As we filter a constant, A is equal to 1. We will see in the next section how A is adapted in order that the filter could manage non-constant signals.

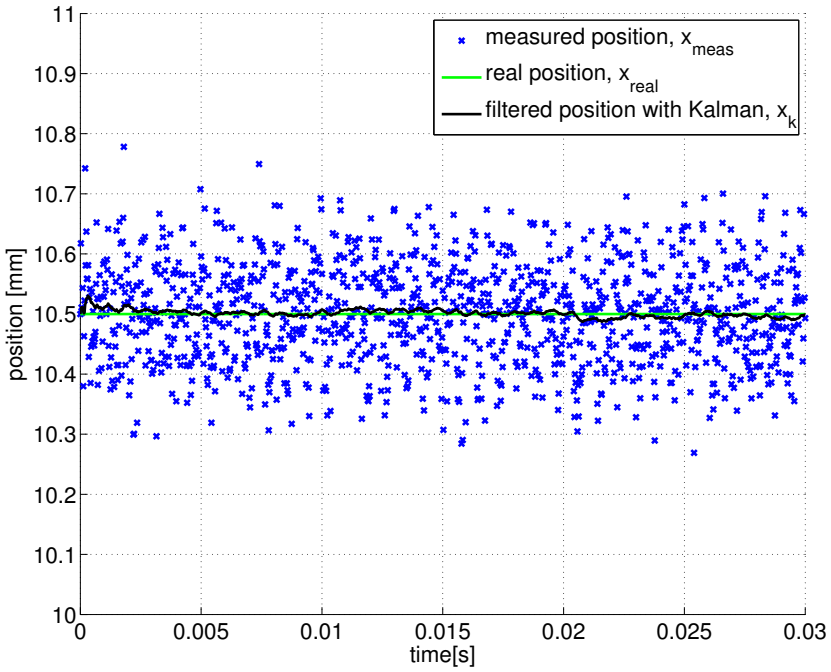

Figure 4.4: Filtering of a random constant using the adapted Kalman filter (x = 10.5 mm)

As an example, Fig. 4.4 shows a measured constant position (x = 10.5 mm, R = 10 and $Q = 10^{-5}$) and this position filtered with the adapted Kalman filter. We see that the signal is well filtered.

4.3.4 Adapted Kalman filter applied to actuator signals

In our application, the position is not constant but varies with time. Fig. 4.5 shows that the filter is not effective anymore. It introduces a delay, so that the measured position does not match the real one.

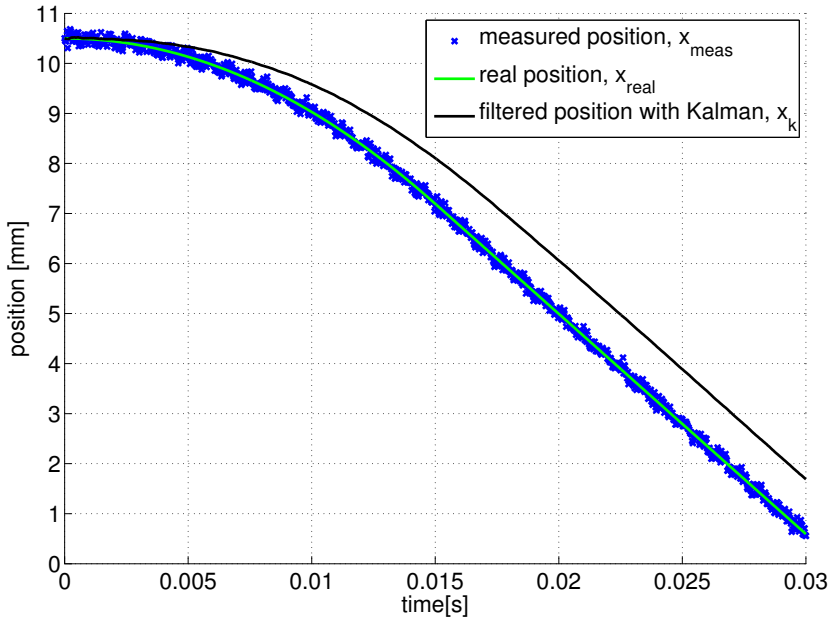

Figure 4.5: Filtering of a non-constant signal using the adapted Kalman filter

This problem is solved by correcting $\hat{x}_k^-$ with the slope of the position reference x_{ref}.

$$x_{ref} = \int v_{ref} dt \tag{4.17}$$

It means that the position reference is used to help filtering (even in the case when it differs from the real one). It could be seen as a modification of the parameter A in equations (4.7) and (4.8). Consequently, (4.12) is replaced by:

$$\hat{x}_k^- = \hat{x}_{k-1} + (-x_{ref,k-1} + x_{ref,k}) \tag{4.18}$$

Fig. 4.6 shows the resulting filtered position. The gain K is evaluated at each step and Fig. 4.7 shows its value versus time. In this case we also supposed that the position differs from its reference. This value of K is calculated in (4.14) which consumes a lot of calculation lines when implemented in the DSP mainly because of the division.

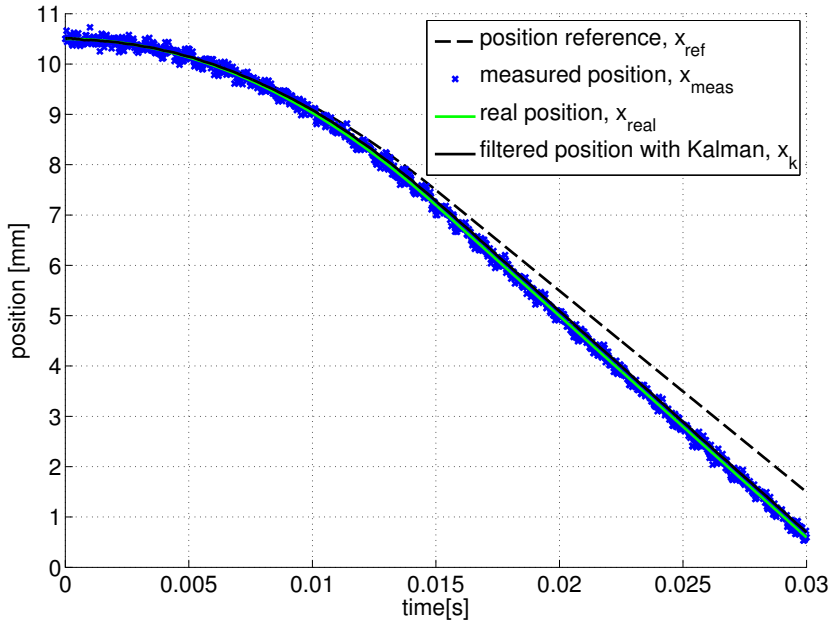

Figure 4.6: Filter with slope correction

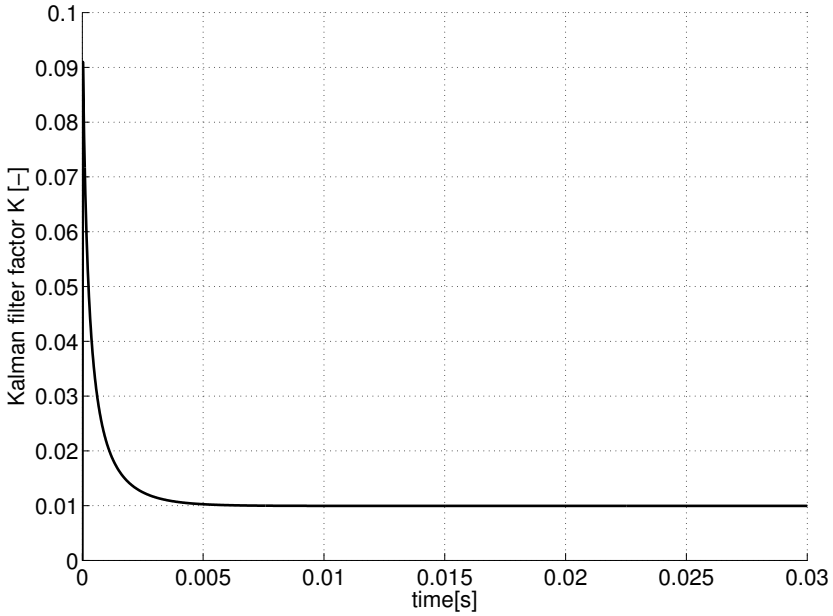

Figure 4.7: Kalman filter factor K versus time

4.3.5 Kalman filter with a constant K

In order to further reduce the calculation time, we consequently used a constant K and Fig. 4.8 shows the filtering when K is a constant value.

In order to choose its optimal value, we search the K that minimizes the difference between the

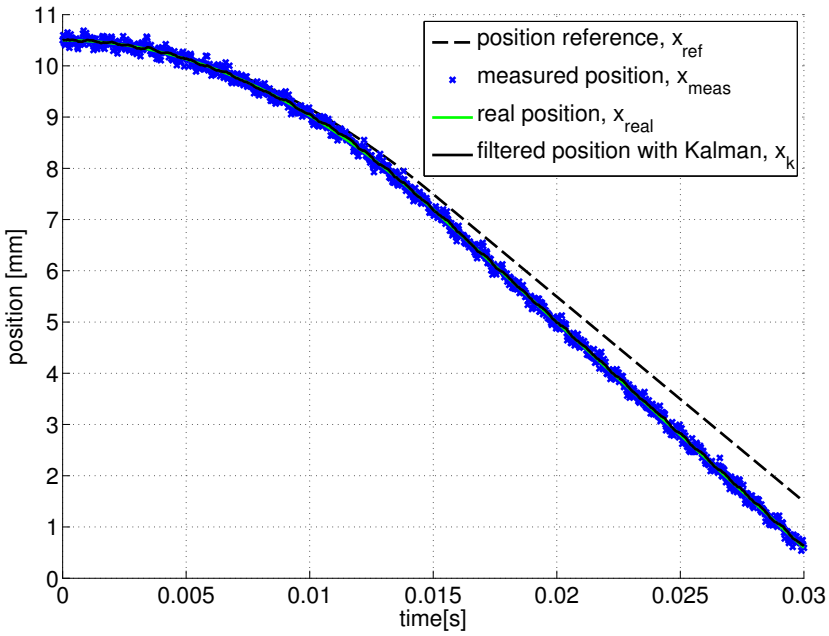

Figure 4.8: Adapted Kalman filter with constant K

filtered position x_k and the real position x_{real} using the least square method (Fig. 4.9), which gives finally $K = 58.1 \cdot 10^{-3}$ [35].

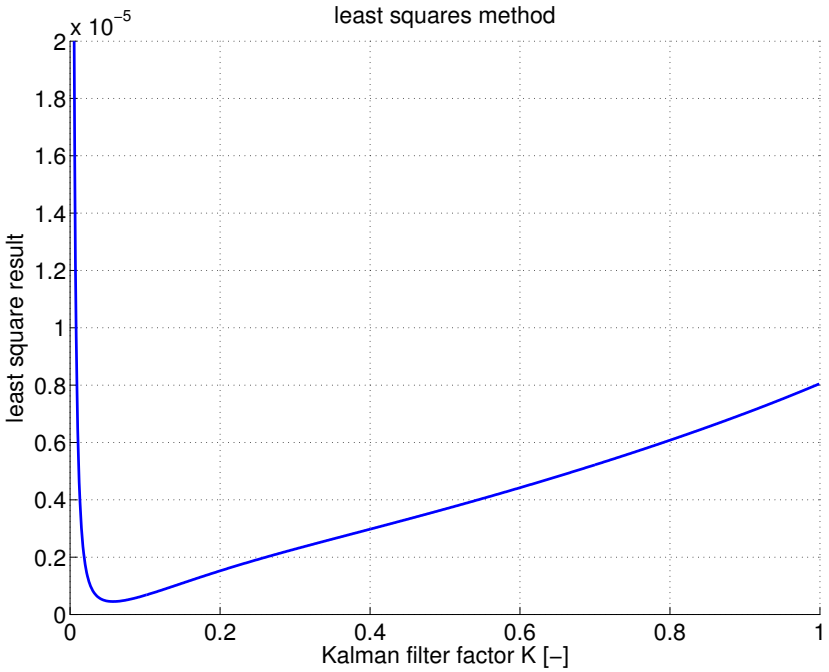

Figure 4.9: Determination of K with the least square method

4.3.6 Practical explanation

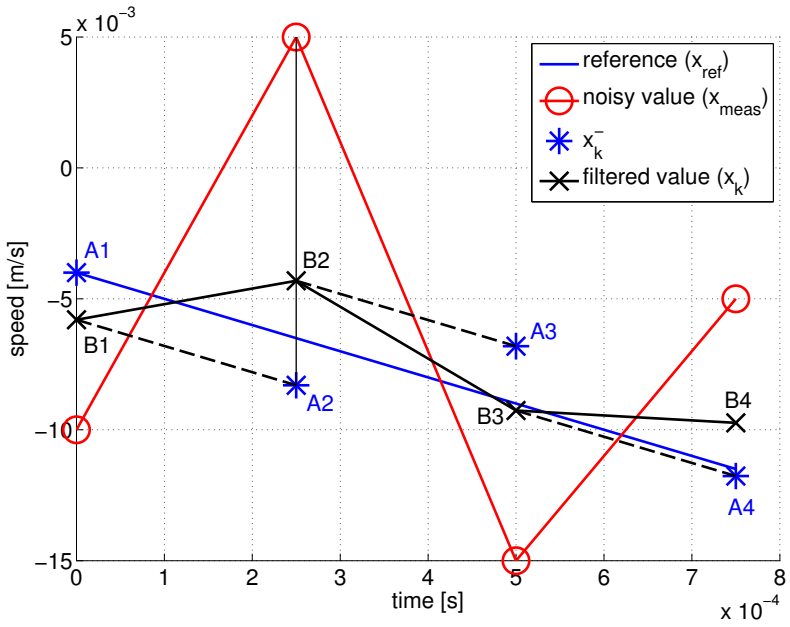

Figure 4.10: Kalman filtering explanation

Fig. 4.10 explains how the presented method works practically. First, $\hat{x}_k^-$ is set to the first value of the reference v_{ref} (Here, $\hat{x}_1^- = -0.004$, point A_1). Then, the error E between the noisy value v_{meas} and $\hat{v}_k$ is calculated:

$$\begin{aligned} E_1 &= x_{meas,1} - \hat{x}_1^- \\ &= -0.01 - (-0.004) \\ &= -0.006 \end{aligned} \tag{4.19}$$

In order to illustrate this example we choose the value $K = 0.3$ and consequently the filtered value $\hat{v}$ (point B_1) is:

$$\begin{aligned} \hat{x}_1 &= \hat{x}_1^- + K \cdot E_1 \\ &= -0.004 + 0.3 \cdot (-0.006) \\ &= -0.0052 \end{aligned} \tag{4.20}$$

Then, the second value of $\hat{x}^-$ is a correction of $\hat{x}$ with the slope of the reference (point A_2):

$$\begin{aligned} \hat{v}_2^- &= \hat{v}_1 - v_{ref1} + v_{ref2} \\ &= -0.0052 - (-0.004) + (-0.0065) \\ &= -0.0077 \end{aligned} \tag{4.21}$$

This process is repeated at each step to filter the signal properly. The array B_1, B_2, B_3... will form the filtered signal.

4.3.7 Interpretation of factor K

Factor K ($0 \leq K \leq 1$) is actually a coefficient that determines the proportions of reference and measurement that the filter takes into account. $K = 1$ means that the measured signal is not filtered at all, whereas $K = 0$ means that the measured signal does not have any influence on the result and that only the reference plays a role in determining the filtered signal. The optimal value of K is determined using the least square method between the filtered signal x_k and the real one x_{real}.

4.3.8 Comparison with sampling filter

The DSP works at 40 kHz and the contactor is closing in 30 ms. This means that there are 1200 points of position evaluation. A good way to filter could be to sample these points. Fig. 4.11 shows the position sampled at every 32 points, x_f.

Fig. 4.12 shows that the position filtered with the adapted Kalman filter x_k is less delayed compared to x_f and above all there is no need to stock in the memory of the DSP all the former values of speed. We can see in Fig. 4.13 that the filtered speeds v_f, derived from x_f, and v_k derived from x_k are less noisy than the speed directly derived from the measurement of the position x_{meas} shown in Fig. 4.3.

In the next section, we will see exactly how we filter both signals (position and speed) and also show the measurements on the test bench when we apply the Kalman filter factors calculated with the described method.

4.4 Application of the filter to the prototype

4.4.1 Determination of the Kalman filter factors K_x and K_v

The speed v_k obtained by deriving the position filtered using the adapted Kalman filter x_k is also filtered using the same method. Consequently, there exist two Kalman filter factors, K_x for the

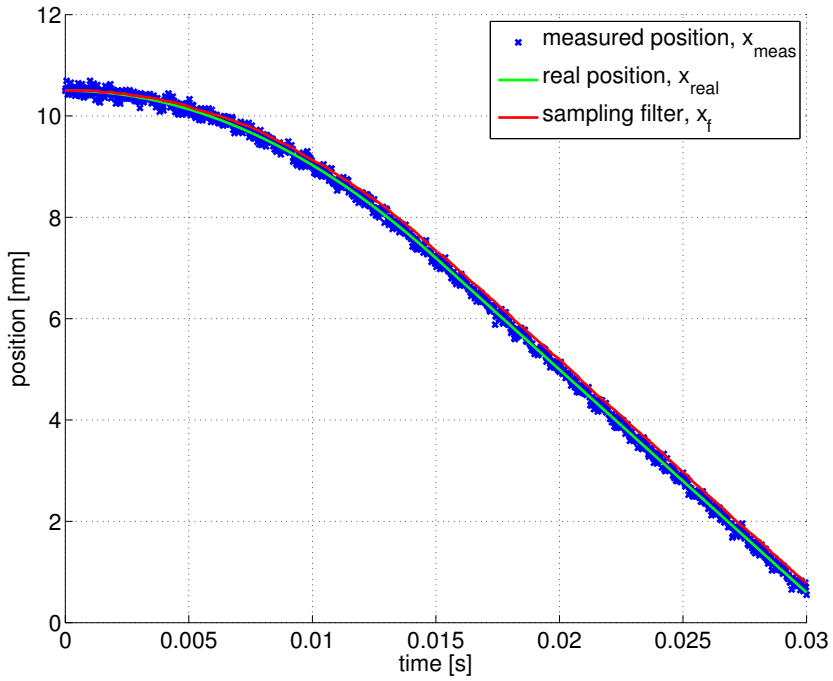

Figure 4.11: Filtered position on 32 points

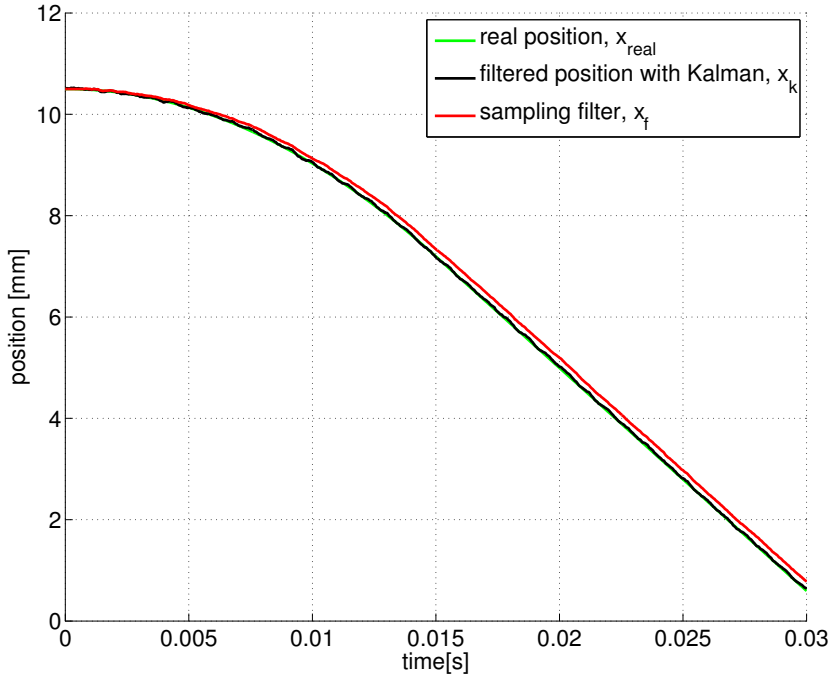

Figure 4.12: Speed comparison between Kalman and sampling filter on the position

position and K_v for the speed.

In order to determine these Kalman filter factors we have minimized the difference between the

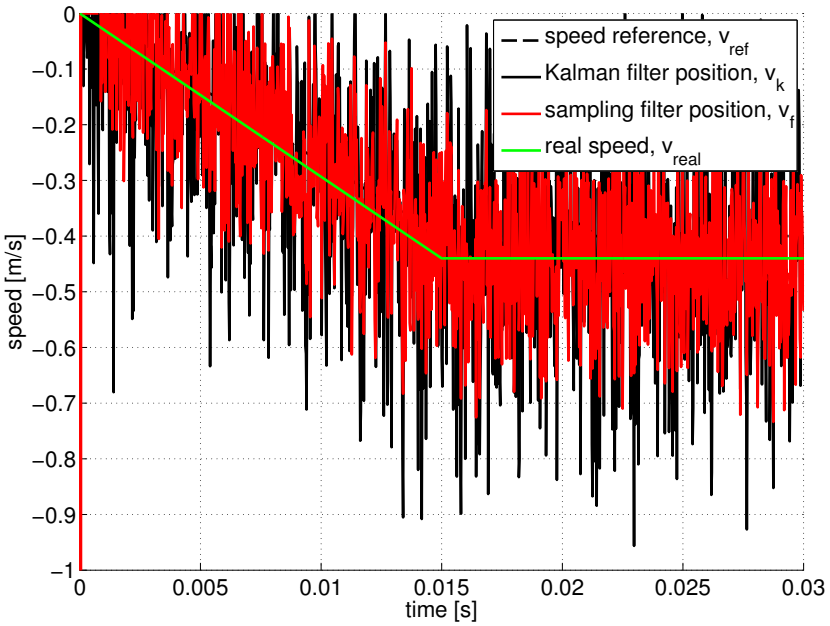

Figure 4.13: Speed comparison between Kalman and sampling filter on the speed

filtered speed v_k and the speed reference v_{ref} using the least square method for both K.

We have already seen that if the least square method is directly performed on the noisy signal x_{meas}, it appears that the best way to filter the signal is to set both K_x and K_v to 0 (filtered signal equal to the reference). And, in this case, the system will not be able to detect any difference between the real speed and its reference (which we can call speed offset) due to various perturbations (unexpected temperature rise, spring or contact wear).

In order to be able to detect a speed of 10% around its reference (as we suppose that 10% is a maximal expected difference between the two signals), two more speed signals that are 10% below (v_{real2}) and above (v_{real3}) the reference ($v_{real} = v_{ref}$) are introduced as (Fig. 4.14):

$$v_{real2} = (1-0.1)\,v_{ref} = 0.9\frac{dx_{ref}}{dt} \tag{4.22}$$

$$v_{real3} = (1+0.1)\,v_{ref} = 1.1\frac{dx_{ref}}{dt} \tag{4.23}$$

Actually v_{real3} is v_{real} presented in section 4.3.

Using equations (4.2) and (4.3), it is possible to determine the 3 measured positions x_{meas}, x_{meas2} and x_{meas3} from v_{real}, v_{real2} and v_{real3}. Then, the artificial noise is added to those positions to obtain the 'measured' ones.

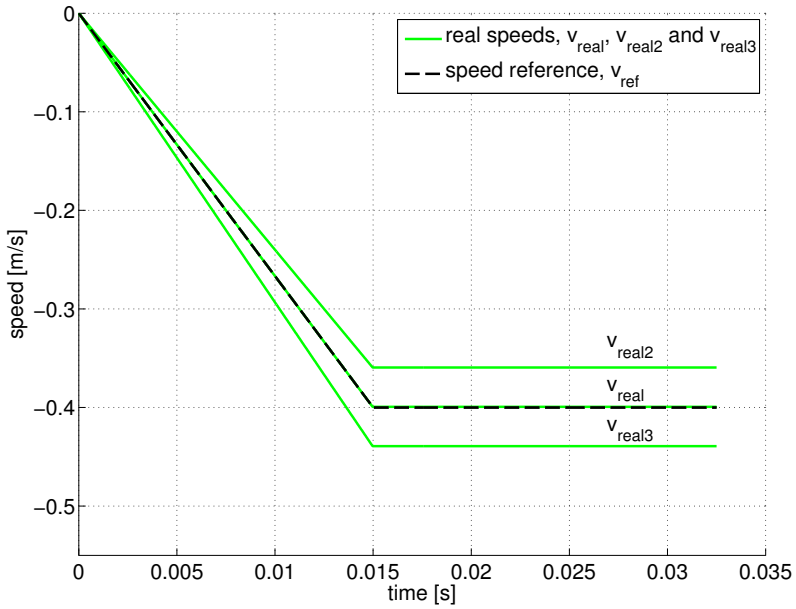

Figure 4.14: 10% speed offset around the reference

These 3 measured positions are filtered with the Kalman filter to obtain the filtered positions x_k, x_{k2} and x_{k3}. The speeds v_k, v_{k2} and v_{k3} are derived from those filtered positions. They are then filtered to obtain v_{kk}, v_{kk2} and v_{kk3}. Factors K_x and K_v are calculated with the least square method that is applied to all three speeds in order to minimize F:

$$F = \sum[(v_{real} - v_{kk})^2 + (v_{real2} - v_{kk2})^2 + (v_{real3} - v_{kk3})^2] \tag{4.24}$$

Fig. 4.15 shows that the optimal values are $K_x = 13 \cdot 10^{-3}$ and $K_v = 12 \cdot 10^{-3}$.

Fig. 4.16 shows the resulting filtered speed using these Kalman filter factors.

It is interesting to compare this filter with the sampling filter. Fig. 4.17 shows the speed filtered over 32 sampling points for the positions and 64 for the speed. It is possible to have better filtered results by increasing the sampling periods but the delay becomes a problem that we do not have with the Kalman filter.

4.4.2 Results

We now apply these Kalman factors to the industrial contactor. Figs. 4.18 and 4.19 show the result before and after Kalman filtering.

There are still some fluctuations but the speed is completely usable and it is possible to be regulated by adapting the current reference if, for any reason, this speed deviates from the

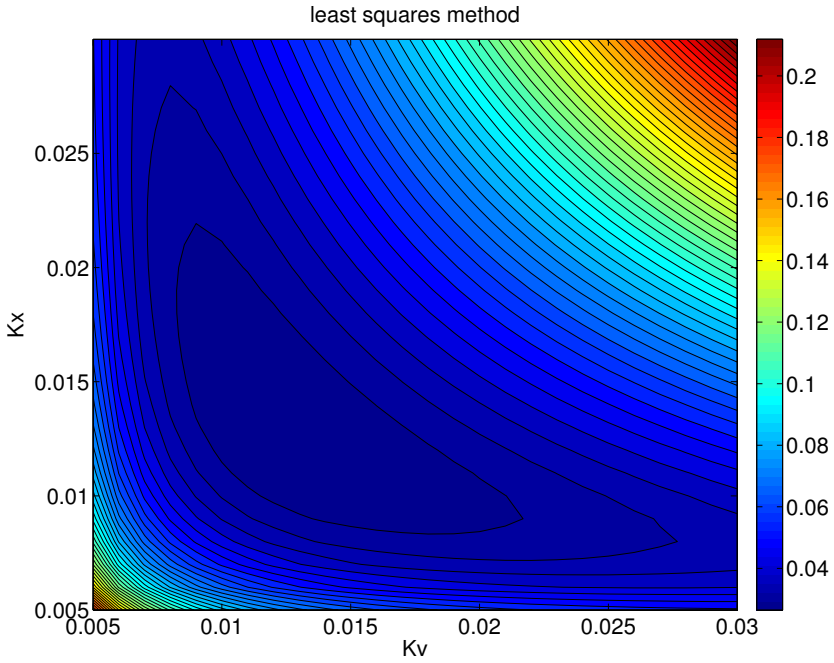

Figure 4.15: Least square method for determination of K_x and K_v

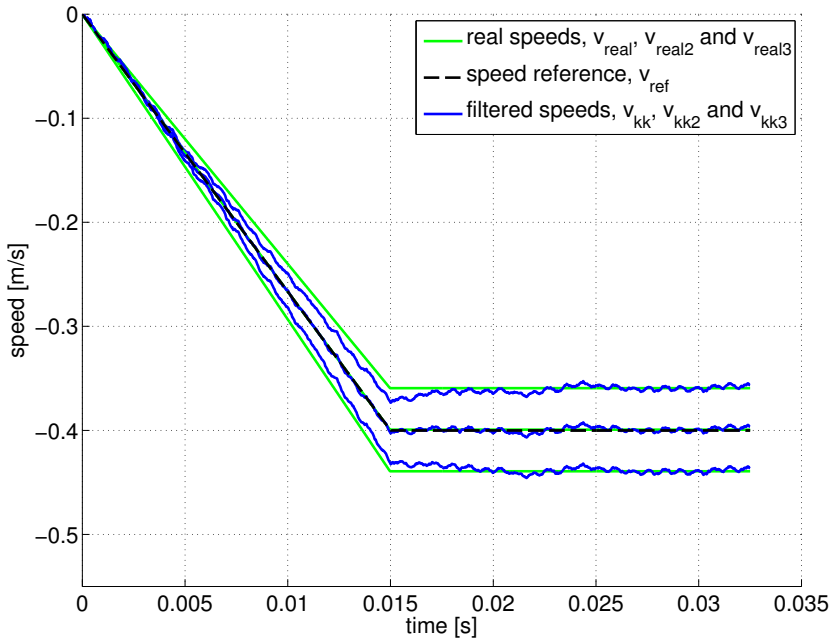

Figure 4.16: Kalman filter of position and speed with a 10% offset around the reference

reference. The next section will show how we manage to control the speed of the mover.

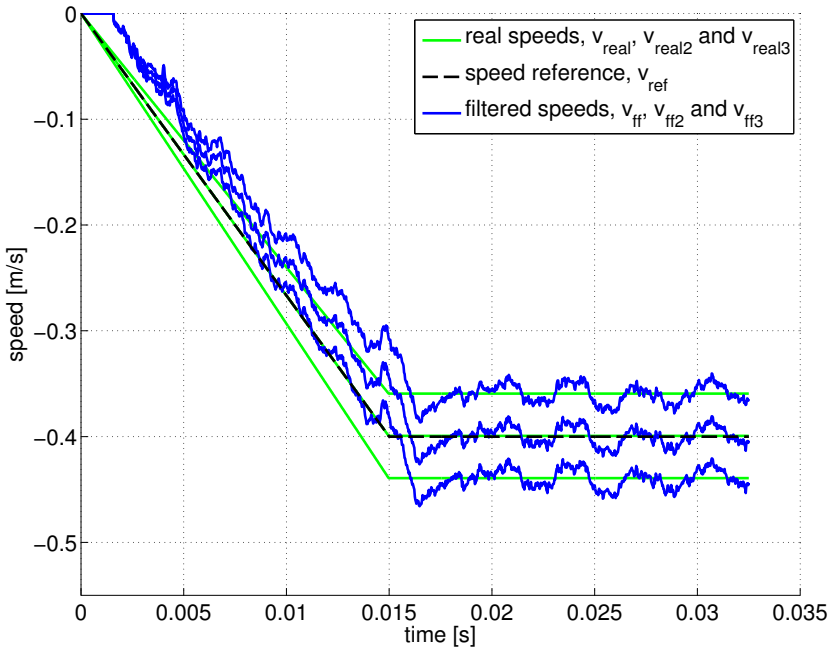

Figure 4.17: Sampling filter of position and speed with a 10% offset around the reference

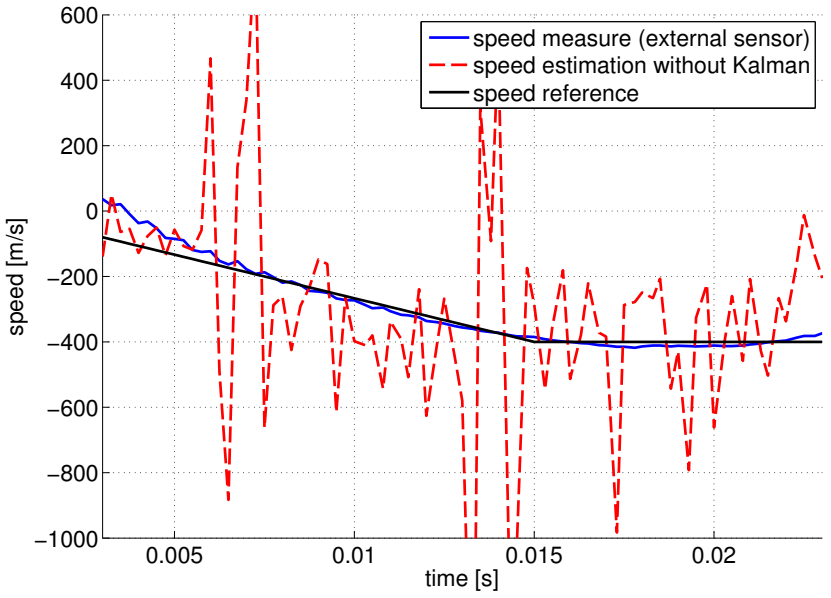

Figure 4.18: Test bench measurement without filter

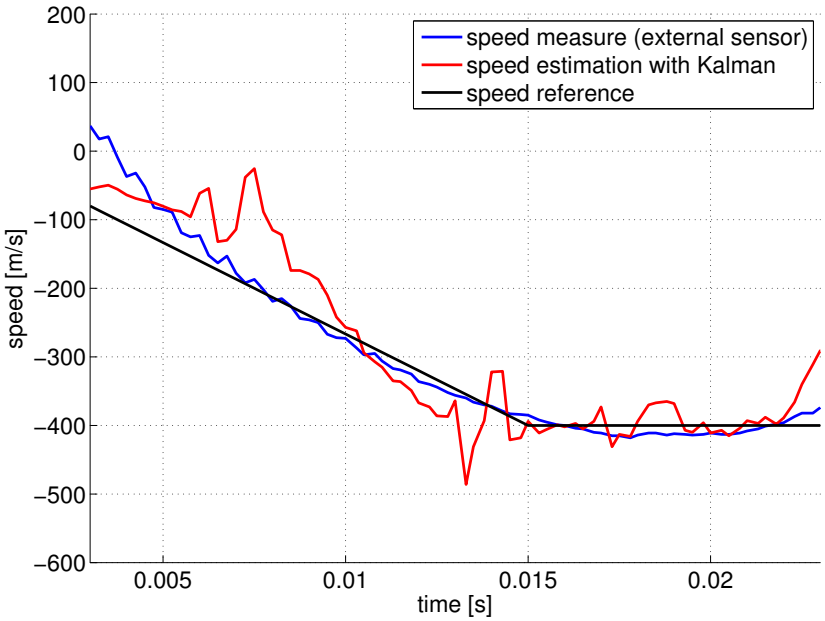

Figure 4.19: Test bench measurement with Kalman filter

5 Sensorless speed control of the electromechanical actuator

5.1 Introduction

Now that we have designed the actuator in chapter 2, detected without sensor the position of its mover in chapter 3 and filtered the position and speed in order to measure the speed simply and accurately in chapter 4, we will see in the present chapter different strategies to control the speed of the actuator's mover.

In the first part of this chapter, we will use Matlab-Simulink in order to simulate the main control strategies. In the second part, we will apply these strategies to the industrial contactor. We will begin by using an external sensor in order to validate the control and then we will present the chosen strategy that is applied for the sensorless speed detection.

Finally, we will present the speed measurement on the prototype described at the end of chapter 2.

5.2 State of the art

The speed control is based on the theory explained in [24], which treats the digital control of dynamic systems.

Bühler [3] offers a broad introduction to all the knowledge needed to design automated systems, from the use of analog and digital signals to methods of analysis and theoretical synthesis and processes to automate.

Espinosa [13] uses fuzzy logic to control the speed at closing of a contactor and to limit the wear of the contacts. A fuzzy controller uses the position and speed as inputs and provides as output an intensity set point that controls the speed of the mover at the impact with the contacts. A low-cost electronic module that drives the control system is directly implemented in the contactor.

Ustun [48] uses a PID control implemented on a DSP to control the speed in a linear actuator with a NdFeB magnet excitation and a printed-circuit armature. A classical position-loop-gain controller is used with a PI speed controller and an inner-current control loop. Position and speed information are obtained from a linear sensor.

Lim [22] proposed a control solution by transforming a simple contactor “on/off” in an actuator known as “proportional”, which means that the speed is controlled all along the mover trajectory. A fast inner loop current controller and a slower PID outer loop trajectory controller are employed. He used an external sensor to estimate the position.

Braune [7] controls a linear motor for an electric valve with a PD control. A nonlinear feed-forward block, containing the inverse reluctance characteristics, is used to compensate the non-linear effects of the actuator and to ensure the stationary accuracy. He plans to study control strategies without sensors.

[15] studies the control of an electromagnetic actuator which can be used in various applications like electromagnetic valve, artificial heart actuators, magnetic levitation or electromagnetic brakes. The control is done by linear-varying parameter (LVP) control that consists in working at different equilibrium positions, where the system can be considered linear. Consequently a great part of the paper discusses different linearization techniques. The system gives good results but the time of closing is apparently very long and the computational calculations during the closing have to be taken into account for an implementation on a DSP for an application that is as fast as ours.

5.3 Control strategies

We studied the performances of the system in open and closed loop, with "all or nothing" (full voltage or zero) control or with a PID in order to finally keep 3 control strategies:

a) Open loop (All or nothing and voltage reference).

b) Closed loop (PI control).

c) PI control with an a priori reference.

5.3.1 Open loop control

Fig. 5.1 shows the open-loop block diagram.

In this control strategy, the loop is broken off before the block ’A priori’. Therefore, it is this block which gives the voltage reference u_{ref} to the actuator. x_l is the measurement of the position of the mover with an external sensor and x_e is the detected position obtained thanks to the scan current i. The position (x_l or x_e) is then derived to obtain the measured speed v_{meas} but, again, the loop is, in this particular case, not closed and the control is only done by the “a priori” block.

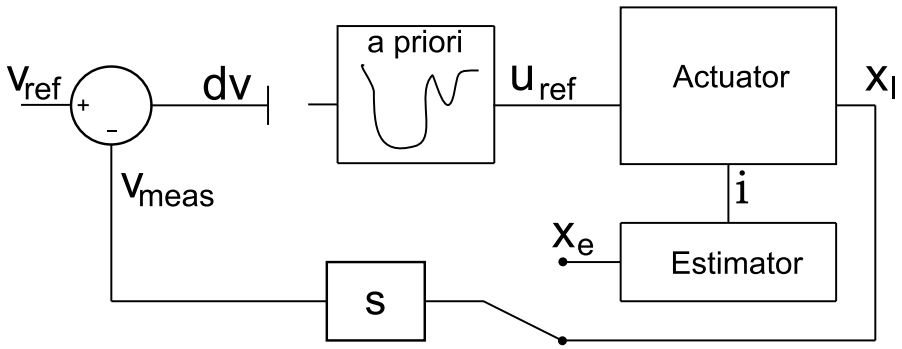

Figure 5.1: Block diagram of open-loop control

The objective of the specifications is to obtain the speed profile presented in Fig. 2.12 of subsection 2.4.2 but, as the speed at the impact is important, it seemed also interesting not to follow the profile but to have a speed of 0.4 m/s at the impact as the only objective. Knowing this, we decided to work with 2 different voltage reference profiles:

1) All or nothing reference between 0 and u_{max} (105 V).

2) Reference for a speed profile as close as possible to the one shown in Fig. 2.12 of subsection 2.4.2

5.3.2 Closed loop control

Fig. 5.2 shows the block diagram of the closed loop control.

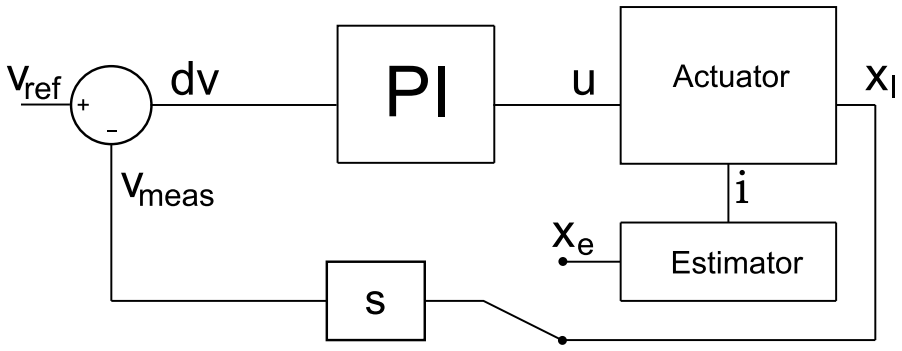

Figure 5.2: Block diagram of closed-loop control

Here the loop is closed and the measured speed v_{meas} is compared to the speed reference v_{ref} in order to obtain the speed difference dv. This difference is then used by the PI regulator to calculate the voltage u that drives the actuator.

We decided not to use the differential term of the PID regulator and to only work with a PI because the term D appeared not useful in this case and additionally, it generates some instabilities difficult

to remove. Indeed, when the speed is controlled, the term D derivate the noise, which becomes acceleration that perturbs the speed.

5.3.3 PI control of an a priori reference

Fig. 5.3 shows the block of the closed loop control of an a priori reference. It is actually a combination between the two precedent strategies. The a priori control voltage is u_{ref}. The PI controller issues a Δu in addition to the a priori value u_{ref} to generate the drive voltage u of the actuator. The speed difference dv allows to close the loop and to calculate Δu.

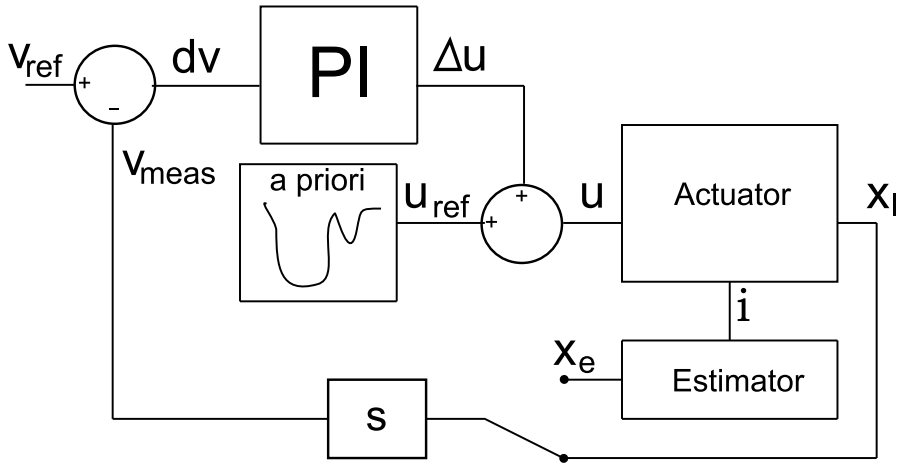

Figure 5.3: Block diagram of closed-loop control (CL) of an a priori reference

5.4 Simulink models of the industrial contactor

The objective of the Simulink model is to test the control algorithms before their implementation on the real DSP controlling the actuator.

5.4.1 Simulink overall model

Fig. 5.4 shows the overall model. The system consists of three main parts:

- The physical model of the linear actuator (grey block "Actuator model")
- The dynamic equation of motion (cyan block "Dyn equation")
- The speed control (green block "Regulation")

The black lines represent the values and subsystems containing pseudo-continuous values (clock frequency: 10 MHz), the red lines represent the discrete values and subsystems (f_e = 100 kHz)

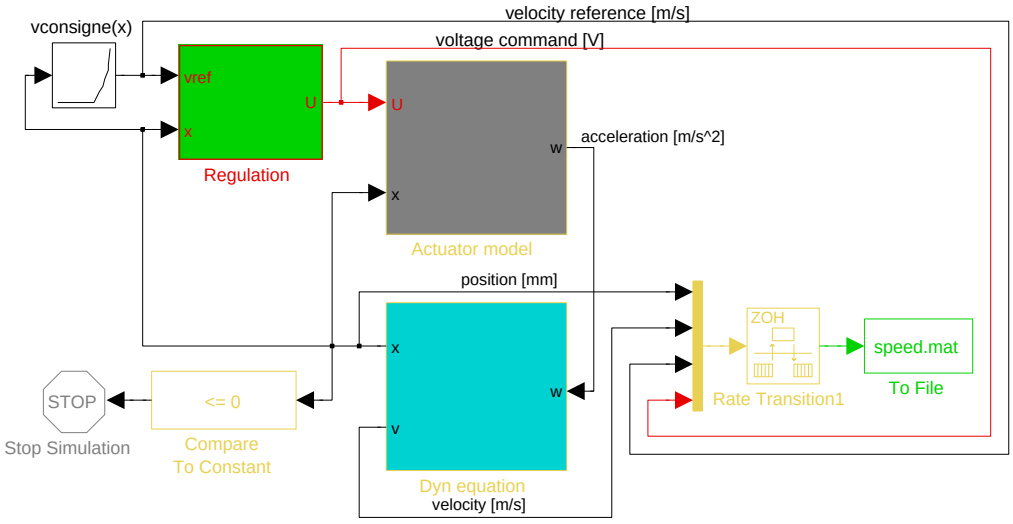

Figure 5.4: Simulink model of the actuator and its speed control

and beige lines represent mixed sub-systems.

5.4.2 The physical model of the linear actuator

Fig. 5.5 describes the actuator with the inputs, the voltage u and the airgap value x and the output, the acceleration w. The acceleration is calculated as:

$$w = \frac{F_L + F_{tot}}{m_{mob}} \tag{5.1}$$

F_{tot} is function of x and i, and is defined in a look-up table (Fig. 5.6) that is the result of FEM simulations. m_{mob} is the mass of the mover.

The grey block "I(x,U)" in Fig. 5.5 is detailed in Fig. 5.7 and models the equation derived from (3.1):

$$i = \frac{U - \frac{d\Psi}{dt}}{R} \tag{5.2}$$

Ψ is also defined by a lookup table resulting from the FEM simulations (Fig. 5.8).

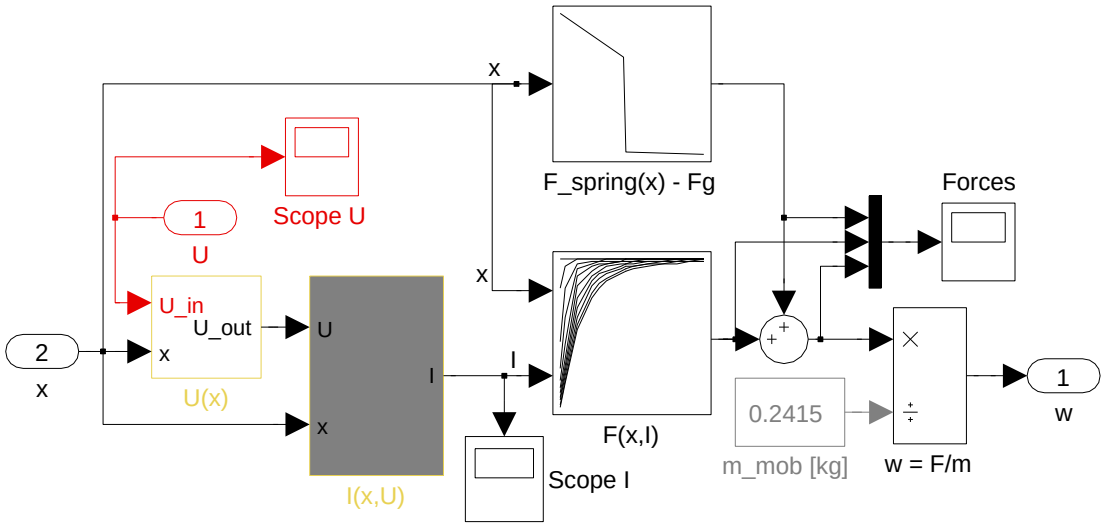

Figure 5.5: Physical model of the linear actuator

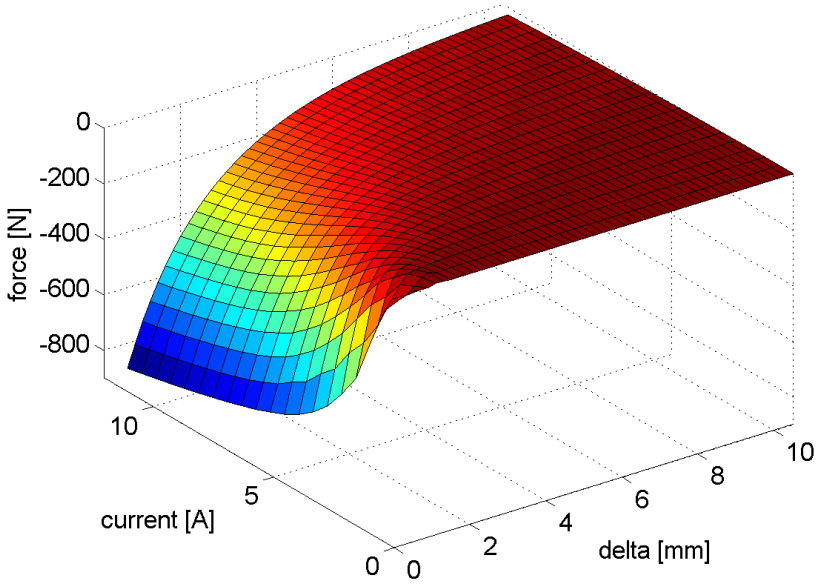

Figure 5.6: "lookup table" of forces simulated with Flux 2D

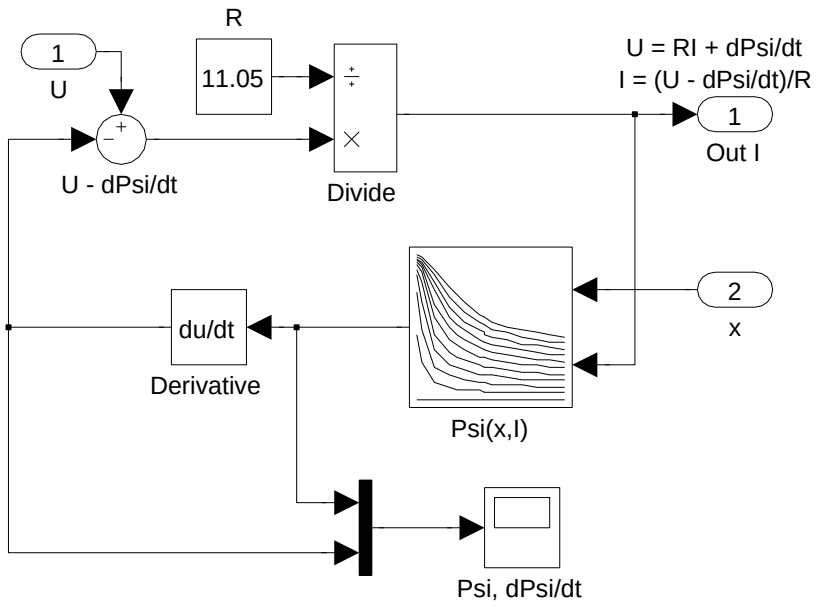

Figure 5.7: $I = f(U, x)$

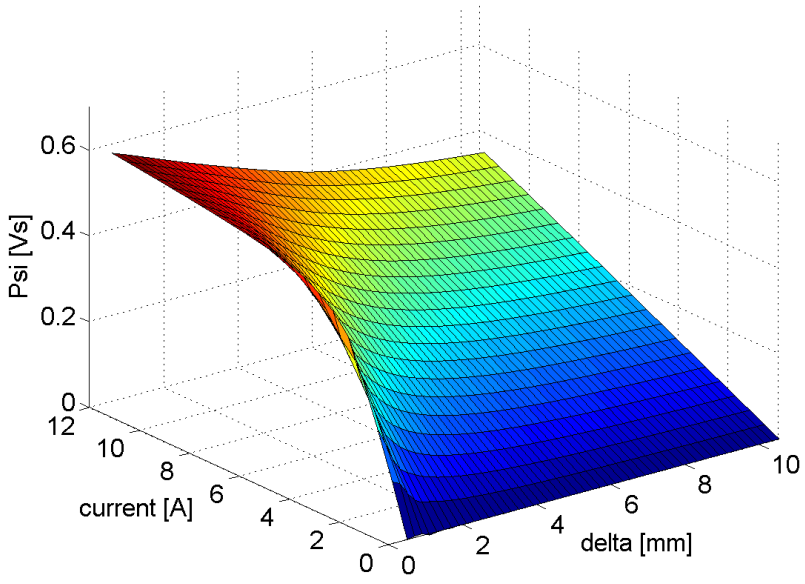

Figure 5.8: "lookup table" of the flux simulated with Flux 2D

5.4.3 The dynamic equation of motion

Fig. 5.9 describes how the speed and the position are calculated from the acceleration w. Speed v is the integral of acceleration, and the position x is the integral of this speed, therefore:

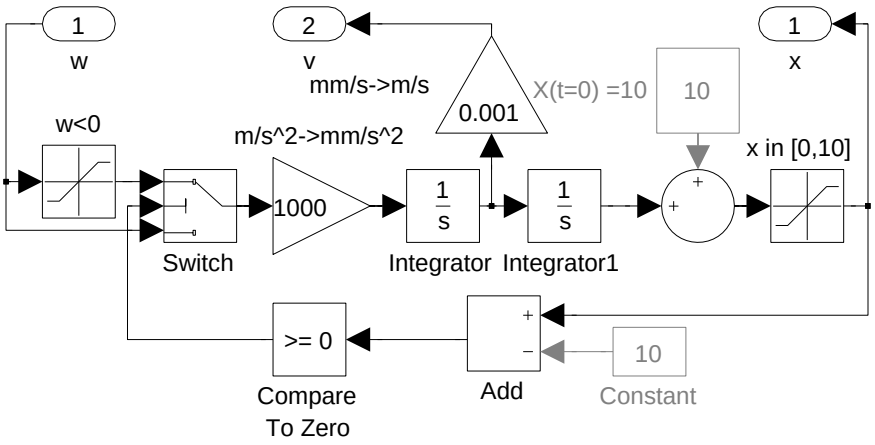

Figure 5.9: The dynamic equation of motion $\int_0^{t_x}\int_0^{t_x} w\ dt^2$

$$v = \int_0^{t_x} w\ dt \tag{5.3}$$

$$x = \int_0^{t_x}\int_0^{t_x} w\ dt^2 \tag{5.4}$$

with t_x the time when evaluating the position and speed. The position of the mover x is between 0 and 10 mm. The acceleration w is negative and the open position is x = 10 mm.

5.4.4 Regulation

There are 3 different regulation blocks for the 3 different control strategies defined in subsection 5.3.

Open loop control

Fig. 5.10 shows the open loop control strategy (a), we only take the “a priori command" which is just applied to the system input without any feedback.

The a priori voltage reference profile depends on the position x and the speed reference v_{ref} is not used as the loop is open.

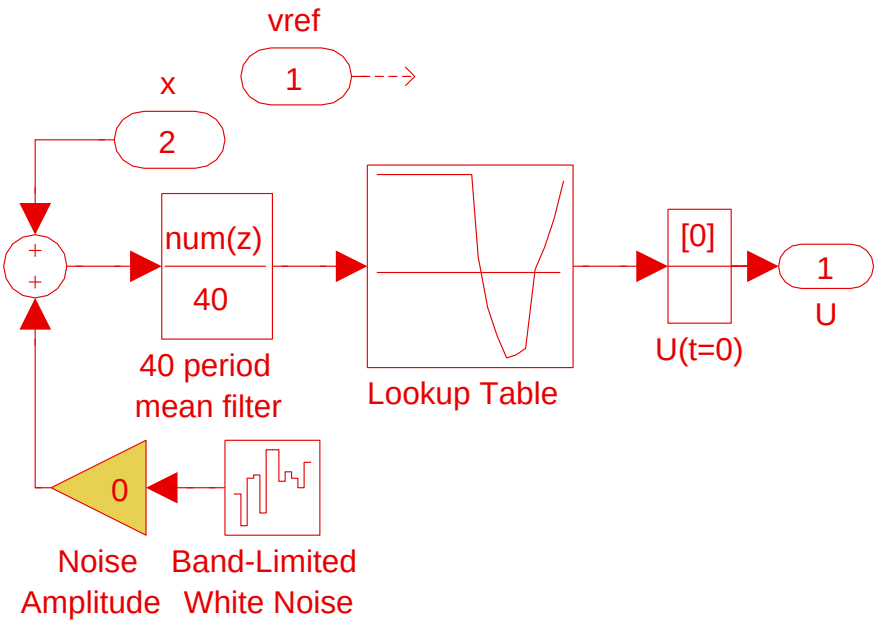

Figure 5.10: A priori voltage reference

Closed loop control

For the PI closed loop control strategy (b), the block regulation is modified to obtain the diagram presented in Figs. 5.11 and 5.12 in order to control the drive voltage u.

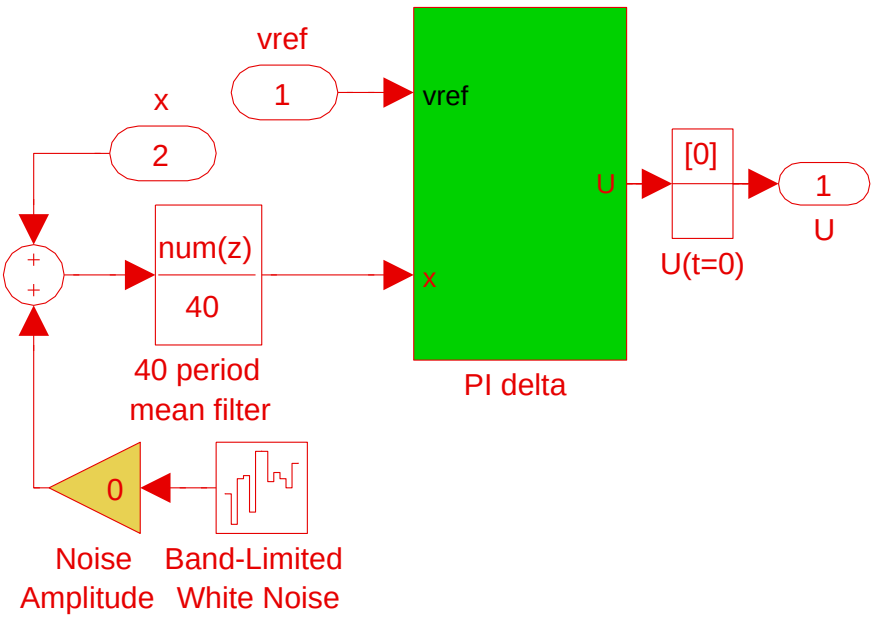

Figure 5.11: Closed-loop control

The PI control is implemented in Matlab function "Delta u, PI regulation", where we can change

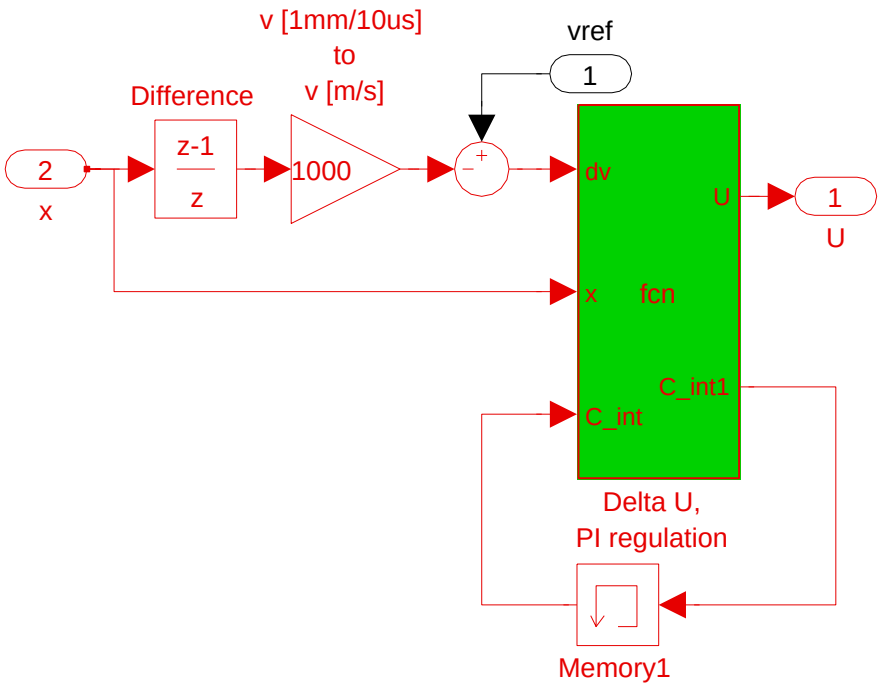

Figure 5.12: Closed-loop control (position derivation)

the settings of the proportional and integral components K_p and K_i of the PI regulator. The function also describes the "anti reset windup" which limits the instability of the integral term when the drive voltage is limited.

For PI control, we must first evaluate the speed difference dv between the measured speed v_{mes} and the speed reference v_{ref}:

$$dv = v_{ref} - v_{mes} \tag{5.5}$$

In order to perform the anti reset windup, we calculate an intermediate parameter u':

$$u' = C_{int} + (K_p + K_i)\, dv \tag{5.6}$$

And limit u' to obtain U:

$$U = \begin{cases} U_{max}, & \text{if } u' > U_{max} \\ U_{min}, & \text{if } u' < U_{min} \\ u', & \text{if } u' \in [U_{min}, (U_{max})] \end{cases} \tag{5.7}$$

The integration constant C_{int} limits the drift of the integrator term of the PI for a better control of the system. It is calculated as:

$$dv_{lim} = dv - \frac{(u' - u)}{K_p + K_i} \tag{5.8}$$

$$C_{int} = C_{int} + K_i \, dv_{lim} \tag{5.9}$$

Voltages U_{min} and U_{max} are set to 15 % and 85 % of the full voltage range that goes from $-U_{DC}$ = -150 V to U_{DC} = 150 V, therefore:

$$U_{max} = 0.85(2\ U_{DC}) - U_{DC} = 105\ V$$
$$U_{min} = 0.15(2\ U_{DC}) - U_{DC} = -105\ V$$

The margin of 15% is left in order to allow the superimposition of the scan signal which is used for the position detection (blue arrow in Fig. 5.13).

PI control of an a priori reference

Figs. 5.14 and 5.15 describe the control strategy (c) for PI control with an a priori reference.

In this case we have implemented an intentionally bad calibrated a priori voltage reference u_{ref} and the PI control manages the voltage difference Δu to get closer to the speed reference. In the Matlab function the code is modified and the equations (5.6) to (5.9) become:

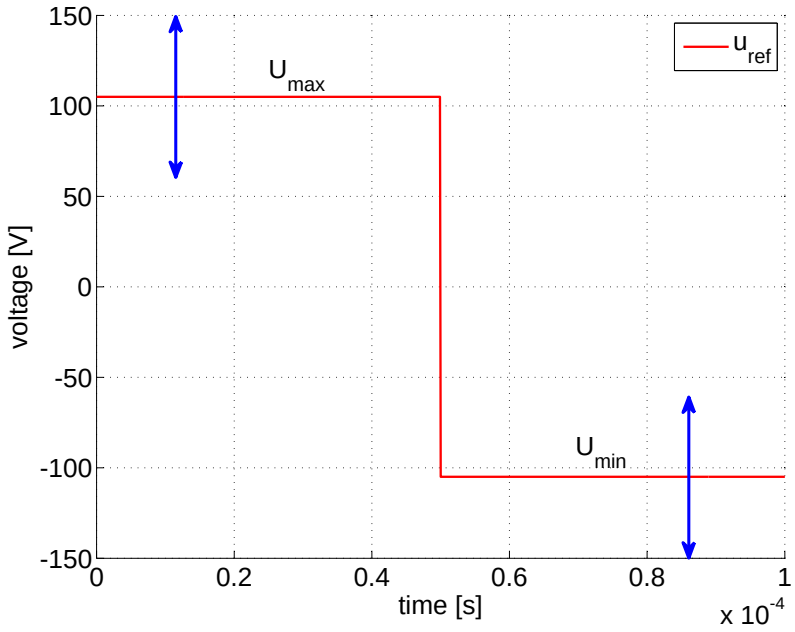

Figure 5.13: Limits of the drive voltage

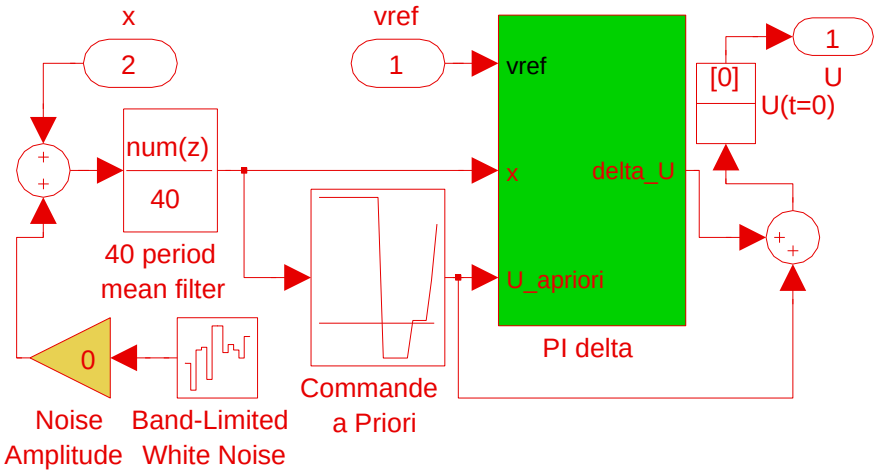

Figure 5.14: PI control and a priori voltage reference

$$\Delta u' = C_{int} + (K_p + K_i)\, dv \tag{5.10}$$

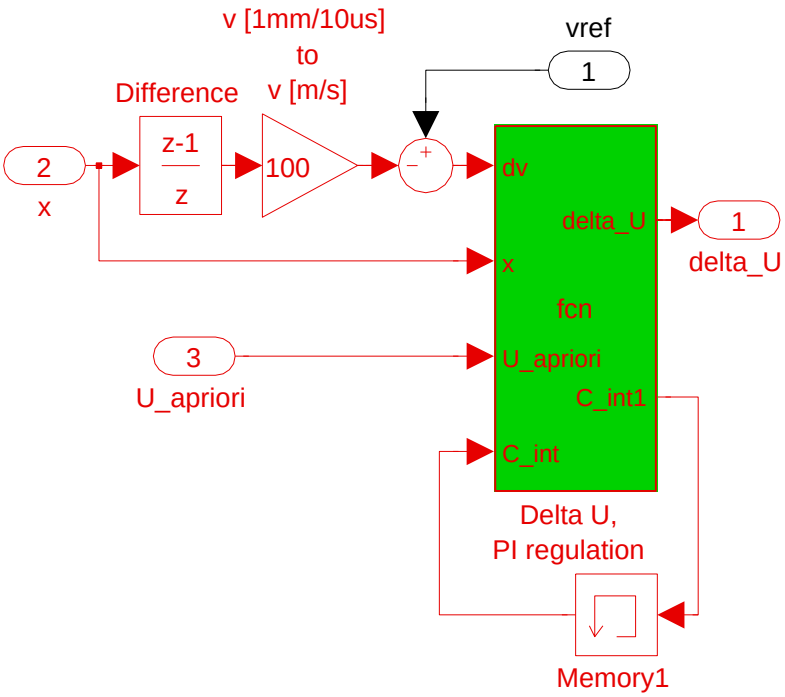

Figure 5.15: PI delta

which will test the voltage limits u and that is calculated according to:

$$\Delta u = \begin{cases} (U_{max} - u_{ref}), & \text{if } \Delta u' > (U_{max} - u_{ref}) \\ (U_{min} - u_{ref}), & \text{if } \Delta u' < (U_{min} - u_{ref}) \\ \Delta u', & \text{if } \Delta u' \in \left[U_{min} - u_{ref}), (U_{max} - u_{ref})\right] \end{cases} \tag{5.11}$$

$$dv_{lim} = dv - \frac{(\Delta u' - \Delta u)}{K_p + K_i} \tag{5.12}$$

$$C_{int} = C_{int} + K_i \, dv_{lim} \tag{5.13}$$

5.5 Simulation results

5.5.1 Simulation results - Open loop control

The first step in forming the open loop control is to analytically create the voltage reference u_{ref}.

When the actuator is not saturated, the force is directly proportional to the square of the current

density. Consequently, to determine the necessary current density, we apply $J_1 = 1$ A/mm^2 to the optimized actuator and statically simulate the force for air-gap values between 0.2 and 10 mm, which will give the function $F_1(x)$. In this case, the force F_{tot} being proportional to J_{ref}^2, we easily obtain the reference of current density according to the formula:

$$J_{ref} = J_1 \sqrt{F_{tot}/F_1} \tag{5.14}$$

Nevertheless, simulations show that the actuator is saturated for small air-gap values. Consequently, the proportionality between F_{tot} and J_{ref}^2 is not correct anymore and we have to use a new method.

As it is not possible to rebuild mathematically the current reference i_{ref} or the current density reference J_{ref}, we simulate the force F_i for current densities J_i ranging between 0 and 40 A/mm^2 (Figs. 5.16 and 5.6).

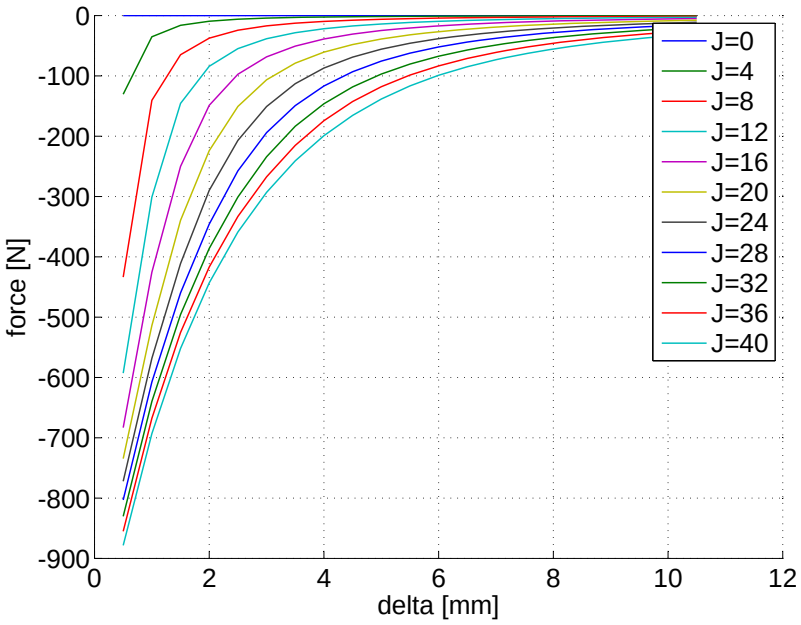

Figure 5.16: Forces versus air-gap values and current (2D)

Knowing the force F_{tot}, it is consequently possible to determine the current density reference $J_{ref}(x, F)$ by interpolation, and Fig. 5.17 shows the obtained function: the current density reference versus the air gap necessary to obtain the required speed profile. The maximum constraint of 40 A/mm^2 is respected.

Then, this current density reference is injected in dynamic FEM simulations. Fig. 5.18 compares the speed reference with the speed resulting from dynamic simulations. The obtained speed

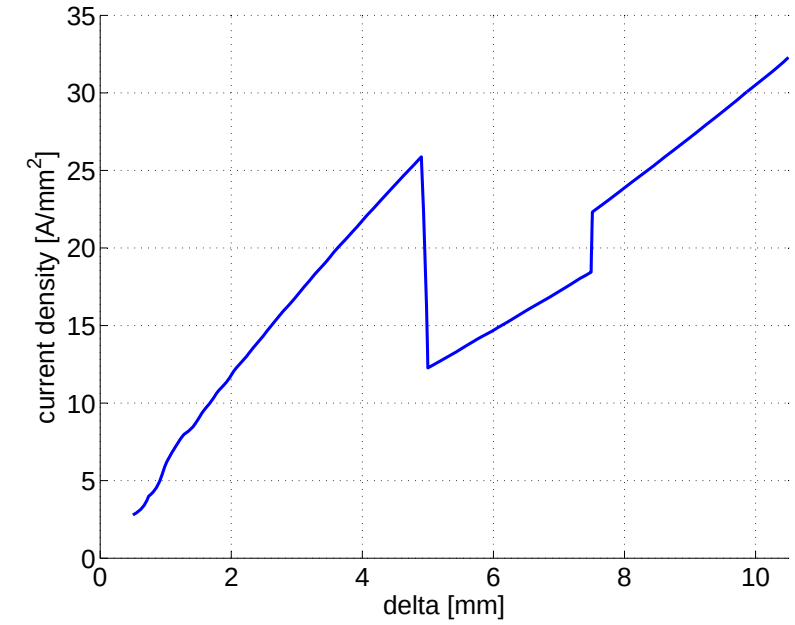

Figure 5.17: Current density reference J_{ref}

corresponds to its referent values.

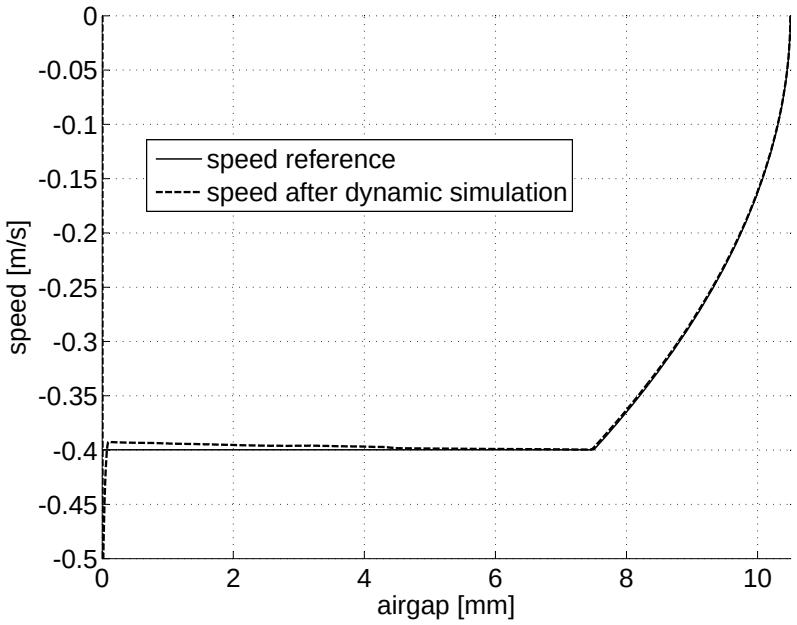

Figure 5.18: Industrial contactor - Speed after dynamical simulation

However, the command is the voltage, and not the current. It is not straightforward to transform the current reference into the voltage reference because of derivation of numerical parameters

like the flux Ψ.

Because of the difficulty to obtain analytically the voltage reference, its 2 profiles described in subsection 5.3.1 are determined by an iterative try-and-error process on Simulink:

For the reference 1), $u_{ref} = U_{max} = 105$ V until $t = t_{off1}$ and then $u_{ref} = 0$. Finally, as the speed is not important after the impact, then at $t = t_{on1}$, $u_{ref} = U_{max}$ again.

For the reference 2), the profile of u_{ref} is built in order to be as close as possible to the speed reference shown in Fig. 5.18. After the impact, at $t = t_{on3}$, $u_{ref} = U_{max}$.

The result of imposing two referent voltages u_{ref} is shown in Fig. 5.19, where it can be seen that the speed of 0.4 m/s at the impact is respected. Figs. 5.20 and 5.21 show the profiles of voltage and current ($t_{off1} = 7.73$ ms, $t_{on1} = 20$ ms and $t_{on2} = 24$ ms)

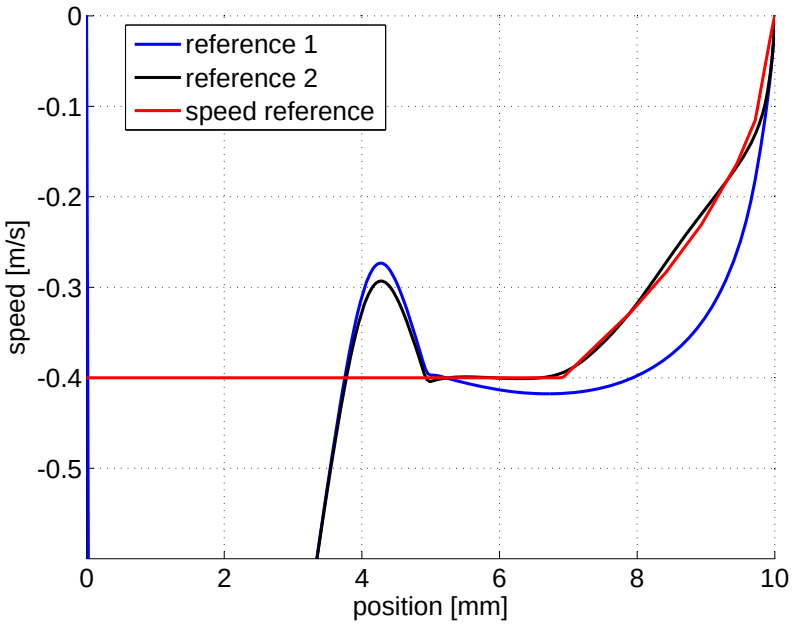

Figure 5.19: Speed versus the position for both references

The time value before impact fluctuates between 21 ms for the reference 1 and 24 ms for the reference 2 (Fig. 5.22). The second reference corresponds exactly to the industrial specifications but the first one is slightly quicker.

We will see later in subsection 5.6.5 that the position detection is easier with a voltage that does not have big voltage jumps and even if it is a little bit slower, the second reference has the advantage to be smoother than the first one.

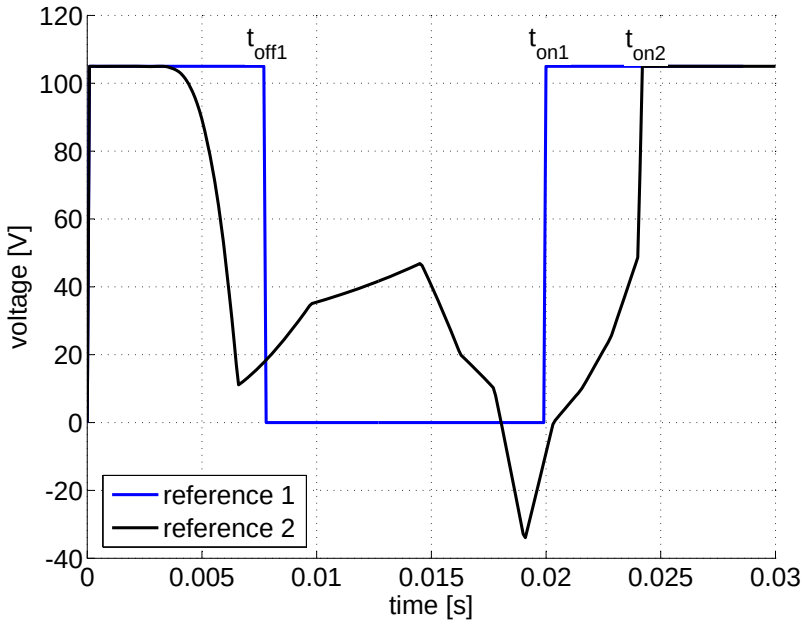

Figure 5.20: Voltage versus the position for both references

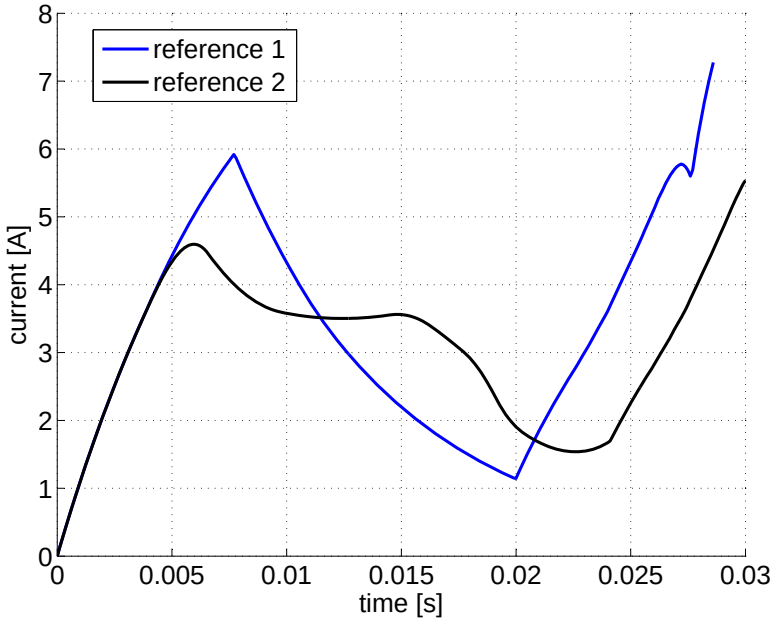

Figure 5.21: Current versus the position for both references

5.5.2 Simulation results - Closed loop control

The principle of the control strategy b) is to eliminate the a priori reference and operate the full PI control. With coefficients $K_p = 10$ and $K_i = 0.4$ we obtain the results shown in Fig. 5.23. The

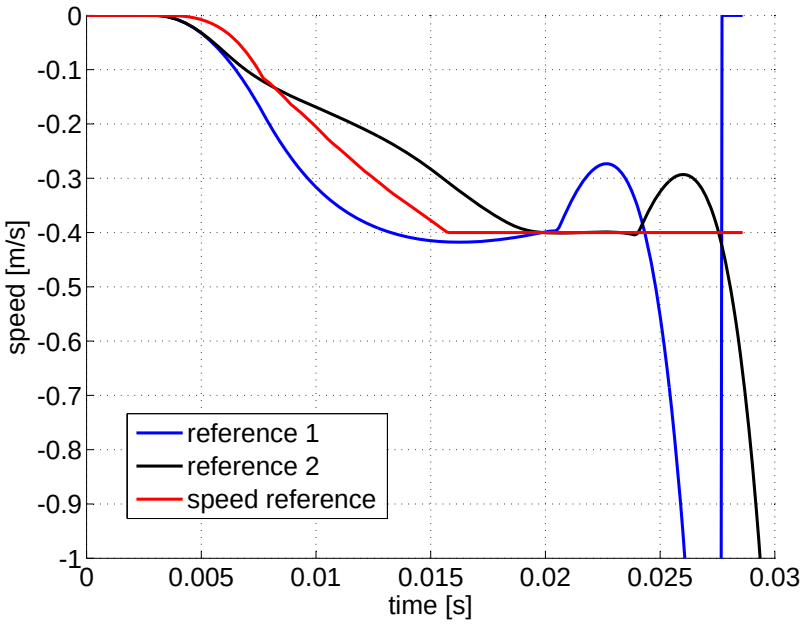

Figure 5.22: Speed versus the time for both references

K_p and K_i coefficients have been determined empirically.

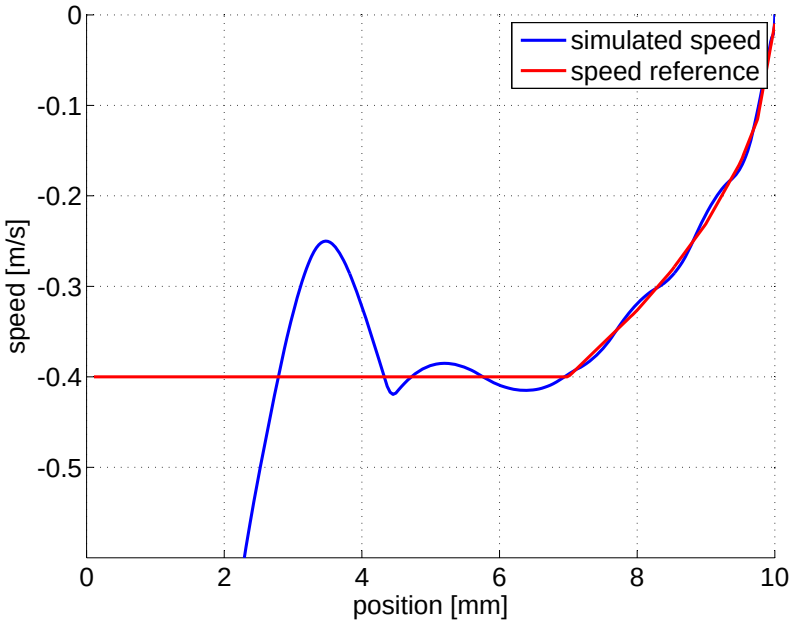

Figure 5.23: Speed versus the position - CL control

It is surely possible to improve the control by finding the optimal values of K_p and K_i but the resulting speed is already accurate enough to validate the strategy. Fig. 5.24 shows the voltage

profile during the control.

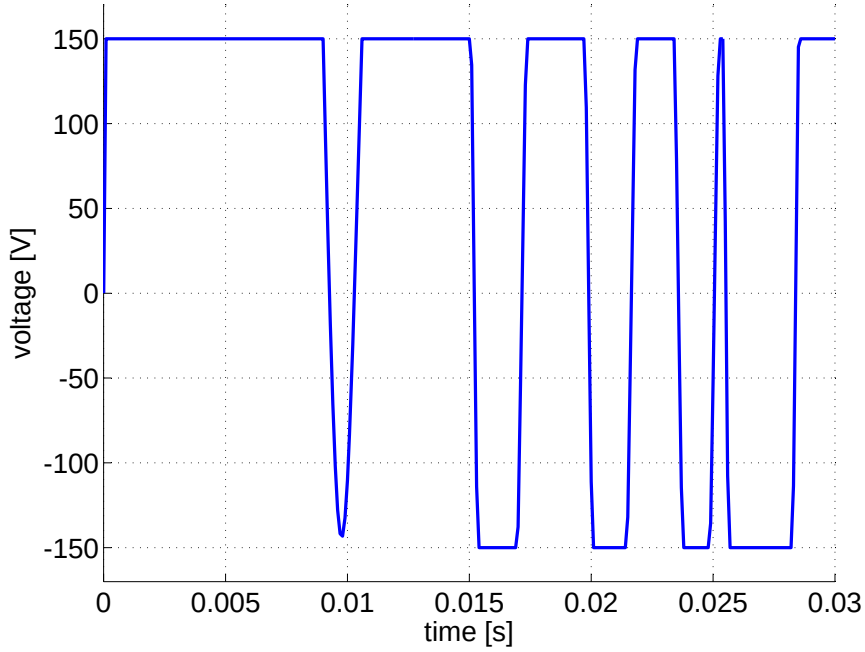

Figure 5.24: Voltage versus time - CL control

5.5.3 Simulation results - PI control of an a priori voltage reference

Fig. 5.25 shows the intentionally bad calibrated voltage reference that produces the speed profile shown in Fig. 5.26. In Fig. 5.27, the PI control is activated and the measured speed approaches the speed reference.

Fig. 5.28 shows how the voltage evolves during the PI control.

The speed is controlled with coefficients proportional $K_p = 6$ and integral $K_i = 0.2$. These coefficients are defined by increasing K_p and then, after reducing it by one third, increasing the term K_i. As shown in Fig. 5.27, the speed oscillates around the reference and it is surely possible to reduce these oscillations but, again, the results are already accurate enough to validate the strategy.

5.6 Experimental measurement on the industrial contactor

5.6.1 Introduction

The three presented control strategies are applied to the industrial contactor presented in section 3.1. The results presented in this section are measured with the test bench described in Appendix

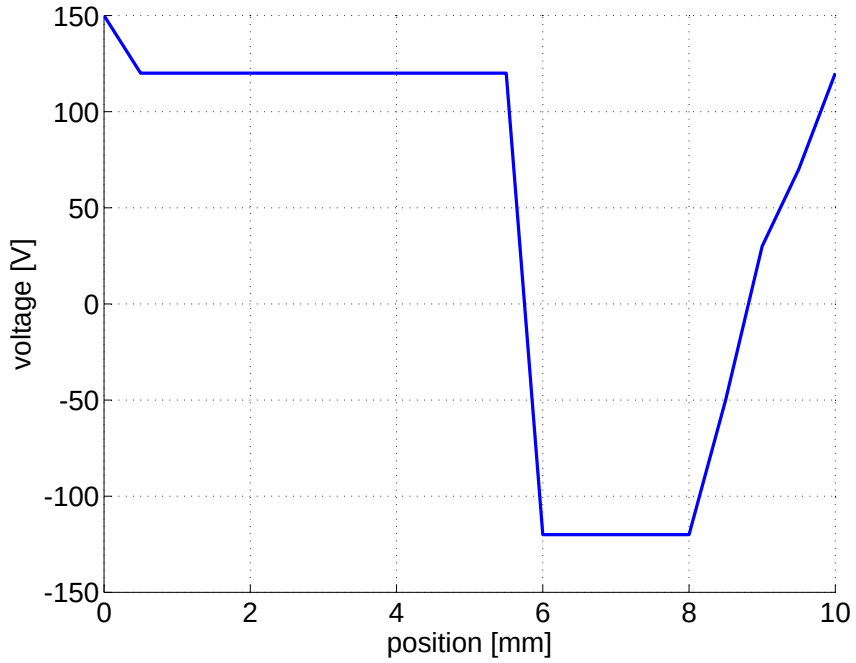

Figure 5.25: Voltage reference

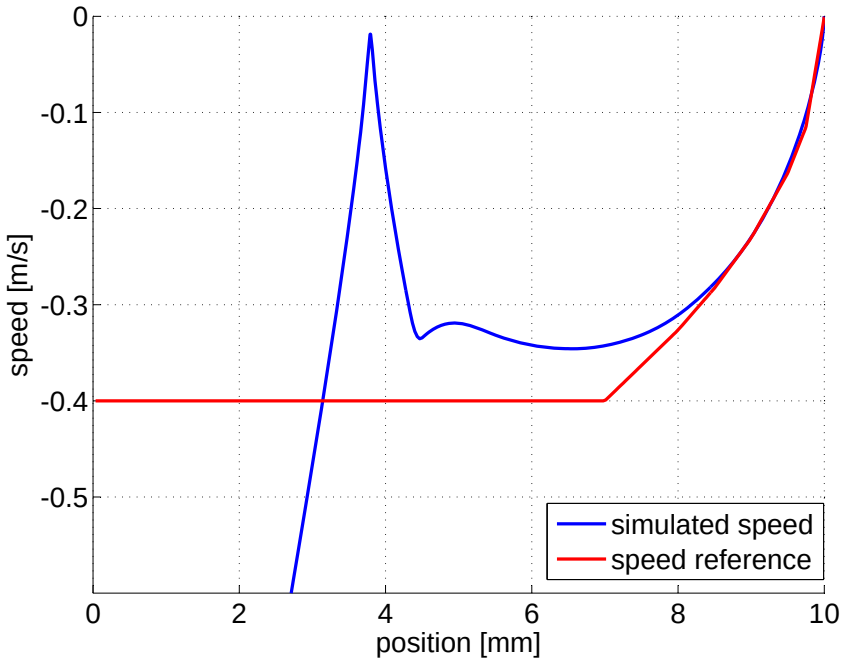

Figure 5.26: Speed versus the position - Open-loop

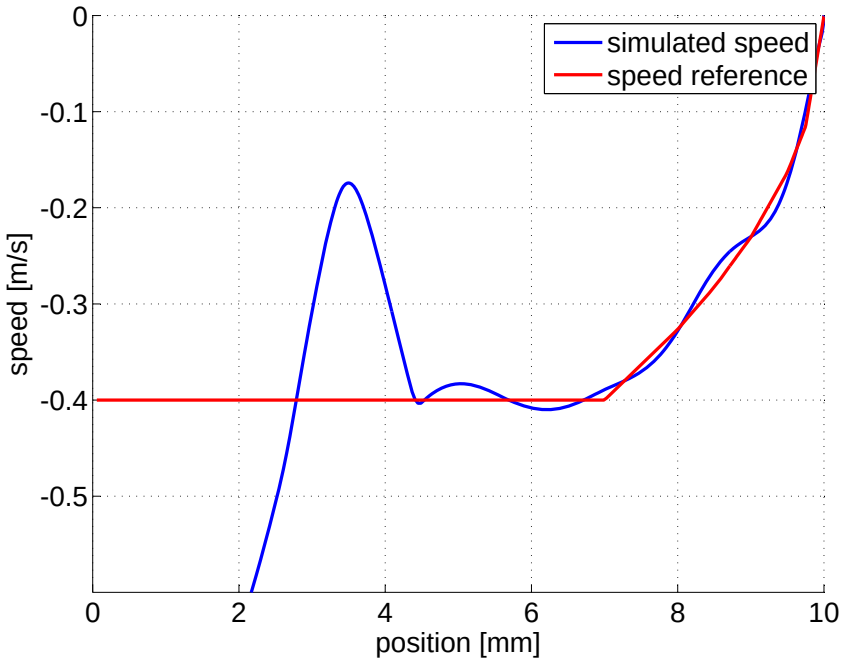

Figure 5.27: Speed versus the position - PI control

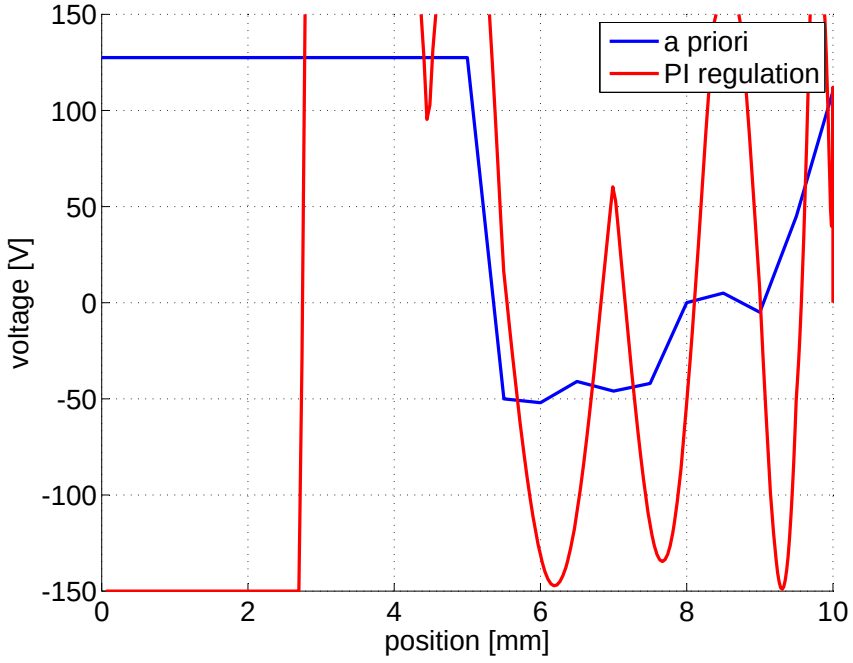

Figure 5.28: Voltage versus position during PI control

B. As the objective of Simulink modeling is only to test different strategies of control, the FEM model that allows the force and flux curves of the industrial actuator is not very precise and a real comparison between simulation and measurement is not very relevant. The parameters (t_{on}, t_{off}, K_i and K_p) used on Simulink were a good starting point for the determination of the parameters on the real test bench but are finally quite different.

The drive voltage is commanded by a PWM and is directly related to the duty cycle k_{pwm}. As the scan signal needs 30% of the overall duty cycle, the drive duty cycle is between 15% and 85% as it is shown in Fig. 5.29.

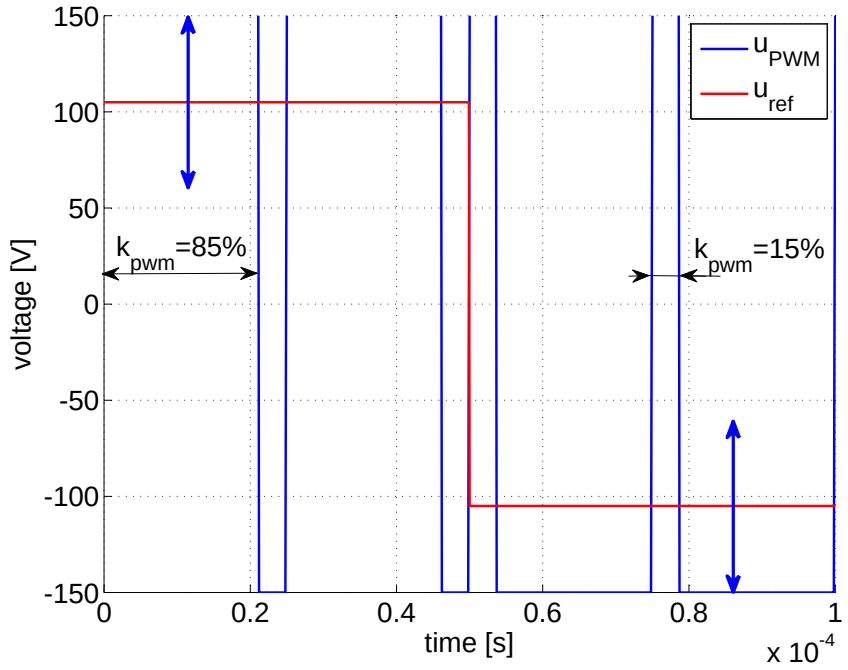

Figure 5.29: Duty cycle limits of the drive voltage

As shown in subsections 5.6.2 to 5.6.4, the laser sensor measures the position which is then transferred to Matlab with the help of the oscilloscope. The speed is then calculated by deriving the position in Matlab. With the oscilloscope, we have the possibility to have a lot of points and to filter relatively easily. In subsection 5.6.5, we will see the results with the position detection and the adapted Kalman filter described in chapter 4.

5.6.2 Experimental results - Open loop control

As in Simulink simulations for the open loop strategy, it is possible to a priori build a PWM's duty cycle reference $k_{pwm,ref}$, which allows the actuator to touch the contacts with the speed required by the specifications.

Fig. 5.30 shows the resulting speed with the reference 1. As we have a better measurement of the position x than the time on the DSP, the transition between U_{max} (k_{pwm} = 85%) and 0 (k_{pwm} = 50%) is performed for $x < 9.7$ mm. We see that the speed at the impact is close to 0.4 m/s.

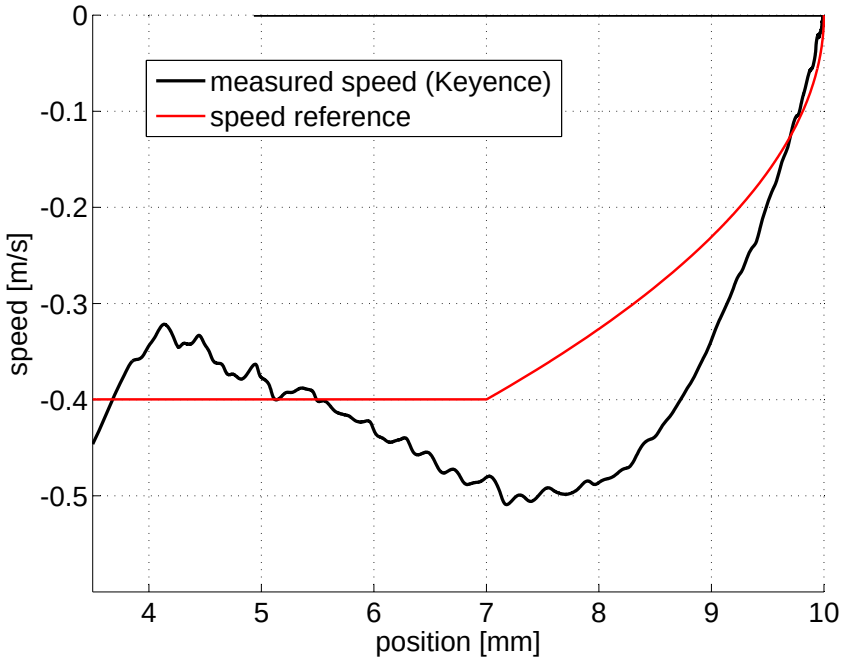

Figure 5.30: Speed versus the position during closing - reference 1

Fig. 5.31 shows the speed in function of time. We see that the impact is made after 24 ms which is slightly longer than the 21 ms simulated on Simulink but still allows the validation of the Simulink model.

Fig. 5.32 shows the resulting speed with the reference 2. The speed corresponds to the specifications and the drive duty cycle is shown in Fig. 5.33.

We can see that the speed is relatively stable around -0.4 m/s from a air gap value of 7 mm. At the impact, the control cannot maintain that speed and the mover slows, without stopping or bouncing according to the specifications.

5.6.3 Experimental results - Closed loop control

In the simulations, the voltage is the control parameter but on the real test bench, the control parameter is actually the duty cycle k_{pwm}, consequently the equations (5.6) to (5.8) that allows the PI control become:

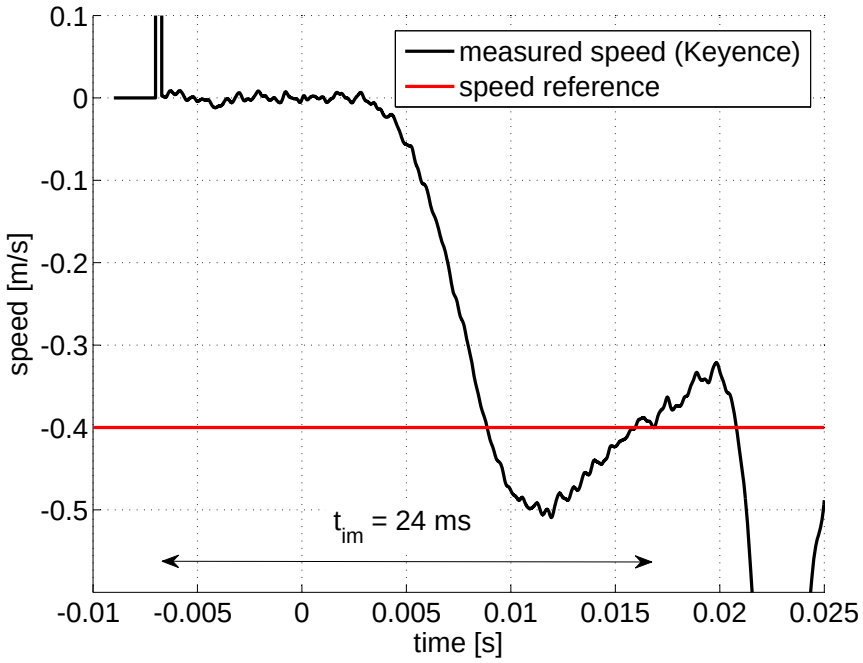

Figure 5.31: Speed versus the time - reference 1

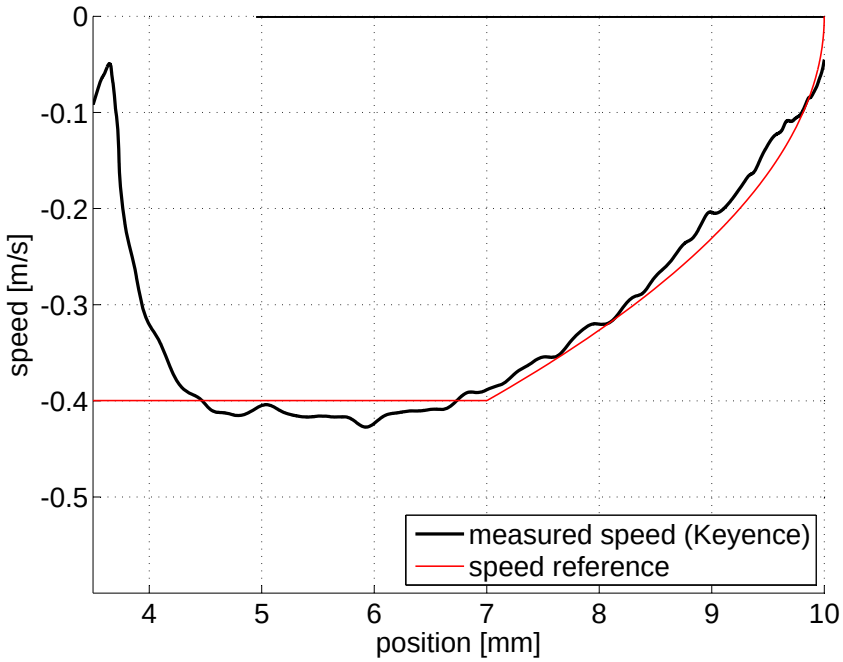

Figure 5.32: Speed versus the position during closing - reference 2

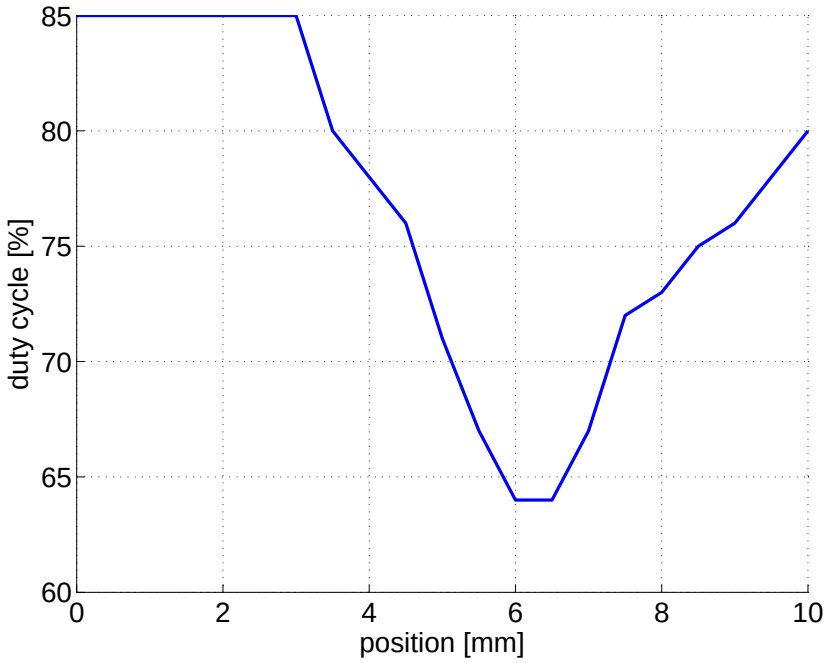

Figure 5.33: PWM's duty cycle reference $k_{pwm,ref}$

$$k'_{pwm} = C_{int} + (K_p + K_i)\, dv \tag{5.15}$$

$$k_{pwm} = \begin{cases} k_{pwm,max}, & \text{si } k'_{pwm} > k_{pwm,max} \\ k_{pwm,min}, & \text{si } k'_{pwm} < k_{pwm,min} \\ k'_{pwm}, & \text{si } k'_{pwm} \in [k_{pwm,min}, k_{pwm,max}] \end{cases} \tag{5.16}$$

$$dv_{lim} = dv - \frac{(k'_{pwm} - k_{pwm})}{K_p + K_i} \tag{5.17}$$

Fig. 5.34 shows the closed loop control of the speed with the proportional gain $K_p = 4$ and integral gain $K_i = 0.1$. The control is made with the speed reference given by the specifications and we can see that the measured speed of the mover is corresponds to the required one.

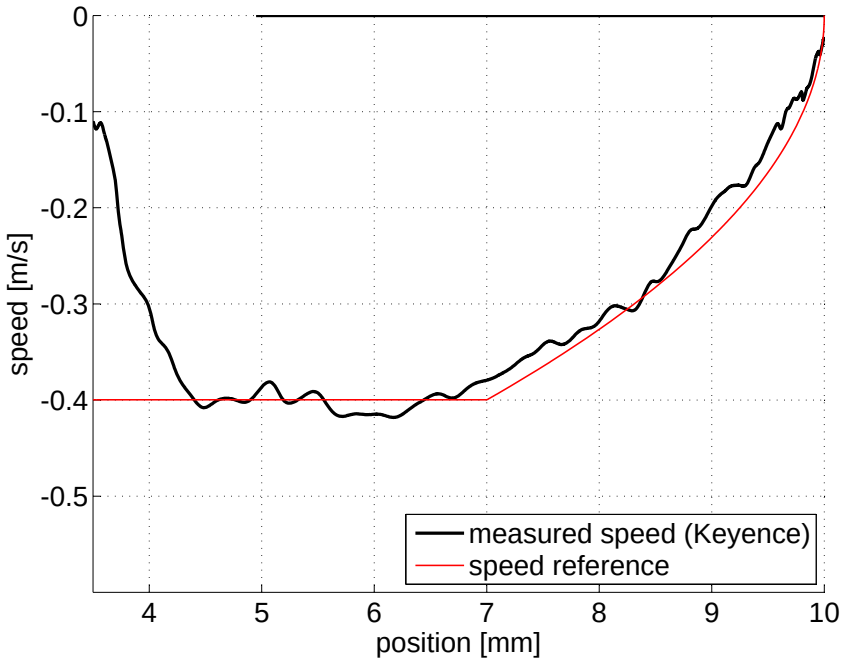

Figure 5.34: Speed versus the position during closing - PI control

5.6.4 Experimental results - PI control of an a priori voltage reference

In this case, the control is similar to the control in Simulink with the drive parameter Δk_{pwm} (instead of Δu) which is added to an intentionally bad calibrated duty cycle reference $k_{pwm,ref}$.

Fig. 5.35 shows the speed generated by a reference intentionally bad calibrated (in blue) and the speed regulated with proportional gain $K_p = 2$ and integral gain $K_i = 0.1$ (in black). We see that the PI control improves the dynamics and allows, as for the PI control alone, a speed between 7 mm and 5 mm relatively stable.

5.6.5 Sensorless results

The method of speed detection presented in chapter 3, where the idea was to measure the amplitude of a scan signal that is directly dependent on the position of the mover. The error between the measured speed and its reference allows the correction of the current reference in order to always follow the speed reference, even in case of wear of contacts or springs.

There remains a lot of noise in the electronic circuit when the PI control is applied. In consequence, it was not possible during the thesis to perform closed loop sensorless speed control. Figs. 5.36 and 5.37 show position and speed measurement with the DSP done on the industrial contactor with an open loop control.

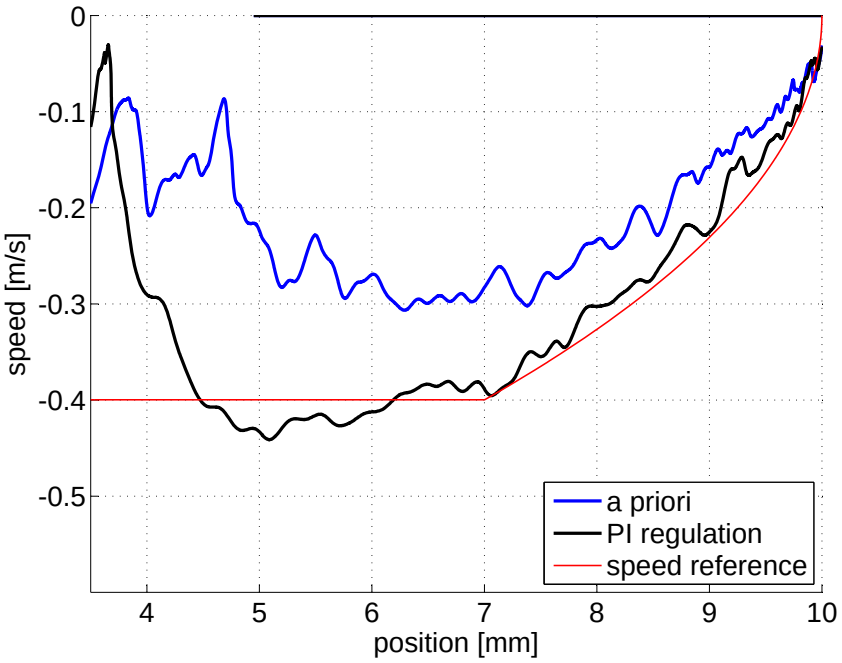

Figure 5.35: Speed versus the position - PI control of an a priori voltage reference

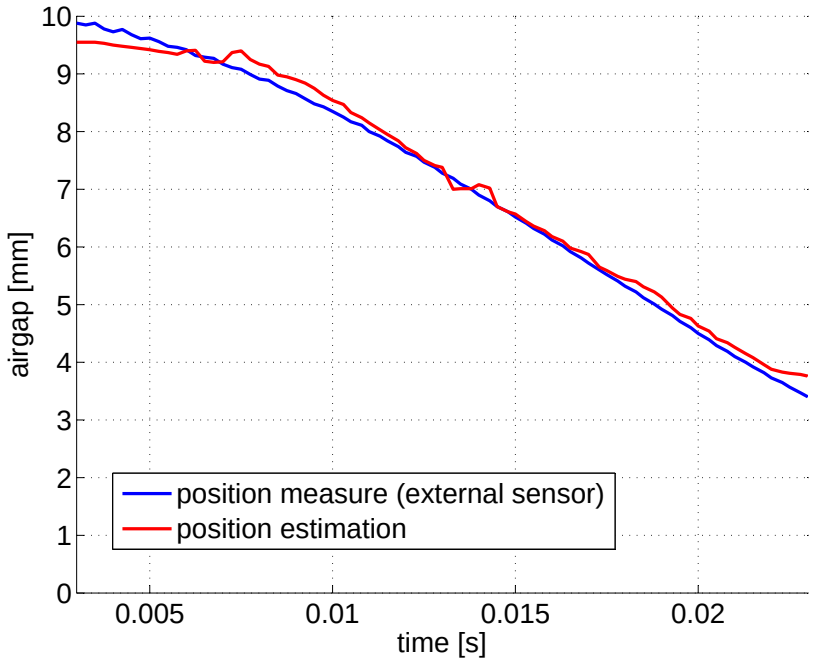

Figure 5.36: Measurement of the controlled position

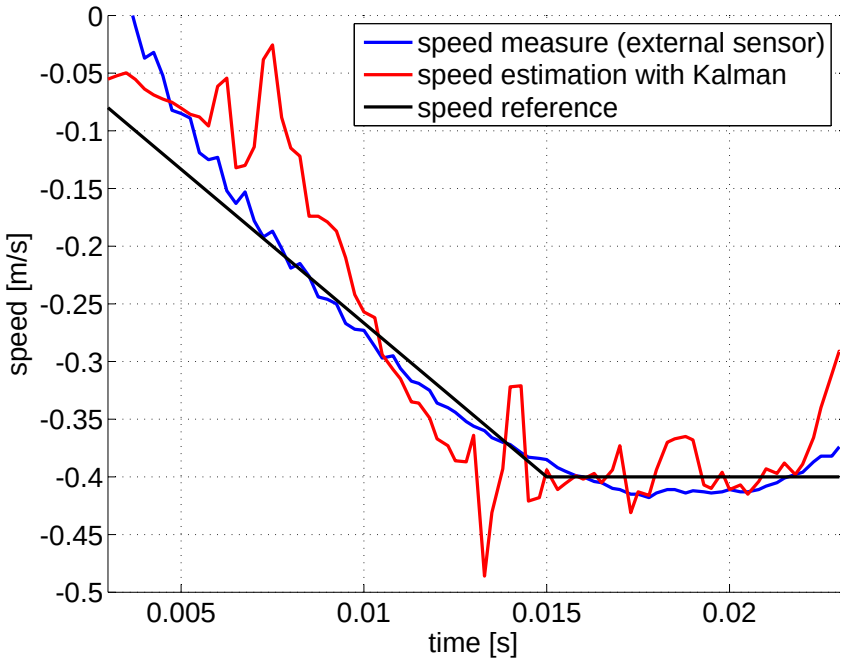

Figure 5.37: Measurement of the controlled speed

We can see that the speed is still noisy but precise enough to tell the user that the speed is conform to the specifications at the impact. It could be now possible to adapt the voltage a priori reference if the speed was not accurate.

5.7 Experimental measurement on the prototype

Fig. 5.38 shows that the difference of amplitude of the scan signal for two extreme mover positions for the prototype is higher than for the industrial contactor. It was not possible to perform measurement like the one shown in Fig. 5.37 with the prototype because of mechanical frictions that introduce noise which perturbs the position detection and speed control.

It is therefore difficult to perform sensorless position detection on the prototype but we can see in Fig. 5.39 that the prototype allows a speed at the impact that corresponds to the speed defined by the specifications (0.4 m/s). This shows that with a well built test bench, the sensorless speed control is possible on the prototype and the position detection should be easier and more accurate than the one performed on the industrial contactor.

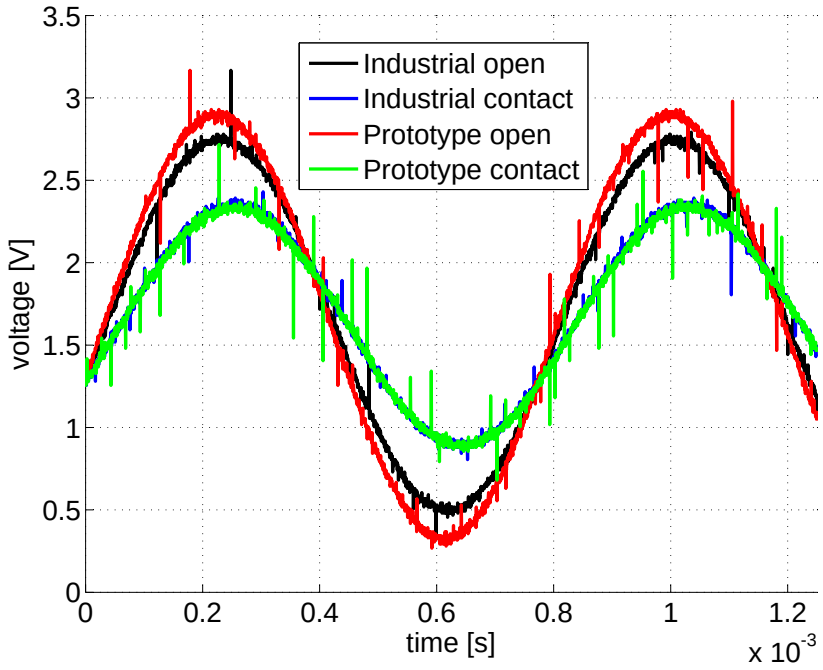

Figure 5.38: Comparison between the scan signals of both prototype end industrial contactor

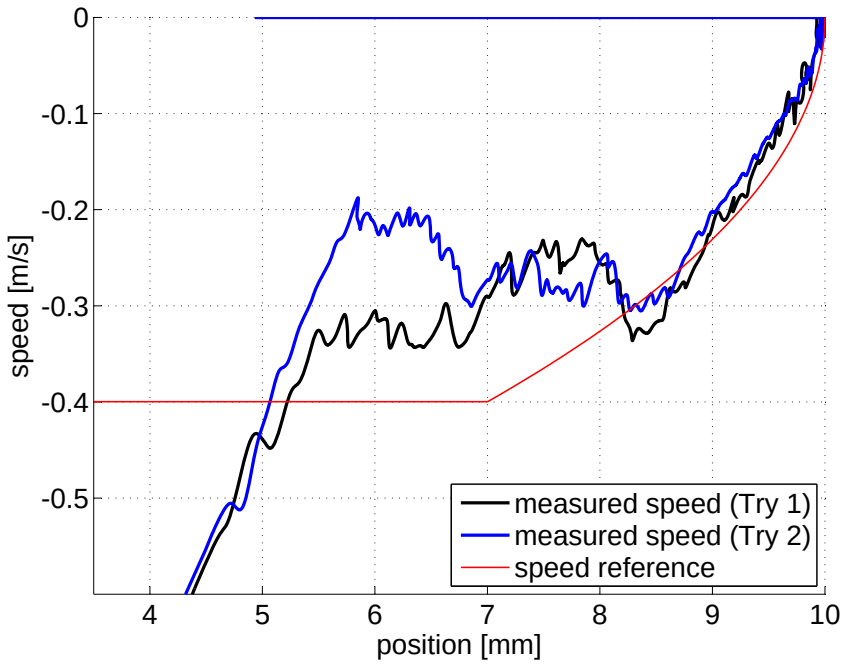

Figure 5.39: Speed versus the position for the prototype

6 Conclusion

The thesis presents a way to design, optimize and control the speed of the mover of an actuator. It is complete in the sense that it shows the entire procedure that fulfills the objectives of sensorless control of the mover's speed.

The thesis is divided into 4 different themes: the optimization of the actuator, the sensorless position detection, the signal processing of the position and the speed by adapting the Kalman filter, and finally the speed control of the moving part of the actuator.

6.1 Main results and innovative contributions

The main results and innovative contributions can be summarized by the following points:

- *Use of static simulations for dynamic optimization*. Because the analytical model is too difficult to obtain, it is replaced by a FEM model. Dynamical simulations are too time-consuming for the optimization and consequently, they are performed for multiple values of airgap by taking into account the load and the acceleration of the mover at each position. This method allows very short calculation time and the success of the optimization.

- *Genetic algorithm and penalty constraints*. The results of FEM simulations can be constrained by applying penalties when they are out of the limits given by the specifications. In the present case, the electromagnetic force has to be large enough to allow the required dynamic and by penalizing the square of the difference between the obtained force and the required one, we manage to have a very good convergence to the optimized solution.

- *Design for self-sensing*. A new actuator configuration was designed to allow a better position detection by optimizing the difference of inductance between 2 extreme positions of the mover. More free parameters and degrees of freedom were given to the optimizer in order that it could built a new actuator that fulfills the specifications. The optimized actuator is designed to have the maximal variations of inductance for high values of airgap,

which are the ones that are interesting for the success of the project objectives.

- *Position detection by superimposing a scan current*. A scan current is superimposed to the main one that drives the actuator. After filtering the total current, the amplitude of the scan current is directly related to the position of the mover. By applying this method to an industrial contactor, it is proven that the position is well detected and corresponds to the one measured with an external sensor.

- *Adaptation of Kalman filter to measure position and speed*. After successful position detection, the important remaining problem is the filtering of both signals, position and speed. Indeed, even if the estimated position corresponds to the one measured with the external sensor, when it is derived to obtain the speed, it becomes too noisy to be exploitable. Therefore, an adaptation of the Kalman filter is developed to enable an effective real-time filtering of the position and speed with a reduced number of calculation lines on the DSP.

- *Sensorless speed control*. A sensorless open loop control has been applied to the industrial contactor. The speed corresponds to the specifications and can be measured with the DSP very accurately. It is now exploitable in order to keep the speed at the impact constant, by adapting the a priori voltage reference, if the mechanic of the contactor changes during its use.

6.2 Future developments

- *Genetic algorithm*. The optimization algorithm that combines Genetic Algorithms with FEM simulations is completely adaptable for various applications. Even without FEM model, it is very interesting because of its reliability and rapidity. For example, it has been used, in the laboratory, to find the starting points for gradient optimization of a non linear curve fitting process. It has also been used by students in order to compare the results between stochastic and heuristic methods for the optimization of an actuator described by its analytical model. The method can be applied to other problems and the convergence and the accuracy of the global solution should be well studied in order to definitely validate a tool that is already very convincing.

- *Winding model*. The winding is very complex to modelize and the influence of the secondary winding has not been completely studied because it was not an issue for the success of the thesis objectives. However, it could be very interesting to well understand the winding and see if it is possible to improve the position detection by optimizing the parameters of the winding like the number of turns, the distance between the wires or the insulation.

- *Test bench*. The test bench has to be improved in order to better filter the scan current. The ground plane should be better implemented in order to avoid instabilities. The Sallen key filter was very convenient because of its simplicity but it may be interesting to study other filters and try to have a more reliable and stable final electronic board. This should

allow sensorless closed loop control of the actuator, which is the next aim to reach before a possible industrialization of the product.

- *Prototype*. The mechanical part of the contactor, which is composed of the support and the springs, should be improved because the mover is not well guided and the friction does not allow good results at the desired speed. A good solution could be to have a prototype comparable to the industrial one where there are no friction issues.
- *Speed regulation*. Open loop regulation: An algorithm should be implemented in order to modify the voltage reference and thus correct the speed if its measurement does not correspond to the specifications anymore.

  Closed loop regulation: If a better filter allows the sensorless closed loop control, a characterization of the regulator using the symmetric and maximally flat criteria should be done in order to have a better real time speed control.

Despite these possible improvements, this thesis proves the possibility of sensorless control of a linear actuator and shows a method, by optimizing the configuration, detecting the position, filtering the position and speed signals and finally controlling the speed of the mover, that contributes to the developpement of the next generation of contactors.

6.3 Perspectives

The collaboration with the industrial partner has enabled the project to have a clear objective that is to perform sensorless speed control of a contactor. But in order to reach this object, many scientific problems have been solved and this has resulted in 4 publications:

- Sensorless position detection of a linear actuator using the resonance frequency (IEMDC 2009) [27]
- Optimization design of a linear actuator using a genetic algorithm (ICEMS 2009) [30]
- Kalman filter to measure position and speed of a linear actuator (IEMDC 2011) [29]
- Design for Self-Sensing of a Linear Actuator (ECCE 2011) [28]

The complete method that combines optimization for self-sensing, position detection, filtering and control of the speed is completely usable in various applications.

[31] uses the combination of FEM simulations and GA to design an in-wheel BLDC motor for a kick scooter and introduces three operating modes for which the motor is optimized in order to reduce the number of FEM simulations. The method is directly inspired by the method of multiple static simulations for a dynamic transient trajectory.

[36] optimizes the design process of a tubular linear synchronous machine. The author has been inspired by the optimization method presented in the thesis and in [30].

[11]has cited our paper on [27] for the position estimation of a plunger and its control for the precise adjustment of oil pressure.

The adapted Kalman filter [29] is very simple to implement on a DSP when the user needs space and can be very interesting for the filtering of signals which are close to a known reference.

In conclusion, the method is based on the development of a linear actuator because it is the application that motivated the project at the beginning but some part of the method or the complete one can be used in various other applications.

A Appendix

The following 2 prototypes have been built after material cost optimization. They have been replaced by the one described in chapter 2. The position detection of these prototypes was impossible because the ferromagnetic parts were massive and the problems described in subsection 3.3.2 due to eddy currents did not allow to fulfill the objectives. But the optimization of these two configuration, and especially the hybrid one, show what the optimization algorithm can perform.

A.1 Reluctant and Hybrid prototypes

1^{st} Configuration description

First, we optimize a configuration composed of a ferromagnetic structure having an "E" shape and a fixed winding (Fig. A.1). Concerning the actuator analytical model, it can be generated, but it is valid only for small values of air gap. Therefore, an optimization using an analytical model is not possible. The configuration is described by 4 parameters.

2^{nd} Configuration description

The second configuration is also composed of a fixed winding but there are permanent magnets on the mobile part (Fig. A.2). This configuration is proposed and patented by the industrial partner. The analytical model cannot be generated: considering that all the parameters will change during the optimization, it is impossible to generate a general analytical model which is correct in all cases [9].

This configuration is described by 18 geometrical parameters. In addition, there is one parameter O_R that describes the orientation of the magnets (Fig. A.2). This parameter is comprised in the interval $[0, 1]$ and is defined by the direction of both magnets O_{R1} and O_{R2} (in degrees with reference to the horizontal axis) as follows:

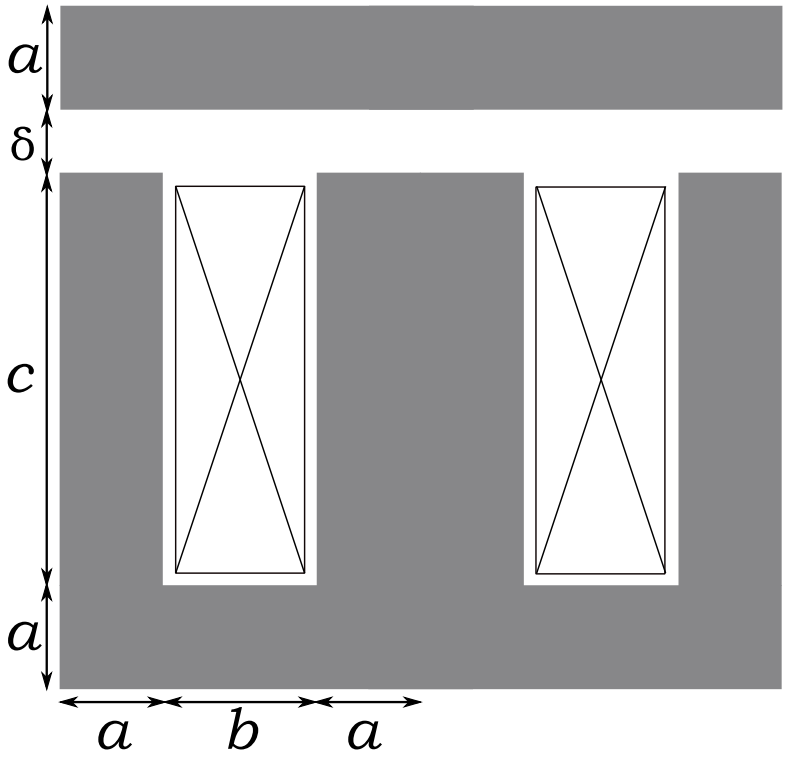

Figure A.1: 1^{st} Configuration to optimize. The axial depth is e

$$\begin{cases} O_{R1} = 0^\circ \\ O_{R2} = 0^\circ \end{cases}, \quad \text{for } O_R \in [0, 0.25]$$
$$\begin{cases} O_{R1} = 180^\circ \\ O_{R2} = 0^\circ \end{cases}, \quad \text{for } O_R \in [0.26, 0.5]$$
$$\begin{cases} O_{R1} = 180^\circ \\ O_{R2} = 180^\circ \end{cases}, \quad \text{for } O_R \in [0.51, 0.75]$$
$$\begin{cases} O_{R1} = 0^\circ \\ O_{R2} = 180^\circ \end{cases}, \quad \text{for } O_R \in [0.76, 1] \tag{A.1}$$

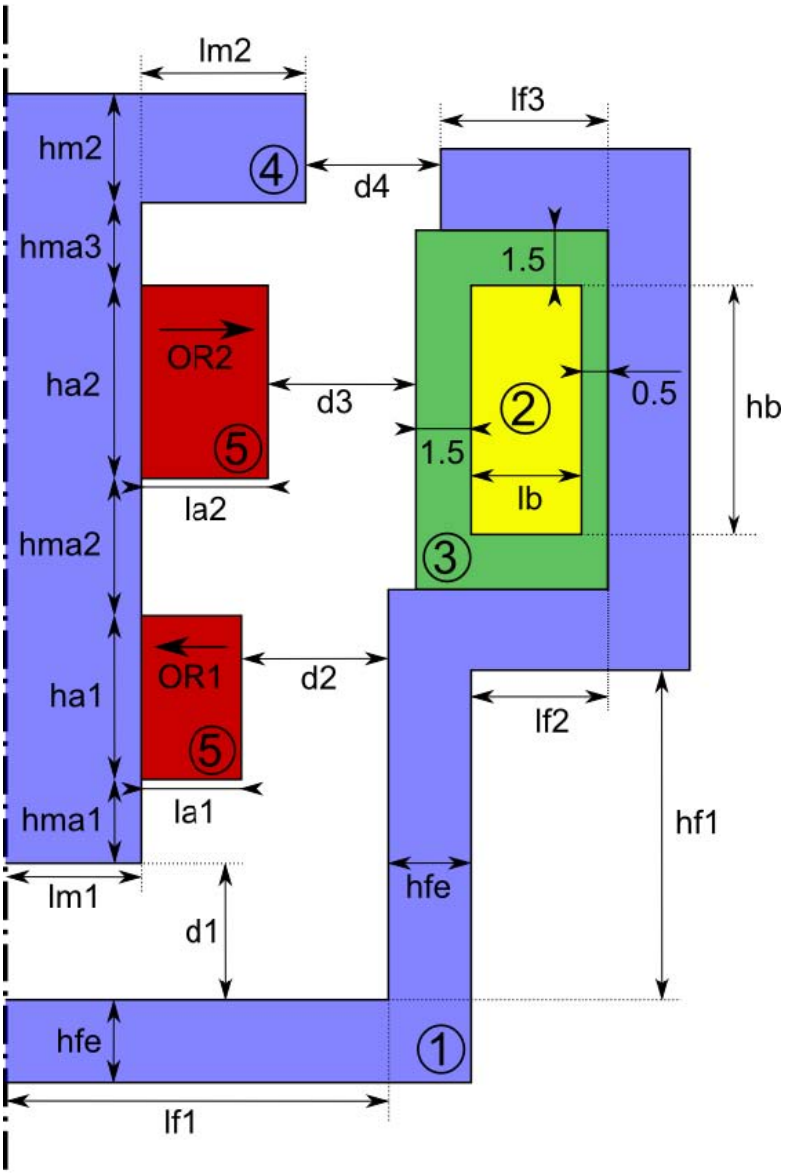

Figure A.2: 2^{nd} Configuration - The axial depth is e (1,4: iron, 2: copper, 3: plastic, 5: magnet)

A.2 Results and comparison

1^{st} Configuration

Fig. A.3 shows the 20 best results after optimization (the cost C is between 1.01 € and 3.17 €). The best of them is represented with the red solid line, and its geometric parameters, mass and cost are presented in Table A.1. For the optimized actuator, all the penalties P_F are equal to 1, therefore $O = C$.

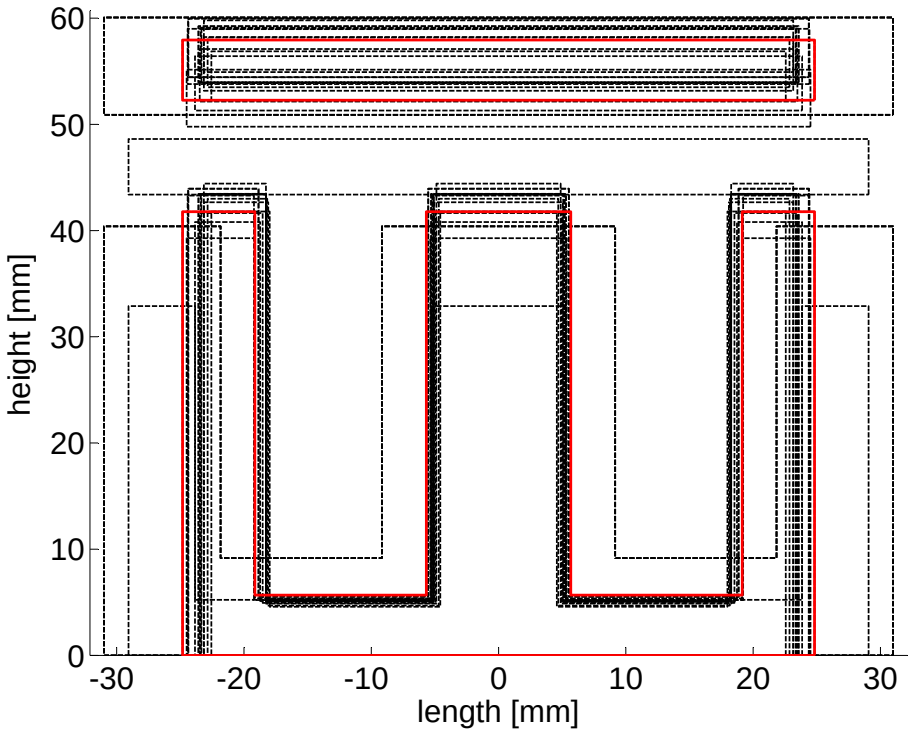

Figure A.3: 1^{st} Configuration - The 20 best results

Table A.1: The optimal 1^{st} configuration

a	2 mm	b	8.8 mm
c	11.5 mm	e	30.5 mm
V_{iron}	37.76 cm^3	V_{copper}	22.01 cm^3
M_{copper}	117.55 g	M_{iron}	294.55 g
M_{tot}		**542.10 g**	
C_{iron}	0.42 €	C_{copper}	0.59 €
C		**1.01 €**	

2^{nd} Configuration

Analysis of the results

The geometries of both optimal configurations are very different but the prices are very similar (1.01 € against 1.09 €). However, the 2^{nd} configuration is much lighter than the 1^{st} (330.7 g against 542.1 g) and the mass could be a second criterion of choice. The magnet significantly reduces the mass, but its high price causes that the total price remains the same.

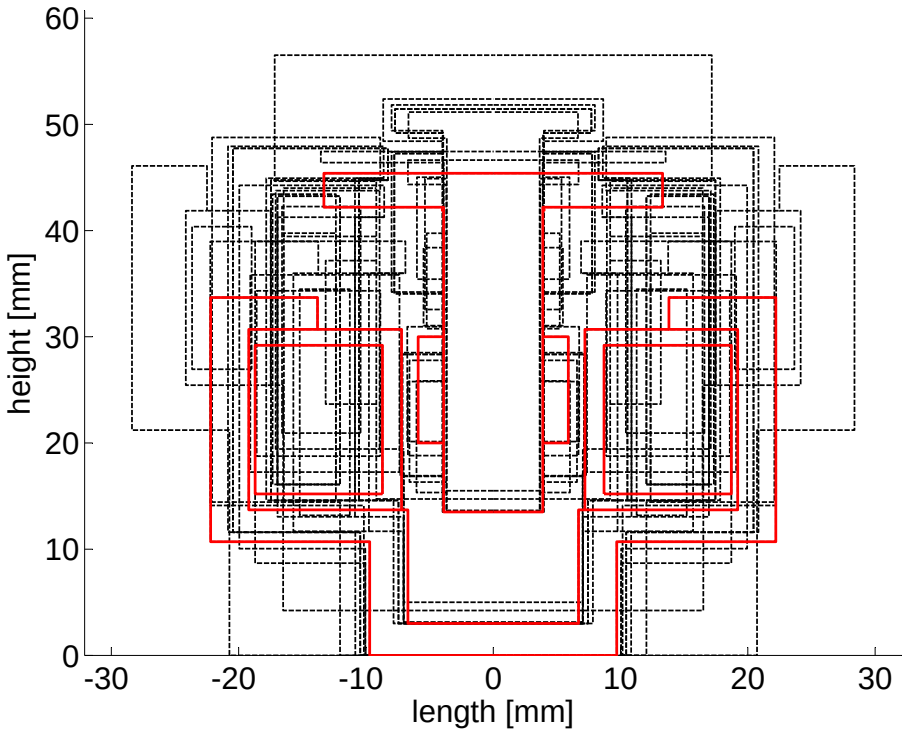

Figure A.4: 2^{nd} Configuration - The 10 best results

Table A.2: The optimal 2^{nd} configuration

l_{m1}	3.9 mm	l_{m2}	9.4 mm
l_{a1}	2.0 mm	l_{a2}	0.1 mm
l_b	10.0 mm	l_{f1}	6.7 mm
l_{f2}	9.5 mm	l_{f3}	5.4 mm
h_{a1}	10.0 mm	h_{a2}	0.1 mm
h_{m2}	3.1 mm	h_{fe}	2.9 mm
h_{f1}	8.0 mm	h_b	14.0 mm
h_{ma1}	6.5 mm	h_{ma2}	11.9 mm
h_{ma3}	0.2 mm	e	21 mm
O_{R1}	180	O_{R2}	180
V_{iron}	13.96 cm^3	V_{copper}	9.59 cm^3
V_{magnet}	0.80 cm^3	M_{iron}	108.89 g
M_{copper}	85.39 g	M_{magnet}	6.40 g
M_{tot}	**330.68 g**	C_{iron}	0.16 €
C_{copper}	0.43 €	C_{magnet}	0.51 €
C		**1.09 €**	

B Appendix

B.1 Test bench

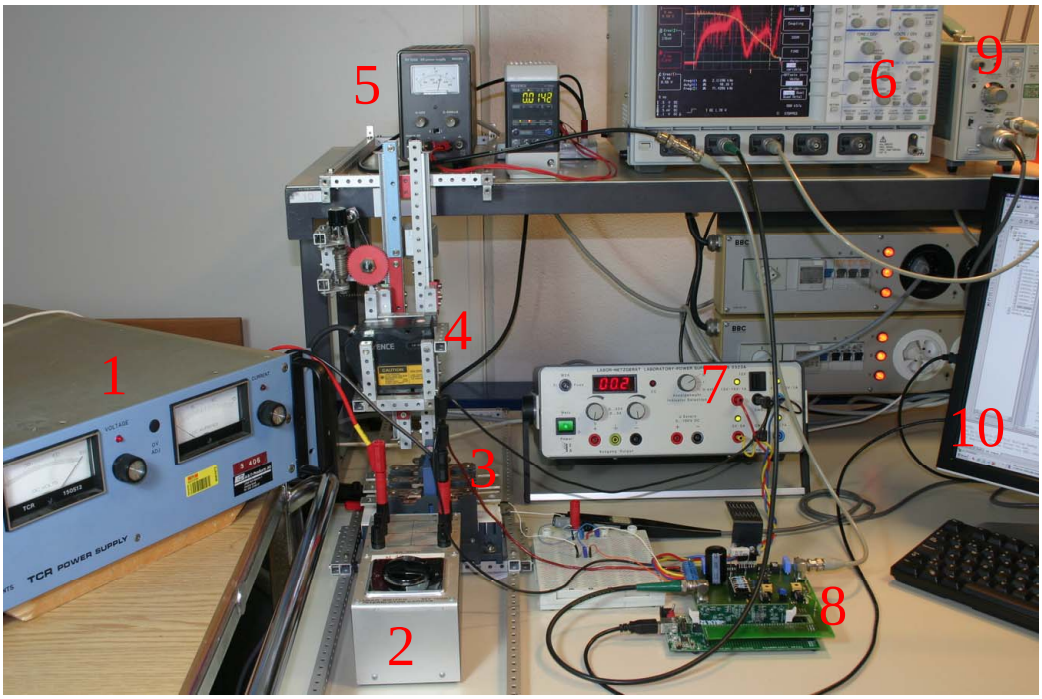

Figure B.1: Test bench

The test bench (Fig. B.1) consists of:

1) DC power supply which can deliver up to 150 V.

2) The switch to be closed to start the closing of the contactor.

3) The tested contactor.

4) The laser external sensor Kayence.

5) The power supply and the control unit of the laser sensor Kayence.

6) The oscilloscope.

7) The power supply (+15V, -15V, and 5V) for supplying the PCB.

8) The PCB with the DSP, filters, and the power stage.

9) A current probe.

10) A PC to control the DSP and analyze the curves provided by the oscilloscope.

B.2 PCB

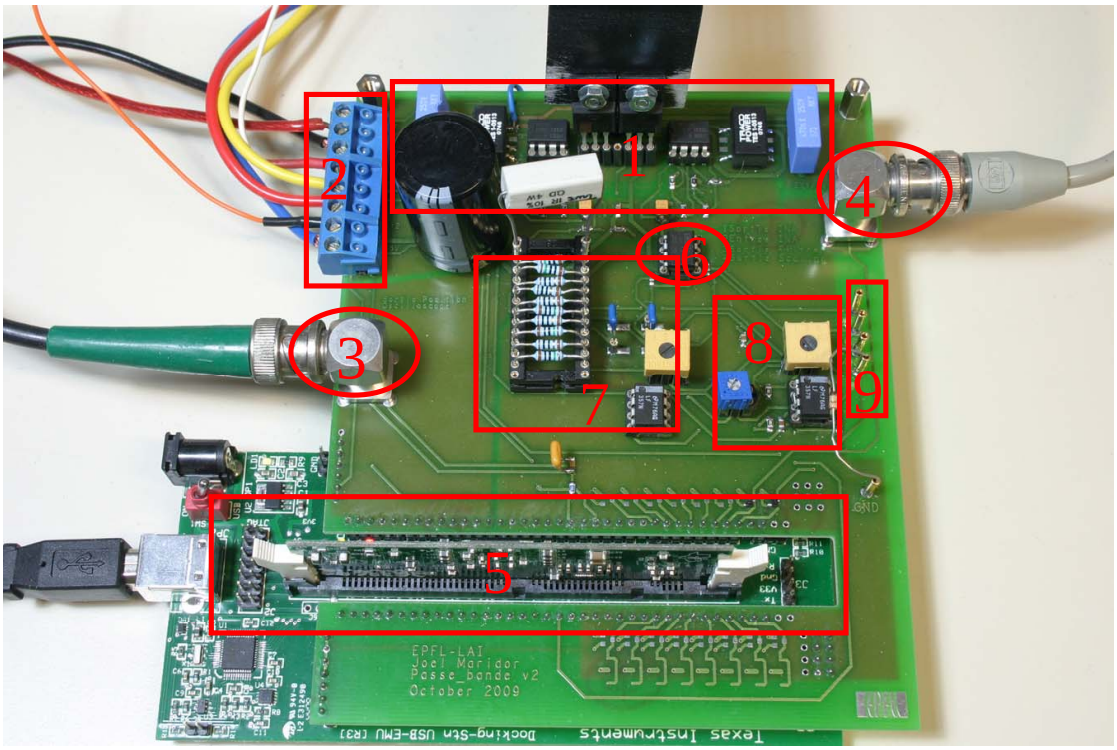

Figure B.2: PCB

The PCB (Fig. B.2) consists of:

1) A power stage with the H-Bridge and the drivers.

2) Power connectors (150 V, +15V, -15V, 5V et GND) and the connectors to the contactor.

3) A connector to see the estimated position at the oscilloscope.

4) A connector to read the position measured by the laser sensor Kayence.

5) A development board which contains the DSP.

6) A differential amplifier INA117.

7) A bandpass filter.

8) A circuit for adjusting the amplitude and the offset.

9) Control connectors.

Bibliography

[1] M. Ali and P. Kaelo. Integrated crossover rules in real coded genetic algorithms. *Eur. J. Oper. Res.*, 176:60–76, 2007.

[2] S. Ali-Loytty, T. Perala, V. Honkavirta, and R. Piche. Fingerprint kalman filter in indoor positioning applications. In *Control Applications, (CCA) & Intelligent Control, (ISIC), 2009 IEEE DOI - 10.1109/CCA.2009.5281069*, pages 1678–1683, 2009.

[3] H. Bühler. *Conception de systèmes automatiques*. EPFL, 1988.

[4] O. Bottauscio, M. Chiampi, and A. Manzin. Advanced model for dynamic analysis of electromechanical devices. *Magnetics, IEEE Transactions on DOI - 10.1109/TMAG.2004.840367*, 41(1):36–46, 2005.

[5] D. Bourlis and J. Bleijs. A wind speed estimation method using adaptive kalman filtering for a variable speed stall regulated wind turbine. In *2010 IEEE 11th International Conference on Probabilistic Methods Applied to Power Systems, PMAPS 2010*, pages 89–94, 2010.

[6] A. Bourquin. Optimisation d'un instrument chirurgical ultrasonique par algorithmes génétiques. Master's thesis, EPFL-LAI (Projet de semestre), 2008.

[7] S. Braune, S. Liu, and P. Mercorelli. Design and control of an electromagnetic valve actuator. In *Computer Aided Control System Design, 2006 IEEE International Conference on Control Applications, 2006 IEEE International Symposium on Intelligent Control, 2006 IEEE*, pages 1657–1662, 2006.

[8] S. Brisset and P. Brochet. Optimization of switched reluctance motors using deterministic methods with static and dynamic finite element simulations. *Magnetics, IEEE Transactions on DOI - 10.1109/20.717664*, 34(5):2853–2856, 1998.

[9] C. Chillet and J.-Y. Voyant. Design-oriented analytical study of a linear electromagnetic actuator by means of a reluctance network. *Magnetics, IEEE Transactions on*, 37(4):3004–3011, 2001.

[10] Design Processing Technologies S.A, http://www.designprocessing.com/. *Pro@design-Expert*. version 2.0.

[11] I. Dulk and T. Kovacshazy. Modelling of a linear proportional electromagnetic actuator and possibilities of sensorless plunger position estimation. In *Carpathian Control Conference (ICCC), 2011 12th International DOI - 10.1109/CarpathianCC.2011.5945822*, pages 89–93, 2011.

[12] A. Espinosa, J.-R. Ruiz, J. Cusido, and X. Morera. Sensorless control and fault diagnosis of electromechanical contactors. *Industrial Electronics, IEEE Transactions on DOI - 10.1109/TIE.2008.925773*, 55(10):3742–3750, 2008.

[13] A. Espinosa, J.-R. Ruiz, and X. Morera. A sensorless method for controlling the closure of a contactor. *Magnetics, IEEE Transactions on*, 43(10):3896–3903, 2007.

[14] P. Eyabi and G. Washington. Model based robust control: An experimental approach. In *Industrial Electronics, 2006 IEEE International Symposium on DOI - 10.1109/ISIE.2006.295577*, volume 1, pages 109–117, 2006.

[15] A. Forrai, T. Ueda, and T. Yumura. Electromagnetic actuator control: A linear parameter-varying (lpv) approach. *Industrial Electronics, IEEE Transactions on DOI - 10.1109/TIE.2007.893077*, 54(3):1430–1441, 2007.

[16] P. Georgilakis. Recursive genetic algorithm-finite element method technique for the solution of transformer manufacturing cost minimisation problem. *Electric Power Applications, IET DOI - 10.1049/iet-epa.2008.0238*, 3(6):514–519, 2009.

[17] C. Gutfrind, X. Jannot, J. Vannier, P. Vidal, and D. Sadarnac. Analytical and fem magnetic optimization of a limited motion actuator for automotive application. In *Electrical Machines (ICEM), 2010 XIX International Conference on DOI - 10.1109/ICELMACH.2010.5608151*, pages 1–6, 2010.

[18] P. Kaelo and M. Ali. Integrated crossover rules in real coded genetic algorithms. *European Journal of Operational Research*, 176(1):60–76, Jan. 2007.

[19] T. Kajima and Y. Kawamura. Development of a high-speed solenoid valve: investigation of solenoids. *Industrial Electronics, IEEE Transactions on DOI - 10.1109/41.345838*, 42(1):1–8, 1995.

[20] C.-C. Lai and C.-C. Tsai. Neural calibration and kalman filter position estimation for touch panels. In *Control Applications, 2004. Proceedings of the 2004 IEEE International Conference on DOI - 10.1109/CCA.2004.1387586*, volume 2, pages 1491–1496 Vol.2, 2004.

[21] L.-J. Li. Method and apparatus for sensing armature position in reluctance electromagnetic actuators. *EUROPEAN PATENT APPLICATION (EP 0 908 904 A2)*, 1999.

[22] K. Lim, N. Cheung, and M. Rahman. Proportional control of a solenoid actuator. In *Industrial Electronics, Control and Instrumentation, 1994. IECON '94., 20th International Conference on*, volume 3, pages 2045–2050vol.3, 5-9 Sept. 1994.

[23] Y. Liu, J. Wan, H. Shen, G. Li, and C. Yuan. Pmsm speed sensorless direct torque control based on ekf. In *Industrial Electronics and Applications, 2009. ICIEA 2009. 4th IEEE Conference on DOI - 10.1109/ICIEA.2009.5138873*, pages 3581–3584, 2009.

[24] R. Longchamp. *Commande numérique de systèmes dynamiques*. EPFL, 1995.

[25] F. Malaguti and E. Pregnolato. Proportional control of on/off solenoid operated hydraulic valve by nonlinear robust controller. In *Industrial Electronics, 2002. ISIE 2002. Proceedings of the 2002 IEEE International Symposium on DOI - 10.1109/ISIE.2002.1026322*, volume 2, pages 415–419 vol.2, 2002.

[26] R. Mancini. *Design Reference - Op Amps For Everyone*. Texas Instruments, advanced analog products edition, August 2002.

[27] J. Maridor, N. Katic, Y. Perriard, and D. Ladas. Sensorless position detection of a linear actuator using the resonance frequency. In *Electrical Machines and Systems, 2009. ICEMS 2009. International Conference on*, pages 1–6, 2009.

[28] J. Maridor, M. Markovic, and Y. Perriard. Design for self-sensing of a linear actuator. In *Energy Conversion Congress & Exposition (ECCE), 2011 IEEE International DOI*, pages 330–335, 2011.

[29] J. Maridor, M. Markovic, and Y. Perriard. Kalman filter to measure position and speed of a linear actuator. In *Electric Machines & Drives Conference (IEMDC), 2011 IEEE International DOI - 10.1109/IEMDC.2011.5994869*, pages 330–335, 2011.

[30] J. Maridor, M. Markovic, Y. Perriard, and D. Ladas. Optimization design of a linear actuator using a genetic algorithm. In *Electric Machines and Drives Conference, 2009. IEMDC '09. IEEE International*, pages 1776–1781, 2009.

[31] M. Markovic, V. Muller, A. Hodder, and Y. Perriard. Optimal design of an in-wheel bldc motor for a kick scooter. In *Energy Conversion Congress and Exposition (ECCE), 2010 IEEE DOI - 10.1109/ECCE.2010.5618023*, pages 292–296, 2010.

[32] D. Meeker. *Finite Element Method Magnetics (FEMM)*. http://femm.foster-miller.net/wiki/HomePage. version 4.2.

[33] M. Montanari, F. Ronchi, C. Rossi, and A. Tonielli. Control of a camless engine electromechanical actuator: position reconstruction and dynamic performance analysis. *Industrial Electronics, IEEE Transactions on DOI - 10.1109/TIE.2004.825230*, 51(2):299–311, 2004.

[34] C. Moon, J. Kim, G. Choi, and Y. Seo. An efficient genetic algorithm for the traveling salesman problem with precedence constraints. *Eur. J. Oper. Res.*, 140:606–617, 2002.

[35] T. Nakano, K. Nagata, M. Yamada, and K. Magatani. Application of least square method for muscular strength estimation in hand motion recognition using surface emg. In *Engineering in Medicine and Biology Society, 2009. EMBC 2009.*, pages 2655–2658, 2009.

[36] A. Oswald and H.-G. Herzog. Automated design of tubular linear generator for use within optimization tool. In *Electrical Machines (ICEM), 2010 XIX International Conference on DOI - 10.1109/ICELMACH.2010.5608032*, pages 1–6, 2010.

[37] D. Pai A, L. Umanand, and N. Rao. Direct torque control of induction motor with extended kalman filter. In *Power Electronics and Motion Control Conference, 2000. Proceedings. IPEMC 2000. The Third International DOI - 10.1109/IPEMC.2000.885344*, volume 1, pages 132–137 vol.1, 2000.

[38] D. Pawelczak and H.-R. Trankler. Sensorless position control of electromagnetic linear actuator. In *Instrumentation and Measurement Technology Conference, 2004. IMTC 04. Proceedings of the 21st IEEE*, volume 1, pages 372–376 Vol.1, 2004.

[39] Y. Perriard, O. Scaglione, C. Koechli, and J. Persson. Self-sensing methods to drive micro-machines. In *Physics of Semiconductor Devices, 2007. IWPSD 2007. International Workshop on*, pages 639–644, 2007.

[40] D. Porto, A. Bourquard, and Y. Perriard. Genetic algorithm optimization for a surgical ultrasonic transducer. *IEEE Ultrasonics Symposium*, 2008.

[41] M. Rahman, N. Cheung, and K. W. Lim. Position estimation in solenoid actuators. *Industry Applications, IEEE Transactions on*, 32(3):552–559, 1996.

[42] Y.-S. Renn, Jyh-Chyang; Chou. Sensorless plunger position control for a switching solenoid. *JSME International Journal Series C*, Volume 47, Issue 2:pp. 637–645, 2005.

[43] F. Ronchi, C. Rossi, and A. Tilli. Sensing device for camless engine electromagnetic actuators. In *IECON 02 [Industrial Electronics Society, IEEE 2002 28th Annual Conference of the] DOI - 10.1109/IECON.2002.1185531*, volume 2, pages 1669–1674 vol.2, 2002.

[44] R. P. Sallen and E. L. Key. A practical method of designing rc active filters. *IRE Trans. Circuit Theory*, CT-2:74–85, 1955.

[45] K. Shi, T. Chan, Y. Wong, and S. Ho. Speed estimation of an induction motor drive using extended kalman filter. In *Power Engineering Society Winter Meeting, 2000. IEEE DOI - 10.1109/PESW.2000.849963*, volume 1, pages 243–248 vol.1, 2000.

[46] C. Silva, G. Asher, and M. Sumner. Hybrid rotor position observer for wide speed-range sensorless pm motor drives including zero speed. *Industrial Electronics, IEEE Transactions on DOI - 10.1109/TIE.2006.870867*, 53(2):373–378, 2006.

[47] L. Snyder and M. Daskin. A random-key genetic algorithm for the generalized traveling salesman problem. *Eur. J. Oper. Res.*, 174:38–53, 2006.

[48] O. Ustun and R. Tuncay. Design, analysis, and control of a novel linear actuator. *Industry Applications, IEEE Transactions on*, 42(4):1007–1013, 2006.

[49] M. Wada, H. Yoshimoto, and Y. Kitaide. Dynamic analysis and simulation of electromagnetic contactors with ac solenoids. In *IECON 02 [Industrial Electronics Society, IEEE 2002 28th Annual Conference of the] DOI - 10.1109/IECON.2002.1182829*, volume 4, pages 2745–2751 vol.4, 2002.

[50] C. Wang and L. Xu. A novel approach of rotor position detection for pm machines based on conventional pwm algorithms. In *National Aerospace and Electronics Conference, 2000. NAECON 2000. Proceedings of the IEEE 2000*, pages 547–553, 2000.

[51] R.-L. Wang and K. Okazaki. An improved genetic algorithm with conditional genetic operators and its application to set-covering problem. *Soft Computing*, Volume 11:687–694, 2007.

[52] G. Welch and G. Bishop. An introduction to the kalman filter. University of North Carolina at Chapel Hill, july 2006.

[53] D. Westmore and W. Wilson. Direct dynamic control of a robot using an end-point mounted camera and kalman filter position estimation. In *Robotics and Automation, 1991. Proceedings., 1991 IEEE International Conference on DOI - 10.1109/ROBOT.1991.131759*, pages 2376–2384 vol.3, 1991.

[54] www.mathworks.com. Genetic algorithm and direct search toolbox 2. User's guide, Matlab, 2007.

[55] L. Xianxing, W. Chao, C. Li, L. Qing, and W. Weiran. Speed-sensorless direct torque control of bearingless permanent magnet synchronous motor based on extended kalman filter. In *Measuring Technology and Mechatronics Automation (ICMTMA), 2010 International Conference on DOI - 10.1109/ICMTMA.2010.712*, volume 3, pages 457–460, 2010.

[56] Z. Xu and M. Rahman. An adaptive sliding stator flux observer for a direct-torque-controlled ipm synchronous motor drive. *Industrial Electronics, IEEE Transactions on DOI - 10.1109/TIE.2007.900328*, 54(5):2398–2406, 2007.

[57] L.-C. Zai, C. DeMarco, and T. Lipo. An extended kalman filter approach to rotor time constant measurement in pwm induction motor drives. *Industry Applications, IEEE Transactions on DOI - 10.1109/28.120217*, 28(1):96–104, 1992.

Curriculum Vitae

Name:	Maridor
Given name:	Joël
Year of birth:	1978
Marital status:	Single
Nationality:	Swiss
E-mail:	joel.maridor@a3.epfl.ch

Studies and professional experience

2011-...	RD Engineer at ETA SA, Grenchen Nord, Switzerland.
2007-2011	Teaching assistant and Ph.D. student at the Integrated Actuators Laboratory (LAI), Ecole Polytechnique Fédérale de Lausanne (EPFL), Switzerland.
2004-2007	EPF Engineer at Service Industriel de Lausanne, Switzerland.
2003	Civil service: Animator for the Elderly at Neuchâtel, Switzerland.
2002	Civil service: Teaching assistant at the Polytechnic of Makassar, Indonesia.
1996-2002	Master of Science in Electricity, Ecole Polytechnique Fédérale de Lausanne (EPFL), Switzerland.
1993-1996	Maturité Type C, Neuchâtel, Switzerland.

Publications

J. Maridor, M. Markovic, Y. Perriard and D. Ladas. Optimization design of a linear actuator using a genetic algorithm. In *Proceedings of the 2009 IEEE International Electric Machines and Drives Conference (IEMDC), Miami, USA, May 3-6, 2009.*

J. Maridor, N. Katic, M. Markovic and Y. Perriard. Sensorless position detection of a linear actuator using the resonant frequency. *Proceedings of the 12th International Conference on Electrical Machines and Systems (ICEMS 2009), Tokyo, Japan, November 15-18, 2009.*

J. Maridor, M. Markovic and Y. Perriard. Kalman Filter to Measure Position and Speed of a Linear Actuator. *Proceedings of the International Electric Machines and Drives Conference (IEMDC), Niagara Falls, Canada, 2011.*

J. Maridor, M. Markovic and Y. Perriard. Design for Self-Sensing of a Linear Actuator. *Proceedings of the third IEEE Energy Conversion Congress and Exposition (ECCE), Phoenix, Arizona, USA, 2011.*